MONITORING AND CONTROL OF MICRO-HOLE ELECTRICAL DISCHARGE MACHINING

by

Chen-Chun Kao

A dissertation submitted in partial fulfillment
of the requirements for the degree of
Doctor of Philosophy
(Mechanical Engineering)
in The University Of Michigan
2007

Doctoral Committee:

Professor Albert J. Shih, Chair
Professor Jun Ni
Professor Yogesh B. Gianchandani
Research Associate Professor Zoran S. Filipi

ACKNOWLEDGEMENTS

First of all, I would like to thank my academic advisor, Prof. Albert J. Shih, for his insightful guidance and relentless efforts on my PhD research. I also wan to thank my committee members, Prof. Jun Ni, Prof. Yogesh B. Gianchandani, and Prof. Zoran S. Filipi, for their valuable comments and careful review of this dissertation.

My research was primarily sponsored by Caterpillar Inc. The assistance and mentorship from Dr. Marion B. Grant during my corporate internship at Caterpillar are greatly appreciated. I am also grateful to John MacGregor, Chuck Sannes, and Geroge Barbulescue of Ann Arbor Machine Company, Chelsea, MI, and Chiao-Chin Shih of Castek Company, Taiwan, for their technical support and professional remarks on my research. I especially thank my friends at S.M. Wu Manufacturing Research Center for their supports and encouragements.

Finally, I would like to express my greatest gratitude to my parents, Yu-Tsai Kao and Lien-Chiao Lo Kao, whose painstaking efforts and incomparable passion to breeding and educating children made me what I am now. I want to thank my sisters, whose warm care and witty humor always bring cheers to our family and bond us strongly together. My wife, Wenqian Hu, you are the one who gives me the strongest support in the challenging, but also rewarding, pursuit of the PhD degree.

TABLE OF CONTENTS

ACKNOWLEDGEMENTS ii

LIST OF FIGURES vi

LIST OF TABLES xi

LIST OF APPENDICES xii

CHAPTER

1. INTRODUCTION 1
    - 1.1. Research Backgrounds, Motivations, and Goals 1
    - 1.2. Micro-Hole Drilling 5
        - 1.2.1. EDM drilling process 5
        - 1.2.2. Development of micro EDM machines 7
        - 1.2.3. Needs of advanced micro-hole EDM technology 8
    - 1.3. Process Monitoring of EDM 8
    - 1.4. EDM Process Controllers 10
    - 1.5. Form Measurement of Micro-Holes 11
    - 1.6. Concluding Remarks 12
2. SUB-NANOSECOND MONITORING OF MICRO-HOLE EDM PULSES. 14
    - 2.1. Background of Micro-Hole EDM Monitoring 15
    - 2.2. Experimental Setup and Monitoring Procedures 17
        - 2.2.1. Micro-hole EDM machine 17
        - 2.2.2. Data acquisition and classification of EDM pulses 17
        - 2.2.3. Input parameters and stages in micro-hole EDM 19
        - 2.2.4. EDM output parameters 23

2.3. Spark and Arc EDM Pulses 25
2.3.1. Spark and arc pulses in Stage 2 (Drilling) 26
2.3.2. Spark and arc pulses in Stage 3 (Penetration)..................... 29
2.3.3. Spark and arc pulses in Stage 1 (Electrode Dressing) 31
2.4. Pulse Rate and Electrode Feed Rate 34
2.5. Concluding Remarks.. 36
3. ADAPTIVE FUZZY LOGIC CONTROLLER FOR MICRO-HOLE EDM .. 38
3.1. Review of the Fuzzy Logic Controller... 39
3.2. Design and Development of the Fuzzy Logic Controller 41
3.2.1. Input and output parameters.. 41
3.2.2. Fuzzy logic inference engine 44
3.3. Fuzzy Logic Controller Tuning 46
3.4. Concluding Remarks.. 47
4. IMPLEMENTATION AND VALIDATION OF ADAPTIVE FUZZY LOGIC CONTROLLER FOR MICRO-HOLE EDM 48
4.1. Platform 1: Gromax Micro-Hole EDM Machine.............................. 48
4.1.1. Overview.. 48
4.1.2. Data acquisition system 50
4.1.3. Adaptive fuzzy logic controller.. 51
4.1.4. The piezoelectric stage.. 54
4.1.5. Characterization of EDM conditions 56
4.1.6. Experimental procedures 59
4.1.7. Experimental results and discussions................................ 61
4.2. Platform 2: AAM Micro-Hole EDM Machine 72
4.2.1. Overview.. 72
4.2.2. Fuzzy logic controller development and tuning process..... 73
4.2.3. Experiment design 79
4.2.4. DOE analysis of EDM parameters for gain scheduling controller (Exp. I)... 80
4.2.5. Tuning of the fuzzy logic controller (Exp. II).................... 85
4.2.6. Selection of fuzzy input parameter (Exp. III) 87

4.2.7. DOE analysis of EDM parameters for fuzzy logic controller (Exp. IV) 89
4.2.8. Deep micro-hole EDM drilling (Exp. V) 90
4.2.9. Small diameter micro-hole EDM drilling (Exp. VI) 95
4.3. Concluding Remarks 100
5. CONCLUSIONS AND FUTURE WORK 103
5.1. Major Contributions 103
5.2. Recommendations for Future Study 106
APPENDICES 108
BIBLIOGRAPHY 147

LIST OF FIGURES

Figure 1.1. The ignition process for internal combustion engines: (a) gasoline engine and (b) diesel engine. 2

Figure 1.2. SEM micrographs of diesel engine injector spray holes: (a) overview and (b) close-up view. 2

Figure 1.3. A schematic diagram of micro-hole EDM drilling. 3

Figure 1.4. Examples of diesel fuel spray pattern: (a) irregular and (b) regular. 4

Figure 1.5. The emission standards of the US and EU.......... 5

Figure 2.1. Characterization of EDM pulses: (a) spark, (b) arc, and (c) short. 16

Figure 2.2. EDM process input and output parameters of sample spark and arc pulses. 20

Figure 2.3. SEM micrographs of the tip of tungsten wire electrode: (a) sharpened electrode tip after EDM Stage 3 and (b) dressed electrode tip after EDM Stage 1 (diameter of wire electrode: 125 μm). 22

Figure 2.4. The effect of EDM Stage 3 Penetration: (a) worn tip of wire electrode causes a narrower hole exit and (b) enlarged hole exit is generated due to the over-travel of wire electrode. 23

Figure 2.5. Sample EDM pulses in Stage 2: (a) spark and (b) arc (125 μm diameter wire electrode).......... 27

Figure 2.6. Close-up view for Periods II and III of sample EDM pulses in Stage 2: (a) box A and (b) box B. 28

Figure 2.7. Sample EDM pulses in Stage 3: (a) spark and (b) arc (125 μm diameter wire electrode).......... 30

Figure 2.8. Sample EDM pulses in Stage 1: (a) spark and (b) arc (125 μm diameter wire electrode).......... 33

Figure 2.9. Rate of spark, arc, and short pulses for 125 and 225 μm wire electrodes in three EDM stages. 34

Figure 2.10. Feed rate for 125 and 225 μm wire electrodes in three EDM stages. 35
Figure 3.1. Schematic diagram of a typical fuzzy logic controller. 42
Figure 3.2. Membership functions for fuzzy logic parameters: (a)ΔR_s and $\delta(\Delta R_s)$, (b) v, and (c) d. 43
Figure 3.3. Sample pulse trains for six levels of EDM status (open circuit voltage V_o = 100 V). 45
Figure 4.1. Configuration of the fuzzy logic micro-hole EDM control system. 49
Figure 4.2. Measured voltage and current and corresponding parameters in a 1 ms sampling duration T. 52
Figure 4.3. Schematic diagram of the adaptive fuzzy logic controller for Gromax EDM machine. 52
Figure 4.6. Bandwidth of the piezoelectric stage with two sinusoidal inputs. 55
Figure 4.7. Continuous position ramp response of the piezoelectric stage at 50 Hz (Travel = 2 μm, velocity = 1.8 mm/s). 55
Figure 4.8. Classification of EDM pulses by ignition delay t_d. 58
Figure 4.9. Gap voltage and current of the EDM pulse train: (a) no fuzzy logic control applied and (b) with the fuzzy logic EDM control (three-input type, d_{max} = 2 μm, v_{max} = 1.8 mm/s, and t_{dt} = 80 μs). 62
Figure 4.10. Effects of the fuzzy logic EDM control on arc pulse and EDM drilling time (three-input type, d_{max} = 2 μm, v_{max} = 1.8 mm/s, and t_{dt} = 80 μs)............... 63
Figure 4.11. Effects of single and multiple input parameters on arc pulses and drilling time (d_{max} = 2 μm, v_{max} = 1.8 mm/s, and t_{dt} = 80 μs). 64
Figure 4.12. Arc pulses and drilling time under different t_{dt} (three-input type, d_{max} = 2 μm, v_{max} = 1.8 mm/s). 66
Figure 4.13. Movements of piezoelectric stage under three levels of d_{max} = 2, 4 and 8 μm (three-input type, v_{max} = 1.8 mm/s, and t_{dt} = 80 μs). 67
Figure 4.14. Effects of v_{max} on EDM drilling time (v_{max} = 0.6, 1.2, 1.8, and 2.4 mm/s).. 69
Figure 4.15. DOE generated surface $F(t_{dt}, v_{max})$ and the locations of optimal F by DOE analysis. 70
Figure 4.16. Experimental results of fuzzy logic EDM control at the optimal t_{dt} and v_{max} (three-input type, d_{max} = 2 μm, v_{max} = 1.82 mm/s, and t_{dt} = 62 μs)............. 71

Figure 4.17. Schematic diagram of the adaptive fuzzy logic controller for AAM EDM machine. 75
Figure 4.18. Discretization level l of membership functions: (a) high (l = 40) and (b) low (l = 10). 78
Figure 4.19. Response surfaces generated by the DOE analysis for 1.14 mm thick AISI 52100 using 150 μm diameter electrode: (a) t_0 and V_o (b) t_e and V_o, and (c) t_e and t_0. 82
Figure 4.20. Comparison of servo position and spark ratio under gain scheduling controller and fuzzy logic controllers from three tuning tests. 84
Figure 4.21. Representative gap voltage and current waveforms for gain scheduling controller and fuzzy logic controller in micro-hole EDM drilling. 87
Figure 4.22. Effects of fuzzy input parameter selection (using the tuned fuzzy logic controller). 89
Figure 4.23. Deep micro-hole EDM drilling under gain scheduling controller and fuzzy logic controller. 91
Figure 4.24. Representative waveforms of different stages in deep micro-hole EDM drilling under gain scheduling controller and fuzzy logic controller: (a) Stage 1, (b) Stage 2, and (c) Stage 3. 94
Figure 4.25. Response surfaces generated by the DOE analysis for 1.14 mm thick AISI 52100 using 75 μm diameter electrode: (a) t_0 and V_o (b) t_e and V_o, and (c) t_e and t_0. 97
Figure 4.26. Small diameter micro-hole EDM drilling using 75 μm diameter electrode under gain scheduling controller and fuzzy logic controller. 98
Figure 4.27. Representative waveforms of Stage 1 in small diameter micro-hole EDM drilling: (a) gain scheduling controller and (b) fuzzy logic controller. 99
Figure 4.28. Representative waveforms of Stage 2 in small diameter micro-hole EDM drilling under gain scheduling controller and fuzzy logic controller. 100
Figure A.1. Schematic diagram of diesel fuel injector micro-holes of an injector nozzle, a needle, and fuel flow. 110
Figure A.2. Classification of shape of a micro-hole for the fuel injector: (a) positive taper, (b) negative taper, and (c) rounded flow entry. 112

Figure A.3. SEM micrographs of the tip of tungsten wire electrode: (a) sharpened electrode tip after EDM Stage 2 and (b) blunted electrode tip after EDM Stage 1 (diameter of wire electrode: 125 μm). 113
Figure A.4. Micro-hole measurement using the combination of optical and contact sensors in a CMM. 114
Figure A.5. Setup of micro-hole measurement: (a) overview of the nozzle, probe, and optical lens and (b) close-up view for the glass fiber probe. 115
Figure A.6. Three setup procedures: (a) align the probe to the CMM machine Z axis, (b) align the micro-hole to the calibrated probe, and (c) locate the top datum circle and reference point of the micro-hole. 117
Figure A.7. The measurement of a micro-hole by the spherical probe tip: (a) the spherical probe tip inside a micro-hole and (b) the spherical probe tip in contact with the micro-hole and the user-defined rectangle for arc identification. 118
Figure A.8. Determination of the contact point between the micro-hole surface and the probe tip. 119
Figure A.9. Shape measurement of micro-holes: (a) orientation of coordinate system and locations of selected measurement points and (b) depths of different sections according to the three EDM Stages. 122
Figure A.10. Diameter of 12 measurement sections in three micro-holes. 128
Figure A.11. Roundness of 12 measurement sections in three micro-holes. 129
Figure A.12. $\sigma_{repeatability}$ of roundness for 12 measurement sections. 130
Figure A.13. 3D wireframe representation of Hole 1: (a) before AFM and (b) after AFM. 132
Figure A.14. Effects of AFM on micro-hole diameter. 133
Figure B.1. Debris accumulation and hole exit enlargement due to secondary discharges. 136
Figure B.2. Effects of the pilot hole in multi-stage EDM drilling. 137
Figure B.3. Negative tapered micro-holes measurement using Werth CMM. 138
Figure C.1. A *RLC* circuit for the modeling of ringing effect. 140
Figure C.2. Schematic diagram of the micro-hole EDM setup. 140

Figure C.3. Envelope curves of the ringing effect for 100, 125, and 225 μm diameter wire electrodes. (V_o = 200 V).. 143

LIST OF TABLES

Table 2.1. Input parameters of micro-hole EDM. 21

Table 4.1. Analogy between the intelligent machine system (Albus, 1992) and the fuzzy logic EDM control system. 50

Table 4.2. Fuzzy inference rules of the fuzzy logic controller for Gromax EDM machine. 53

Table 4.3. DOE experiment setup and associated EDM drilling time. 61

Table 4.4. Fuzzy inference rules of the fuzzy logic controller for AAM EDM machine. 76

Table 4.5. Variable types and discretization level of three fuzzy logic controller tests. 78

Table 4.6. DOE experiment setup for EDM parameter optimization using 150 and 75 μm diameter electrodes. 81

Table A.1. Process parameters of three Stages in micro-hole EDM. 120

Table A.2. Measurement results of three micro-holes before and after abrasive flow machining. 126

Table A.3. Gage R&R and capability tolerance for CMM micro-hole measurement. 130

Table C.1. Parasitic properties C_p and R_p with different electrode size (V_o = 200 V, L_p = 0.288 μH). 144

Table C.2. Parasitic properties C_p and R_p with different open circuit voltage V_o (diameter of wire electrode = 125 μm, parasitic inductance L_e= 0.066 μH, and L_p = 0.288 μH). 145

LIST OF APPENDICES

A. Form Measurement of Micro-Holes 109
B. Negative Tapered Micro-Hole EDM Drilling 135
C. The Ringing Model 139

CHAPTER 1

INTRODUCTION

Electrical discharge machining (EDM) is one of the most common methods for micro-hole fabrication and is currently applied to the drilling of diesel fuel injector spray holes. This research studies the monitoring and control of micro-hole EDM for diesel fuel injector spray holes and characterizes spray hole geometry using state-of-the-art measurement technology. New micro-hole EDM drilling monitoring and control techniques are developed in this research for next generation injector spray holes.

1.1. Research Backgrounds, Motivations, and Goals

The micro-hole drilling has a wide range of applications, such as ink-jet printer nozzles, orifices for bio-medical devices, cooling vents for gas turbine blades, and diesel fuel injector spray holes. The representative industrial application of micro-hole drilling is the high volume production of diesel fuel injector spray holes. Both diesel engines and direct injection (DI) gasoline engines need fuel injectors with precision injector spray holes. For the DI gasoline engine, the combustion process is ignited by a spark plug, as shown in Figure 1.1 (a). For diesel engine, as shown in Figure 1.1(b), a high compression ratio is applied to ignite the atomized diesel fuel, which is injected into the cylinder through injector spray holes. Scanning electron microscopy (SEM) micrographs of diesel fuel injector spray holes with 150 μm diameter are shown in Figure 1.2.

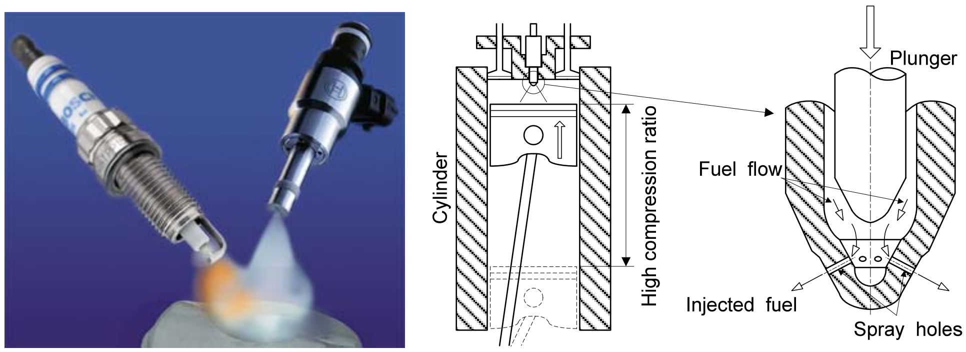

(a) (b)

Figure 1.1. The ignition process for internal combustion engines: (a) gasoline engine[1] and (b) diesel engine.

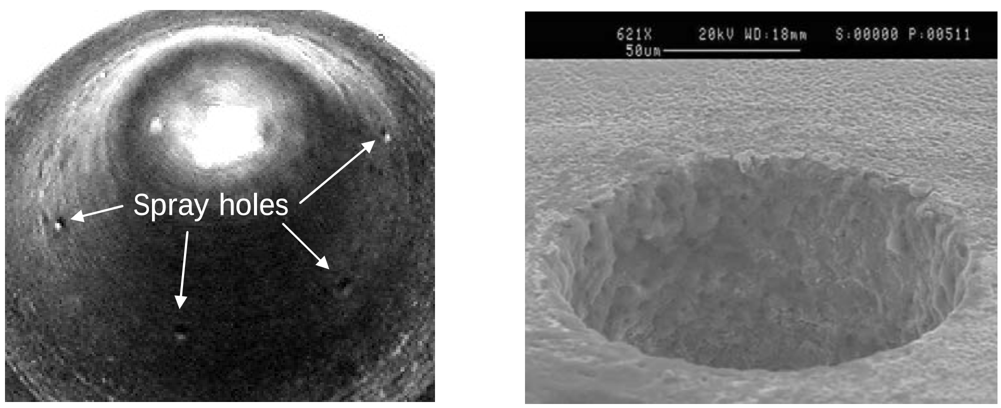

(a) (b)

Figure 1.2. SEM micrographs of diesel engine injector spray holes: (a) overview and (b) close-up view.

The EDM drilling is currently applied for the manufacturing of diesel fuel injector spray holes. This process was first developed in the early 1970s when the injector tip

---

[1] Courtesy of the Robert Bosch GmbH.

material was changed to hardened steel due to the requirement of higher injection pressure for better emission and performance of diesel engines. A schematic diagram of the EDM drilling process for injector spray holes is illustrated in Figure 1.3.

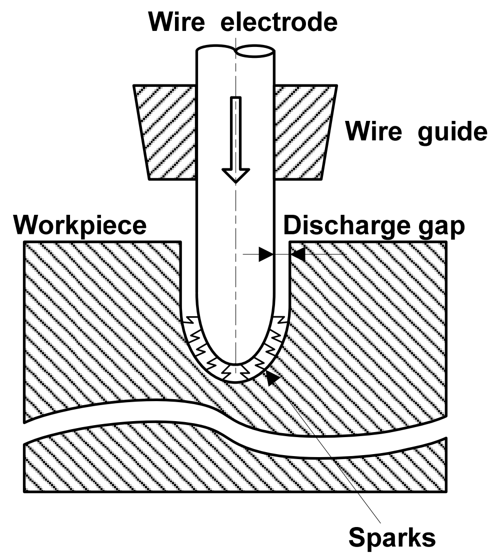

Figure 1.3. A schematic diagram of micro-hole EDM drilling.

A wire electrode is fed through the wire guide, which is usually made of ceramic material for wear resistance, to perform the drilling process. Sparks are generated across the discharge gap at the tip of the wire electrode to remove material from the workpiece and also cause the electrode wear, which sharpens the electrode tip. Tungsten is the most common electrode material because of its high melting temperature (3370°C) and low tool wear rate. Tungsten wire electrodes are centerless ground (Her and Weng, 2001) to achieve uniform size and the smallest diameter can be down to 30 μm. The common specification of state-of-the-art injector spray holes is 150 μm diameter and 1.0 mm depth.

The EDM process affects the dimension and geometry of injector spray holes. The dimension, geometry, flow rate, and surface roughness of the injector spray hole are critical to the spray pattern, fuel atomization, combustion, and emissions of the diesel engine. An example of diesel fuel spray pattern is shown in Figure 1.4.

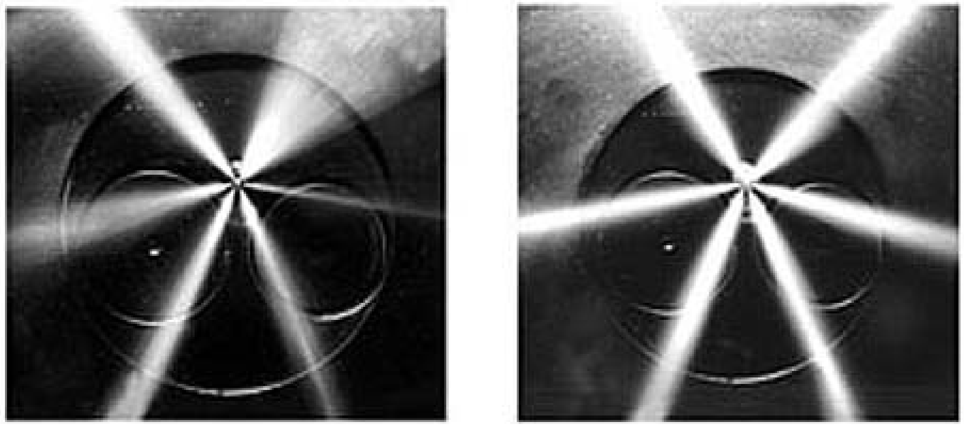

(a) (b)

Figure 1.4. Examples of diesel fuel spray pattern[2]: (a) irregular and (b) regular.

Smaller spray hole diameter (< 100 μm) and higher injection pressure (> 100 MPa) can generate more evenly distributed spray pattern and finer diesel fuel atomization (Nagasaka et al., 2000; Postrioti and Ubertini, 2006), which can lead to lower nitrogen oxide (NO_x) and particulate emission. But the reduction of spray hole dimension will result in a higher aspect ratio (hole depth/diameter), a major technical challenge for the micro-hole EDM. Negative tapered micro-holes, which are truncated cone shaped with the diameter of flow inlet larger than that of flow outlet, can minimize the cavitation problem (Blessing et al., 2003) in diesel fuel injections. New homogeneous charge compression ignition (HCCI) diesel fuel injectors are expected to have small (less than 0.1 mm diameter) and negative tapered spray holes (15 to 20 μm diameter difference). As a result, with the requirement of new diesel combustion technology and ever tightening on-highway diesel emission standards set by U.S. Environmental Protection Agency (EPA) for 2007 and 2010, denoted in Figure 1.5 as US 07 and US 10,

---

[2] Image source: http://www.enertechlabs.com/Inject-R-Clean.htm

respectively, advanced study for the improvement of present micro-hole EDM drilling technology is necessary. This research is thus motivated to investigate the micro-hole EDM drilling process and develop advanced control strategy for better drilling efficiency and capability.

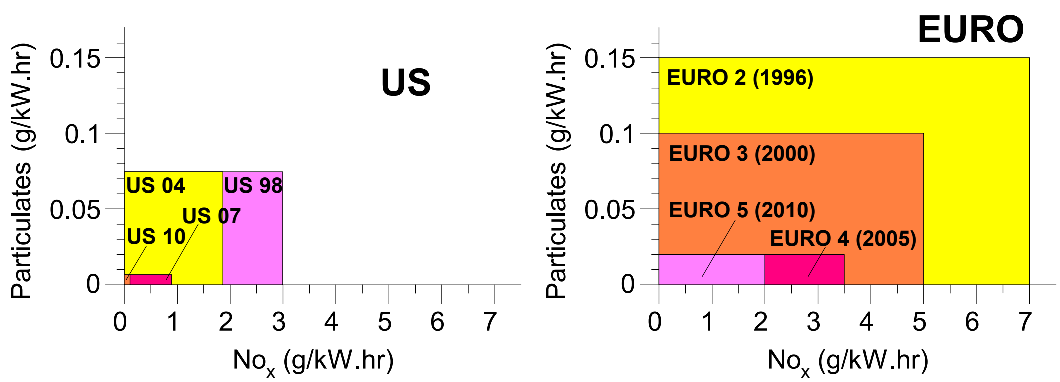

Figure 1.5. The emission standards of the US and EU[3]

The goals in this research are: (1) investigation of the micro-hole EDM drilling through process monitoring and analysis, (2) development of advanced control strategy for better drilling efficiency, (3) design and implementation of innovative EDM drilling techniques for next generation diesel fuel injector spray holes with smaller diameter and negative taper, and (4) form measurement and geometric characterization of injector spray holes to link the manufacturing practice to spray hole design.

1.2. Micro-Hole Drilling

1.2.1. EDM drilling process

One of the first experiments reported on micro-hole EDM drilling was performed

---

[3] Image source: Diesel Progress North American Edition, April 2005.

by Van Ossenbruggen (1969) in the Philips Research Laboratory in the late 1960's. After these groundbreaking experiments, micro-hole EDM has drawn much attention and been extensively applied in the manufacturing industry.

Micro-holes down to 0.1 mm diameter could be achieved with traditional twist drill but it was based on specific prerequisites such as high spindle speeds (up to 140,000 rpm) and efficient cutting fluid supply (Iwata and Moriwaki, 1981). The drill breakage, burrs at hole inlet and exit due to the tool wear, and poor machinability of hard alloys further limited the application of twist drill in micro-hole drilling (Hebbar, 1992). The EDM drilling process, which utilizes thermal effect rather than mechanical force to remove material, is suitable for machining hard materials and is free from burr formation (Masuzawa et al., 1989).

High aspect ratio micro-hole EDM was studied by Masuzawa et al. (1990), Takahata et al. (2000), and Lim et al. (2003). Improvement of micro-hole quality could be obtained by lower discharge energy (Allen and Lecheheb, 1996). Masuzawa (2000) pointed out that the key point for lower discharge energy was the minimization of the stray capacitance between the electrode and workpiece. Effects of polarity, electrode shape, and rotational speed of electrode in micro-hole EDM drilling of carbide were investigated by Yan et al. (1999) and the experimental results showed that positive polarity must be used in micro-hole EDM drilling to reduce tool wear and maintain hole accuracy. The effects of two electrode materials, copper and tungsten carbide, on micro-hole EDM drilling were studied by Her et al. (2001) and it was reported that the copper electrode could provide better surface roughness, lower electrode wear, but lower MRR than the tungsten carbide electrode.

Blind micro-hole EDM drilling is difficult because the debris concentrated at bottom is hard to completely flush away and can lead to excessive electrode wear. A new approach employing planetary movement to produce self-flushing for blind micro-hole EDM was presented by Yu et al. (2002). Recent research on micro-hole EDM showed that very high aspect ratio over 20 could be obtained (Kaminski and Capuano, 2003).

1.2.2. Development of micro EDM machines

Higher accuracy and miniaturization are always the goals for the development of micro EDM machines. In the past fifteen years the two goals are partially fulfilled with the introduction of piezo-driven actuators and precision DC motors.

A concept of impact drive mechanism, which utilized the inertial force and friction generated by the quick deformation of piezoceramics, was applied in the miniature EDM machine (Higuchi et al., 1991; Furutani et al., 1997). An electrical discharge device directly driven by piezoelectric elements was developed by Morita et al. (2000). The bandwidth of this device was 5 kHz and the micro-hole drilling capability ranged from 100 to 500 μm diameters. An inchworm type actuator was applied to a micro-hole EDM machine (Li et al., 2002), which was able to drill a 50 μm diameter micro-hole with aspect ratio 10.

Development and investigation of multi-axis micro EDM machines were reported. A 4-axis micro EDM machine using DC servo motors was developed by Zhao et al. (2004). A granite base was used to decrease the stray capacitance for lower discharge energy. A 25 μm diameter micro-hole with aspect ration over 10 was drilled on this machine. A 3-axis local actuator module for micro EDM was developed by Imai et al.

(2004). This module had 200 Hz bandwidth and utilized the electromagnetic force for the holding and positioning of the electrode. A 60 μm diameter micro-hole with aspect ratio over 16 was machined by this module.

1.2.3. Needs of advanced micro-hole EDM technology

Precision micro-holes with smaller diameter, larger depth and accurate geometry are required for next generation fuel injector spray holes due to requirements of stringent EPA standards on future diesel engine emissions. Advanced EDM drilling technology is needed for next generation injector spray holes. This goal can be achieved by developing advanced EDM process controllers and precision tool servos, e.g. piezoelectric stages, to reduce the EDM drilling cycle time and improve dimensional consistency of drilled micro-holes.

1.3. Process Monitoring of EDM

Process monitoring plays an important role in the EDM process. It provides the real time machining status, which can be analyzed for the optimization of EDM process parameters. By monitoring the EDM process, the pulse types can be classified and information regarding the EDM machining condition can then be acquired. There are two methods for the EDM pulse classification. The most common method is to monitor the variation of EDM pulse parameters, such as gap voltage and gap current. The other method is to analyze the of emitted radio frequency (RF) signals of EDM pulses.

Dauw et al. (1983) developed an algorithm using preset voltage and current threshold values to identify distinctive EDM pulses from the recorded pulse trains (Gangadhar et al., 1992). Pandit et al. (1987) presented a method based on the data dependent system to discriminate pulse types. Ignition delay time of an EDM pulse was used as a discriminator for the pulse identification (Weck and Dehmer, 1992).

Artificial intelligence has been applied in the classification of EDM pulses. The application of fuzzy set theory in EDM process monitoring was regarded as a reliable tool to discriminate EDM pulses (Ho and Newman, 2003). A fuzzy pulse discriminating system for the EDM process was developed by Tarng et al. (1997). Applications of neural networks and abductive networks on the recognition of EDM pulses were conducted by Kao and Tarng (1997) and Liu and Tarng (1997), respectively. To handle the transient non-stable signals generated from EDM process, wavelet transform was applied to filter noise and extract waveform features of gap voltage and current (Yu et al., 2001).

An EDM process monitoring system based on the RF signals was developed by Bhattacharyya et al. (1978; 1980). For the spark pulse, the RF emitted from the EDM region was higher than that of the arc pulse. As a result, the frequency level of RF signals was used to classify the EDM pulses.

EDM has slow material removal rate (MRR) and needs to be improved for better machining cycle time. This improvement is particularly important to micro-hole EDM because its MRR is further limited due to the narrower gap between electrode and workpiece, which makes debris flushing difficult. EDM process monitoring can further investigate effects of EDM parameters for better process stability and efficiency, through analyzing waveforms of gap voltage and current to characterize the stochastic generation of EDM discharges. This is the major advantage of EDM process monitoring and can thus contribute to higher MRR for more efficient EDM drilling.

1.4. EDM Process Controllers

The pulse generation in the EDM process is highly stochastic and complicated, which increases the difficulty of controller design and development. Several controllers have been investigated for the EDM process control for years and will be discussed in this section.

The proportional-integral-derivative (PID) controller is commonly used for EDM process control. The PID controller utilizes a predefined mathematical model to dynamically adjust the servo movement according to sensor feedback. The difficulty of using a mathematical model to precisely describe the EDM process renders the PID controller less competitive in preventing the undesired arc and short circuit pulses (Wang and Rajurkar, 1992; Rajurkar and Wang, 1997).

Pulse width modulation (PWM) is another commonly used EDM process control method. The PWM controller adjusts the servo position by varying the duty cycle of input voltage pulses. PWM controller, relying on the variation of pulse duty cycles, lacks the EDM condition feedback and operates with a severe non-linearity known as the deadband, which degrades the controller performance significantly (Ko and Good, 2005).

Research on advanced control strategy for micro-hole EDM is needed to develop more capable controllers for the nonlinear, stochastic EDM process. Competent EDM process controllers should be able to distinguish the rapid changing EDM status to generate correct servo commands for the minimization of undesired pulses and faster drilling cycle time. In this study, an advanced fuzzy logic controller for micro-hole EDM will be developed. Design and implementation of the fuzzy logic controller will be discussed in Chapters 3 and 4, respectively.

1.5. Form Measurement of Micro-Holes

The shape of diesel fuel injector spray holes is critical to the spray pattern and exhaust emissions. This section discusses the measurement methods and the desired negative taper for the new generation diesel fuel injector spray holes.

Micro-holes are difficult to characterize by optical microscopes and conventional coordinate measuring machines (CMM) due to the small diameter and high aspect ratio (Masuzawa et al., 1993). Common practice to study the spray hole shape uses either the destructive method (Diver et al., 2004) to cut a cross-section of the hole or the plastic molding to make a replica of spray holes (Hebbar, 1992). Both methods provide limited information of the shape and dimension of spray holes.

New technologies were developed since the 90s to enable the shape measurement of spray holes. A new technology called the vibroscanning method was developed by Masuzawa et al. (1993). This method utilized the vibration of a very thin conductive probe to detect and derive the distance between the probe and the hole surface. The measured hole profile was obtained by successive detections along the hole depth. Advanced studies on the vibroscanning method were conducted by Masuzawa et al. (1997), Kim et al. (1998), Kim et al. (1999), Yamamoto et al. (2000), Pourciel et al. (2001), Lebrasseur et al. (2002), and Pourciel et al. (2003).

A multi-sensor measurement technology, which combined the contact (tactile) and non-contact (optical) sensors into an integrated CMM, was developed by Werth GmbH (Christoph, 2004). The Werth multi-sensor CMM was used in this study for the form measurement of micro-holes and gage repeatability and reliability (R&R) study. The working principles, measurement procedures, as well as the gage R&R study using the Werth CMM are discussed in Appendix A.

A multi-stage EDM drilling method for negative tapered injector spray holes was proposed in this research. A brief introduction of the multi-stage EDM drilling and its preliminary results using the Werth CMM are discussed in Appendix B.

The reduced size of next generation injector spray holes highlights the importance of new CMM technology and necessitates the needs for more complete and precise form measurement of micro-holes. Advanced research on non-conventional CMMs, such as the Werth CMM, is needed to fully measure the dimension, as well as characterize the geometry, of micro-holes. This is especially advantageous for negative tapered spray holes because conventional CMMs are unable to measure the inner, tapered portion. The gage R&R study can provide gage capability tolerance specifications, which are particularly beneficial for product design and metrology engineers.

1.6. Concluding Remarks

The research backgrounds, motivations, and goals are discussed in Sec. 1.1. An overview of micro-hole drilling is presented in Sec. 1.2. EDM process monitoring technology is reviewed in Sec. 1.3. Common EDM process controllers are discussed in Sec. 1.4. Form measurement of micro-holes, including the multi-stage EDM drilling technique, are introduced in Sec. 1.5.

This research has three major parts. Chapter 2 introduces the EDM process monitoring, analyzes EDM pulses at the sub-nanosecond (sub-ns) level, and establishes a foundation for the theoretical modeling of discharge ringing phenomenon. Chapter 3 presents the design and development of the adaptive fuzzy logic controller for micro-hole EDM. Chapter 4 discusses the implementation and validation of the adaptive fuzzy logic controller under two test platforms. Conclusion s and future work are summarized in Chapter 5.

Form measurement of micro-holes, multi-stage EDM drilling, and the ringing model are presented in Appendices A, B, and C, respectively.

CHAPTER 2

SUB-NANOSECOND MONITORING OF MICRO-HOLE EDM PULSES

Monitoring the gap voltage and current in micro-hole EDM using high speed data acquisition with 0.5 ns sampling period is conducted. The spark and arc pulses at three stages, namely electrode dressing, drilling, and penetration, of the micro-hole EDM are recorded. The EDM process parameters are setup to use negative polarity to blunt the electrode tip and positive polarity for micro-hole drilling and penetration. A new phenomenon of pre-discharging current is discovered. In the first 20 to 30 ns of spark and arc pulses, the current starts to rise while the voltage remains the same. Effects of EDM process parameters, including the open voltage, electrode diameter, and polarity, on the rate of spark and arc pulses and electrode feed rate are investigated. The monitoring technique developed in this research can assist in the selection and optimization of micro-hole EDM process parameters.

2.1. Background of Micro-Hole EDM Monitoring

Monitoring of EDM pulses using high speed data acquisition is an essential part of the EDM process control and optimization. The voltage and current across the gap between the electrode and workpiece greatly influence the MRR in micro-hole EDM. To enable efficient MRR in micro-hole EDM, very short (less than 1 μs) pulse duration and high (above 200 V) open circuit voltage, as compared with conventional wire and die-sinking EDM, are typically utilized. The high pulse rate in micro-hole EDM requires a high speed data acquisition system to record the rapid change of gap voltage and current. In this study, an oscilloscope with 2 GHz sampling rate (0.5 ns sampling period) is utilized for EDM process monitoring.

The efficiency and quality of EDM drilling can be improved with the rotation of electrodes (Yan et al., 1999; Soni and Chakraverti, 1994; Mohan et al., 2004). But for micro-hole EDM for fuel injector spray holes, to achieve the required hole dimensional and form accuracy and the stringent flow rate specification, the rotation of the thin, 100 to 150 μm diameter, electrode is not desirable. Because the electrode extends 2 to 3 mm from the wire guide, the rotation of electrode will introduce excessive error motion at the electrode tip and cause inconsistency in the micro-hole EDM drilling for diesel engine spray hole applications. Stationary electrode without rotation is investigated in this study.

At the end of discharging, due to the parasitic inductance and inherent capacitance of the EDM circuit, the voltage does not immediately reduce to the steady-state value. This has been recognized as the so-called ringing effect (Kuo et al., 2002), as illustrated in Figure 2.1. The ringing effect is an unavoidable phenomenon in EDM. For micro-hole EDM, the ringing effect is significant. The voltage oscillates for a long period of time after the discharging and slowly reduces to a steady-state value. Shortening the time duration of ringing could lead to more frequent EDM pulses and higher MRR. To better understand the ringing effect, a model of the EDM circuit at the discharge stage is necessary. The *RC* circuit (Takahata and Gianchandani, 2002; Wong et al., 2003) and field effect transistor (FET) circuit (Han et al., 2004) have been proposed to model the EDM discharging. However, these models are not applicable to studying the ringing effect. A new model based on an expanded serial *RLC* circuit in a linear rail gun proposed by Kuo et al. (2002) is developed. In this study, a model based on a *RLC* circuit including the inductance effect of the wire electrode and voltage probe jumper cable, was proposed. The derivation and calculation of the ringing model is in Appendix C.

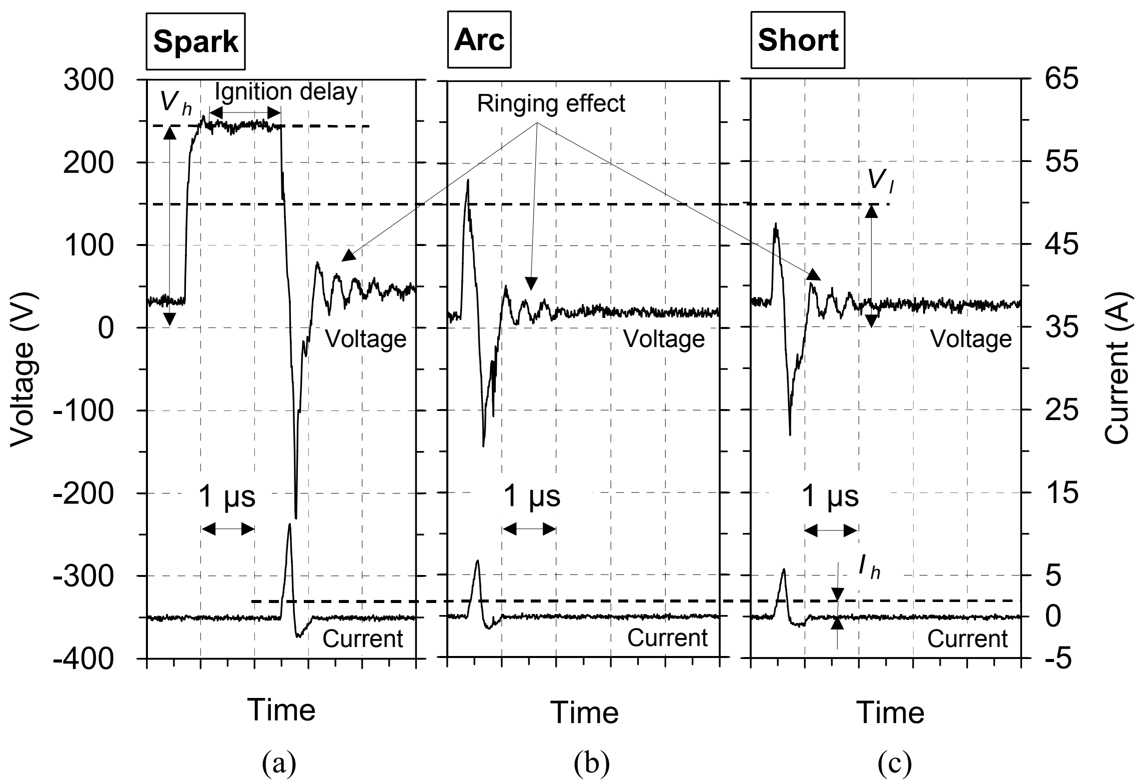

Figure 2.1. Characterization of EDM pulses: (a) spark, (b) arc, and (c) short.

Another phenomenon in micro-hole EDM is the current flowing in the opposite direction near the end of EDM pulse. The parasitic components induce a reverse current (Hebbar, 1992), which can lead to inferior surface roughness and excessive electrode wear (Her and Weng, 2001; Yan et al., 1999). The reverse current is also observed in both spark and arc pulses during this micro-hole EDM study.

In this study, the experimental setup and monitoring procedures are introduced in Sec. 2.2. Characterization of spark, arc, and short pulses in three stages during micro-EDM is discussed in Sec. 2.3. The pulse rate and electrode feed rate are investigated in Sec. 2.4.

2.2. Experimental Setup and Monitoring Procedures

2.2.1. Micro-hole EDM machine

Experiments were conducted in a micro-hole EDM machine, Ann Arbor Machine Model 1S15. Tungsten wire electrodes with 100, 125, and 225 μm diameter were used to drill micro-holes. The spark, arc, and short pulses were recorded. The work-material was through-hardened AISI 52100 steel. Deionized water was the dielectric fluid supplied by controlled dripping into the EDM region.

2.2.2. Data acquisition and classification of EDM pulses

An Agilent Infiniium 54833A digital oscilloscope with 2 GHz sampling rate was used for real time acquisition of the gap voltage and current during micro-hole EDM. This dual-channel oscilloscope was equipped with an Agilent 10076A 250 MHz 100:1

high voltage probe and an Agilent 1147A 50 MHz AC/DC current probe.

The highest sampling rate (2 GHz) was utilized to observe details of the rapidly changing voltage and current of spark, arc, and short pulses in micro-hole EDM. At a reduced sampling rate of 10 MHz, pulse trains of 3 ms (30,000 data points) were recorded every 4 s throughout the micro-hole drilling to study the rate of spark, arc, and short pulses. At least seven sets of 3 ms data were recorded for each micro-hole. Each data set was analyzed to identify and compare the rate of pulses under different EDM setups.

Algorithms developed by Dauw et al. (1983) were applied to classify measured voltage and current behavior as either spark, short, or arc pulses based on preset voltage and current threshold values. Although more advanced EDM pulse classification methods such as the data dependent system (Pandit and Mueller, 1987), artificial intelligence (Ho and Newman, 2003; Tarng, Y.S. et al., 1997; Kao and Tarng, 1997; Liu and Tarng, 1997), and wavelet transform (Yu et al., 2001) are available, the simple method based on Dauw et al. (1983) is efficient and adequate. The spark, arc, and short pulses are identified in EDM pulse trains based on the high and low threshold voltages, V_h and V_l, respectively, and the threshold current I_h, as shown in Figure 2.1. A spark has a long ignition delay, which is marked in Figure 2.1, and the voltage is above V_h before discharging. An arc has no ignition delay because the deionization from the previous pulse is not complete and the remnant plasma channel has a residual conductivity that provides a passage for electric current to flow through (Hebbar, 1992). The peak voltage in an arc is between V_h and V_l. For a short pulse, the contact between the electrode and workpiece causes a high current peak above I_h, and the gap voltage is below V_l. A Matlab program was developed to process the data and automatically count and identify each EDM pulse. The rate of EDM pulses can also be calculated.

2.2.3. Input parameters and stages in micro-hole EDM

Five input or setup parameters are varied in the micro-hole EDM experiments.

- Polarity: Polarity is the pole designation of the workpiece and electrode. Positive polarity sets the workpiece as the anode and the electrode as the cathode, and vice versa for negative polarity. The choice of polarity can greatly affect the wear of wire electrodes. Electrode wear is expected to be high under negative polarity (Her and Weng, 2001). This property is used to blunt the tip of the electrode, a procedure known as electrode dressing. During drilling, to reduce the electrode wear, positive polarity was used.
- Drilling depth: The drilling depth is the travel of the wire electrode from the initial contact with the workpiece. The drilling depth is controlled by the servo motor and affected by the electrode wear.
- Open circuit voltage, V_o: This is the system voltage when the EDM circuit is in the open state and energy has been built up for discharging. An example of an open circuit voltage of 210 V is shown in Figure 2.2.
- Pulse duration time, T_D: As shown in Figure 2.2, T_D is the time duration of the positive discharging current in a single EDM pulse. The measured value of T_D is usually longer than the input value because of the time required for the current to rise and fall during discharging. The input value for T_D of the spark in Figure 2.2 was 0.1

μs. The actual value was about 0.3 μs.

- Pulse off time, T_{off}: This is the time from the end of one EDM pulse to the beginning of the next pulse, as shown in Figure 2.2. During the pulse off time, the pulse generator is in the off state and the current is zero.

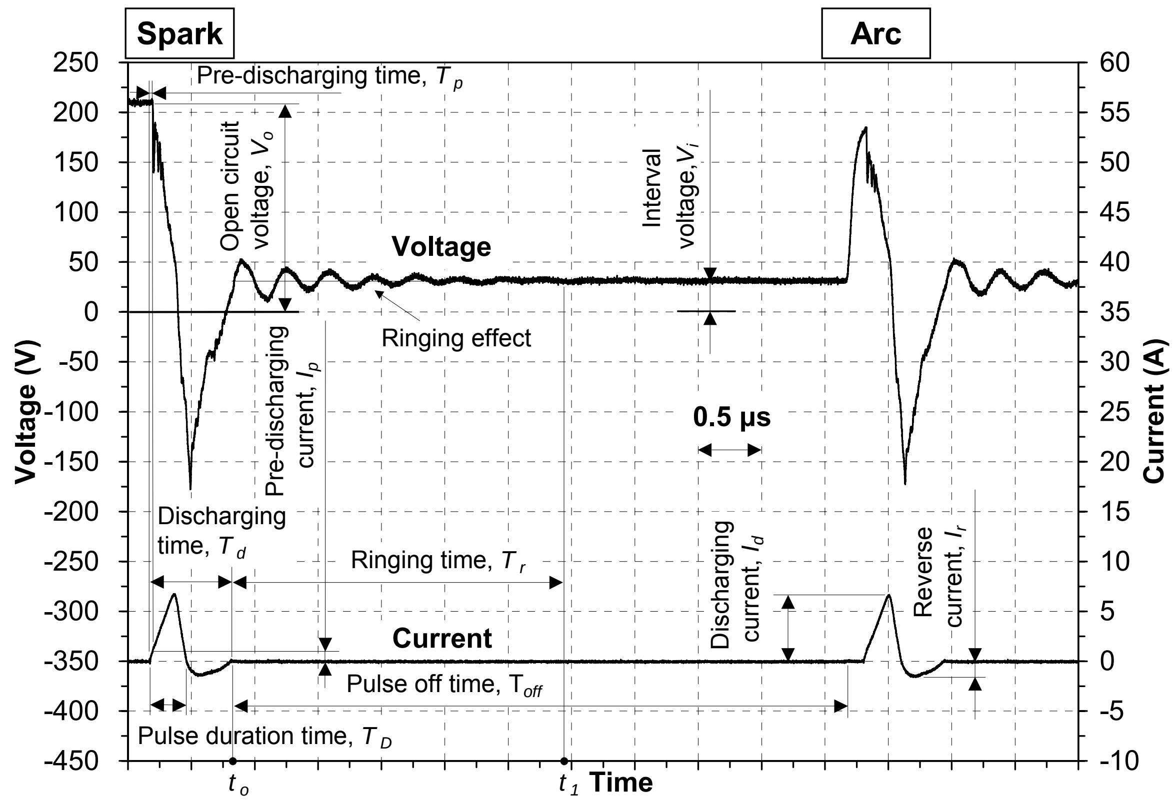

Figure 2.2. EDM process input and output parameters of sample spark and arc pulses.

The EDM process used to drill a micro-hole suitable for a diesel engine injector is composed of three stages: electrode dressing, drilling, and penetration. Each stage, controlled by the drilling depth (without considering electrode wear) has its purpose. The settings of EDM parameters for all three stages are summarized in Table 2.1.

Table 2.1. Input parameters of micro-hole EDM.

Stage	1	2	3
Function	Electrode dressing	Drilling	Penetration
Open circuit voltage, V_o (V)	170	210	240
Level of pulse energy	Low	Medium	High
Polarity	Negative	Positive	Positive
Drilling depth (mm)	0.10	0.76	1.20
Electrode travel relative to the hole depth (%)	11	73	16

- Stage 1. Electrode dressing: The tip of the tungsten wire electrode is sharpened during this micro-hole EDM process. Figure 2.3(a) shows an example of the sharpened electrode tip after completing EDM drilling of a 0.9 mm deep hole. The electrode dressing stage is implemented at the beginning of contact between the electrode and workpiece by using negative polarity to increase the electrode wear and blunt the tip. This has been proven to be important to maintaining the consistency of the micro-hole diameter in practical applications. The open circuit voltage V_o in Stage 1 is low (170 V), compared to other two stages. A low V_o can reduce debris size under negative polarity. The electrode travel in Stage 1 is short, only 0.1 mm. Figure 2.3(b) shows the shape of an electrode tip after Stage 1. The electrode tip is blunted and covered by a thin recast layer.

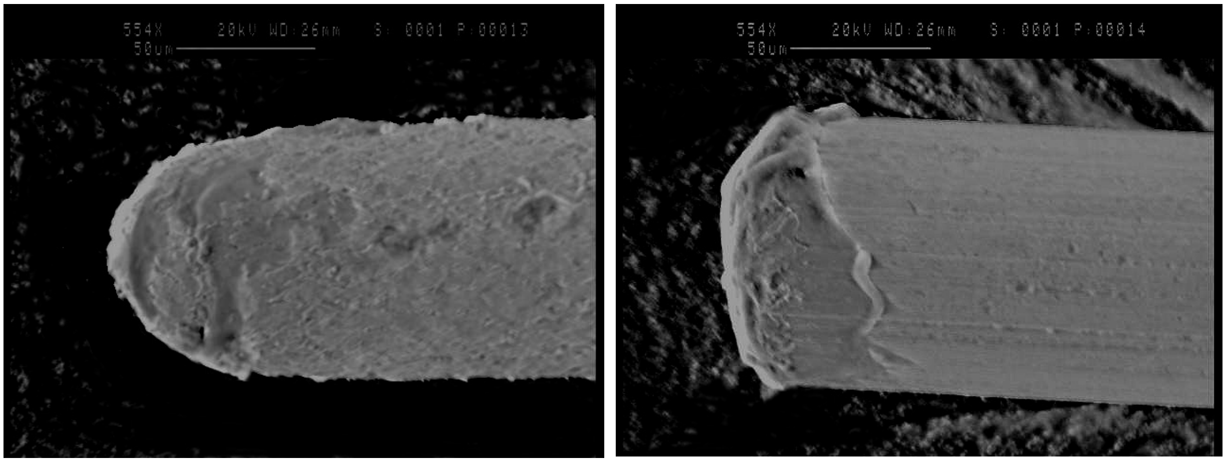

(a) (b)

Figure 2.3. SEM micrographs of the tip of tungsten wire electrode: (a) sharpened electrode tip after EDM Stage 3 and (b) dressed electrode tip after EDM Stage 1 (diameter of wire electrode: 125 μm).

- Stage 2. Drilling: Positive polarity and medium V_o (210 V) were applied in Stage 2 to increase the drilling speed while maintaining reasonable debris size for efficient flushing. This stage accounts for 0.66 mm or 73% of the electrode travel relative to the hole depth.
- Stage 3, Penetration: As shown in Figure 2.4(a), at the time when the sharp electrode tip penetrates the other face of the workpiece, the electrode still needs to move forward by a set distance, called the over-travel, to maintain a consistent diameter inside the hole. From the diesel engine emissions perspective, a larger hole diameter in the final penetration stage, as shown in Figure 2.4(b), is preferred. This is achieved by using a high V_o (240 V) and positive polarity, which increases the gap distance and rounds the fuel inlet edge in the micro-hole.

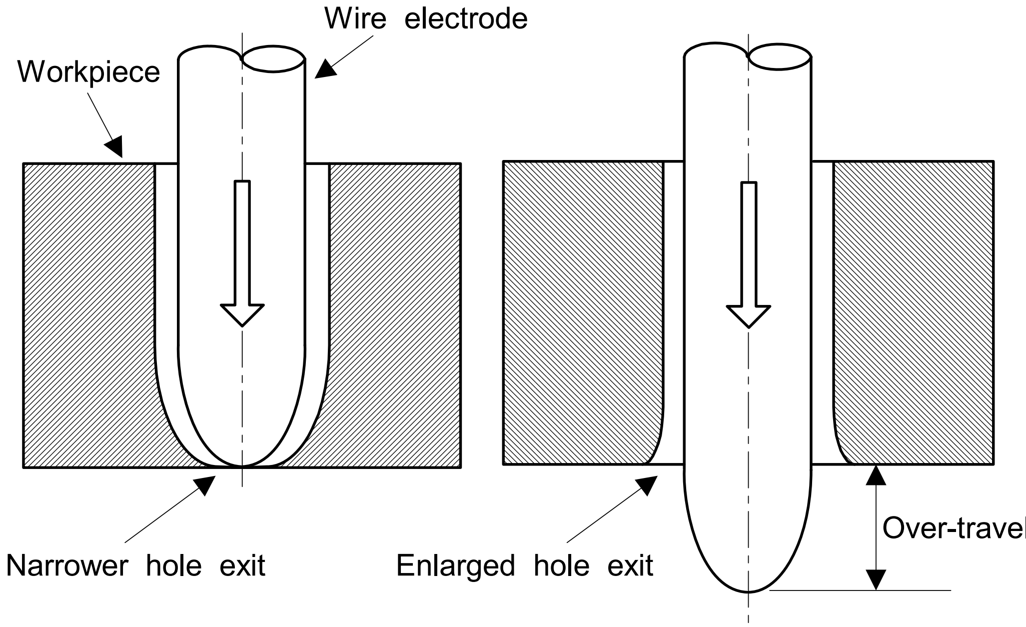

(a) (b)

Figure 2.4. The effect of EDM Stage 3 Penetration: (a) worn tip of wire electrode causes a narrower hole exit and (b) enlarged hole exit is generated due to the over-travel of wire electrode.

The T_D and T_{off} were set at 0.1 and 5 μs, respectively, for all three stages.

The depth of hole was 0.9 mm. The setup for Stage 1 was used for the first 0.1 mm of electrode travel after the initial contact with the workpiece. Due to electrode wear, the actual depth of the hole drilled in Stage 1 was shorter than 0.1 mm. At 0.1 and 0.76 mm drilling depth (D), the EDM setup was changed to Stage 2 and Stage 3, respectively. The EDM process stopped at 1.2 mm drilling depth, which had 0.3 mm of over-travel.

2.2.4. EDM output parameters

Seven EDM output parameters were measured for monitoring of EDM pulses.

All seven parameters are marked in Figure 2.2.

- Discharging current, I_d: This is the peak positive current during discharging.
- Reverse current, I_r: This is the peak negative current during discharging. The reverse current, which has been reported by Hebbar (1992), flows opposite to the discharging current due to the parasitic capacitance of the system (Takahata and Gianchandani, 2002; Kuo et al., 2002).
- Pre-discharging current, I_p: Using the 2 GHz sampling rate, a unique phenomenon was discovered in this study. The current starts to increase before the drop of voltage in discharging. The peak current before the voltage drop is defined as the pre-discharging current.
- Pre-discharging time, T_p: The time duration from the increase of current to the voltage drop in the beginning of discharging is defined as the pre-discharging time, T_p.
- Discharging time, T_d: This is the time duration that the discharging current, both positive and negative, exists.
- Interval voltage, V_i: This is the steady-state voltage after the ringing dissipates. The interval voltage is not constant for all pulses in an EDM pulse train. The value depends on the gap conditions, such as purity of dieletric fluid and concentration of debris.
- Ringing time, T_r: Analogous to the definition of settling time in the transient response analysis of dynamic systems (Ogata, 2004), the ringing time is defined as the time duration from t_o, the instance when the negative current increases to zero, to t_1, when the voltage oscillation reaches and stays within the range of the 5% of the

interval voltage V_i. Both t_0 and t_1 are marked in Figure 2.2.

2.3. Spark and Arc EDM Pulses

Using a 0.5 ns sampling interval, the representative spark and arc of Stages 2, 1, and 3 are presented in Figs. 7, 9, and 10, respectively. Six successive periods, denoted as Period I to VI, are identified in each sample spark and arc pulse.

- Period I: The voltage rises and stays at a specified open circuit voltage V_o while the current remains zero. In Period I, the wire electrode is gradually approaching the workpiece.
- Period II: The current rises and voltage remains the same in this period. The pre-discharging current I_p occurs at the end of Period II. The time duration of Period II is the pre-discharging time T_p. In Period II, the parasitic capacitance (Takahata and Gianchandani, 2002), which is inherent in the EDM circuit, begins to be charged.
- Period III: The voltage drops from the open circuit voltage V_o to zero in this period. In the beginning of Period III, a very rapid voltage drop occurs. The rate of voltage drop will be analyzed in Section 3.1. A high frequency voltage oscillation due to the fast change of the gap impedance (Bhattacharyya and El-Menshawy, 1978) occurs following the rapid voltage drop. The current typically rises to a peak value in Period III.
- Period IV: Period IV begins at the zero voltage and ends when the current reaches zero. The voltage becomes negative in this period.
- Period V: This is the period with the negative reverse current and its peak value I_r

occur.

- Period VI: This is the ringing period.

2.3.1. Spark and arc pulses in Stage 2 (Drilling)

A spark pulse from Stage 2, as is illustrated in Figure 2.5(a), is more representative and, hence, discussed first. In Period I, the open circuit voltage V_o is 210 V and the current is zero. The pre-discharging time T_p is 30 ns and the pre-discharging current I_p is 1.1 A in Period II. A close-up view of the voltage drop, as marked by box A in Figure 2.5(a), is shown in detail in Figure 2.6(a). The rate of voltage drop is –37.6 V/ns. In Period III, the discharging current I_d is 6.3 A and the time duration is 230 ns. In Period V, the reverse current I_r reaches –1.2 A. The discharging time T_d, which is the time duration from Period II to Period V, is 652 ns. The interval voltage V_i is estimated to be 28 V in Period VI.

An arc pulse from Stage 2 is shown in Figure 2.5(b). In Period I, the voltage gradually rises but does not stay at the V_o before the discharging. In Period II, the duration T_p is 23 ns and I_p is 1.2 A. In Period III, the rapid voltage drop begins at 172 V, which is 38 V lower than the V_o. The close-up view of the voltage drop, as marked by box B in Figure 2.5(b), is shown in Figure 2.6(b). The rate of voltage drop is –14.7 V/ns, which is lower than that in the spark pulse. Hebbar (1992) has proposed to use the rate of voltage drop at discharge to differentiate between the spark and arc pulses. In Period III, the amplitude of the high frequency voltage oscillation can also be seen. The current I_d is 6.5 A in Period III. The duration of Period IV is 69 ns. In Period V, the I_r is –1.5 A and the duration is 344 ns. The T_d is 690 ns, about 6% longer than that of the spark pulse.

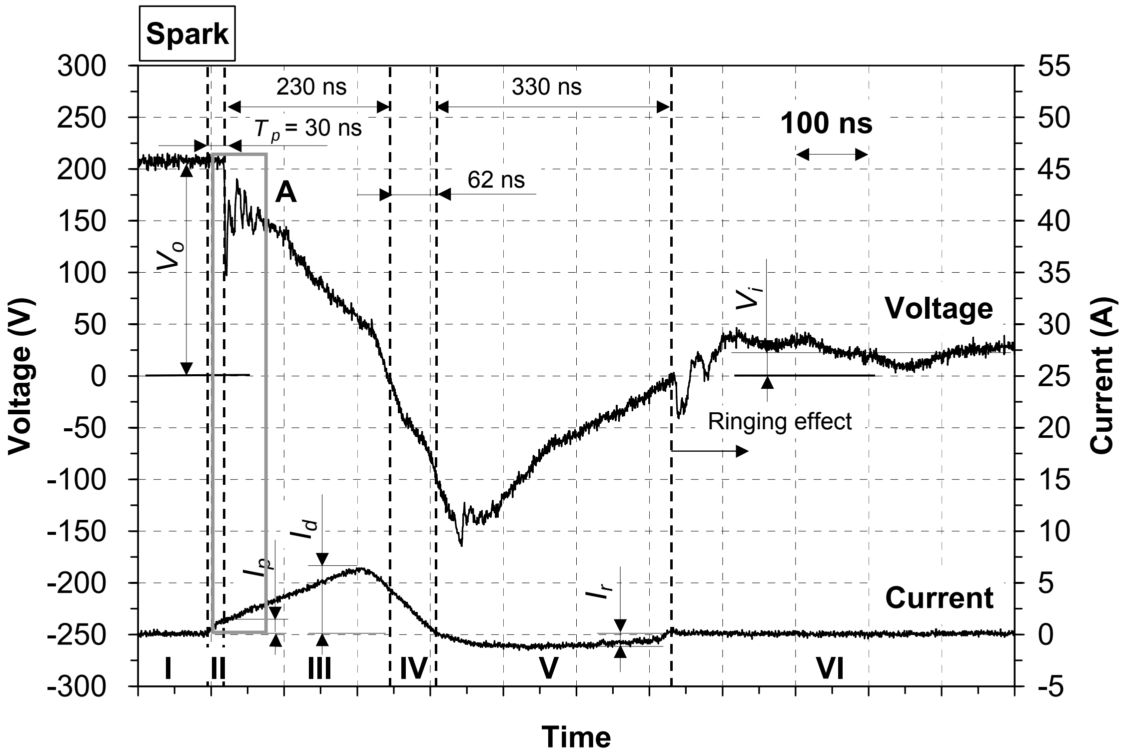

(a)

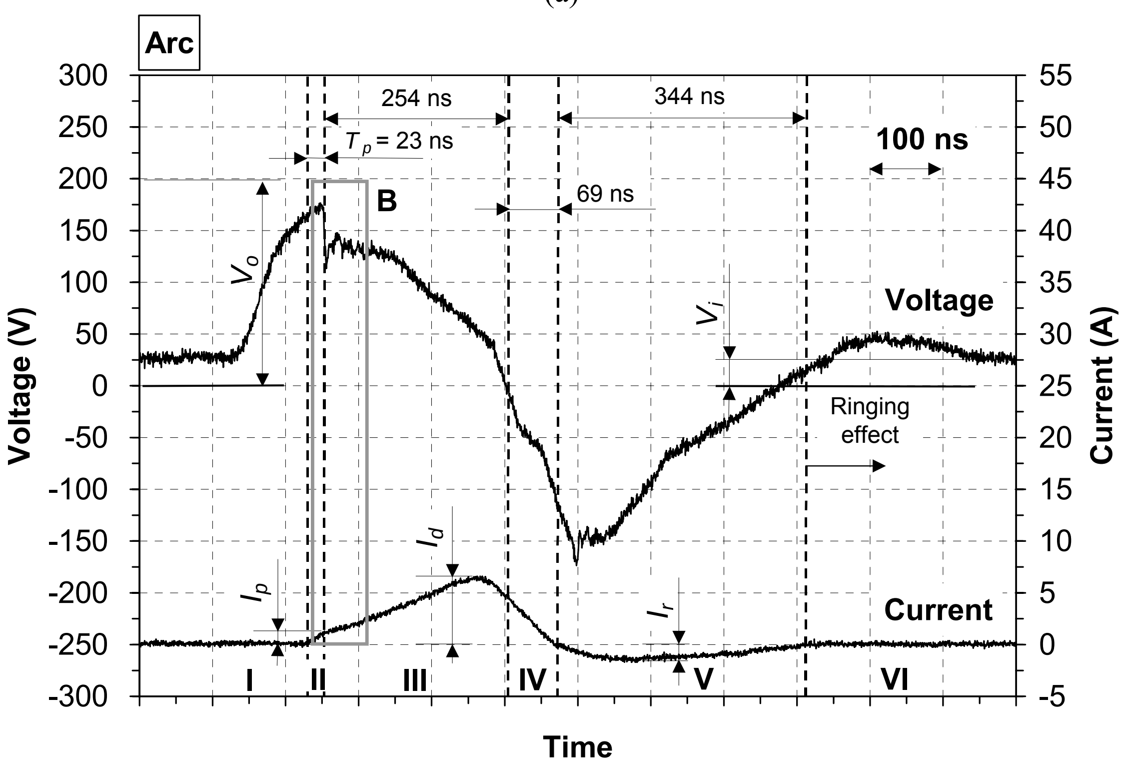

(b)

Figure 2.5. Sample EDM pulses in Stage 2: (a) spark and (b) arc (125 µm diameter wire electrode)

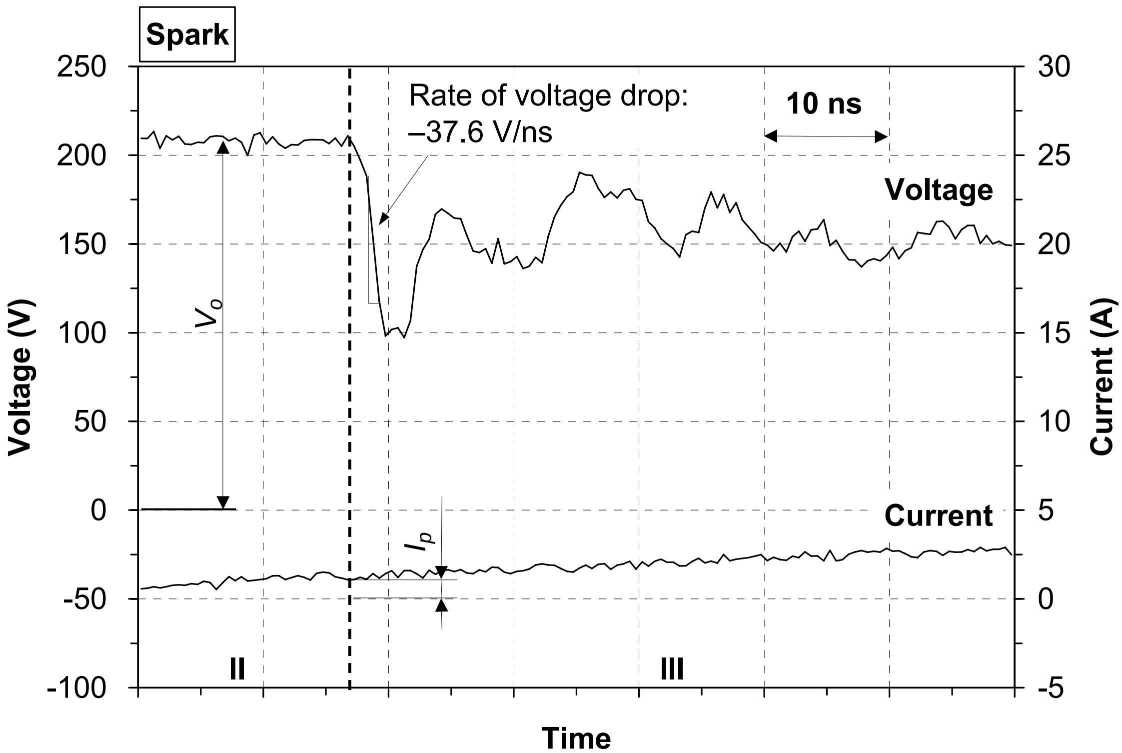

(a)

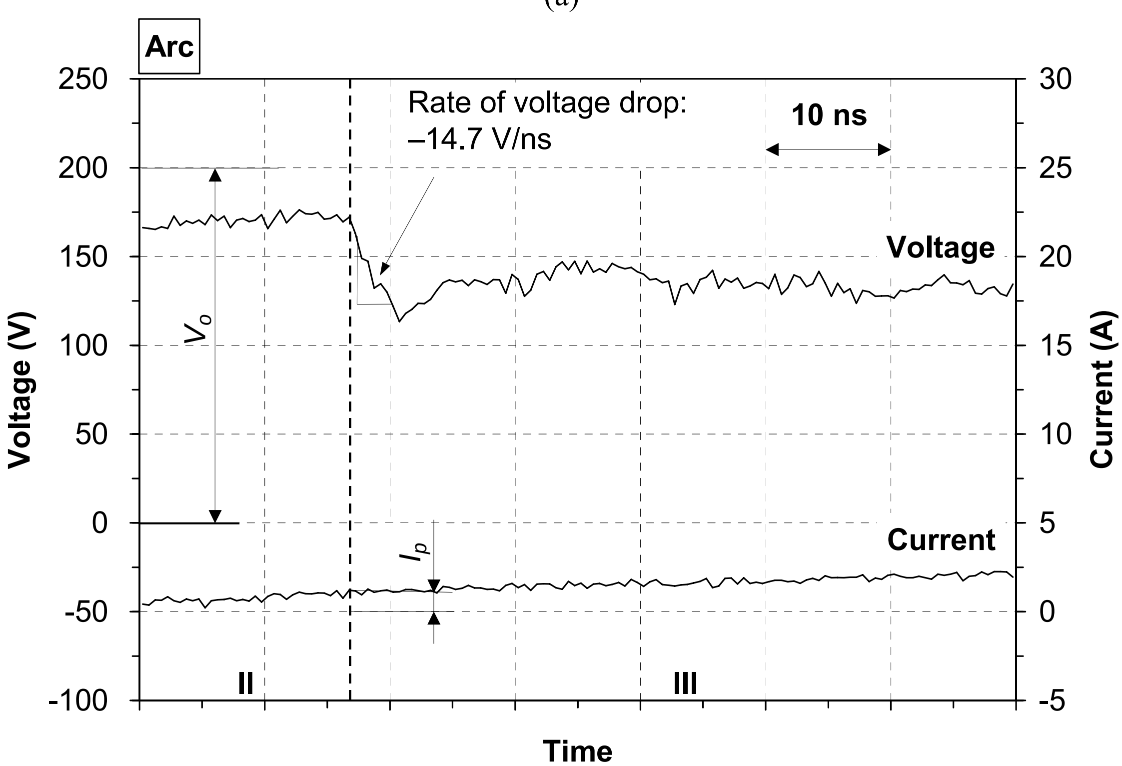

(b)

Figure 2.6. Close-up view for Periods II and III of sample EDM pulses in Stage 2: (a) box A and (b) box B.

The interval voltage V_i is estimated as 25 V in Period VI. In general, the duration of pre-discharging, the voltage at discharge, and the rate of voltage drop at the beginning of discharging are all lower in an arc than those in a spark.

2.3.2. Spark and arc pulses in Stage 3 (Penetration)

A spark pulse in Stage 3 is shown in Figure 2.7(a). In Period I, the open circuit voltage V_o is 240 V, and the current is zero. In Period II, the pre-discharging time T_p is 25 ns and pre-discharging current I_p is 1.6 A. In Period III, the voltage drops quickly, at a rate of –51.7 V/ns. The discharging current I_d is high, 7.6 A. In Period V, the reverse current I_r is –1.6 A, also higher than that of the spark in Stage 2. The discharging time T_d is 646 ns, about the same as that of a spark in Stage 1. In Period VI, the interval voltage V_i is 43 V, higher than that of the spark in Stage 2.

An arc pulse in Stage 3 is shown in Figure 2.7(b). A gradual voltage increase occurs in Periods I and II. The peak voltage is 220 V, 20 V lower than the specified V_o, at the end of Period II when the voltage starts to drop. In Period II, the T_p = 28 ns and I_p = 1.4 A. The rate of voltage drop is –20.9 V/ns, which is lower than that in spark in Stages 2 and 3. In Period III, the I_d is high, 7.9 A. The I_r in Period V is –1.7 A. The T_d is 668 ns, slightly longer than that of the spark pulse in Stage 3. The interval voltage V_i was estimated as 35 V in Period VI.

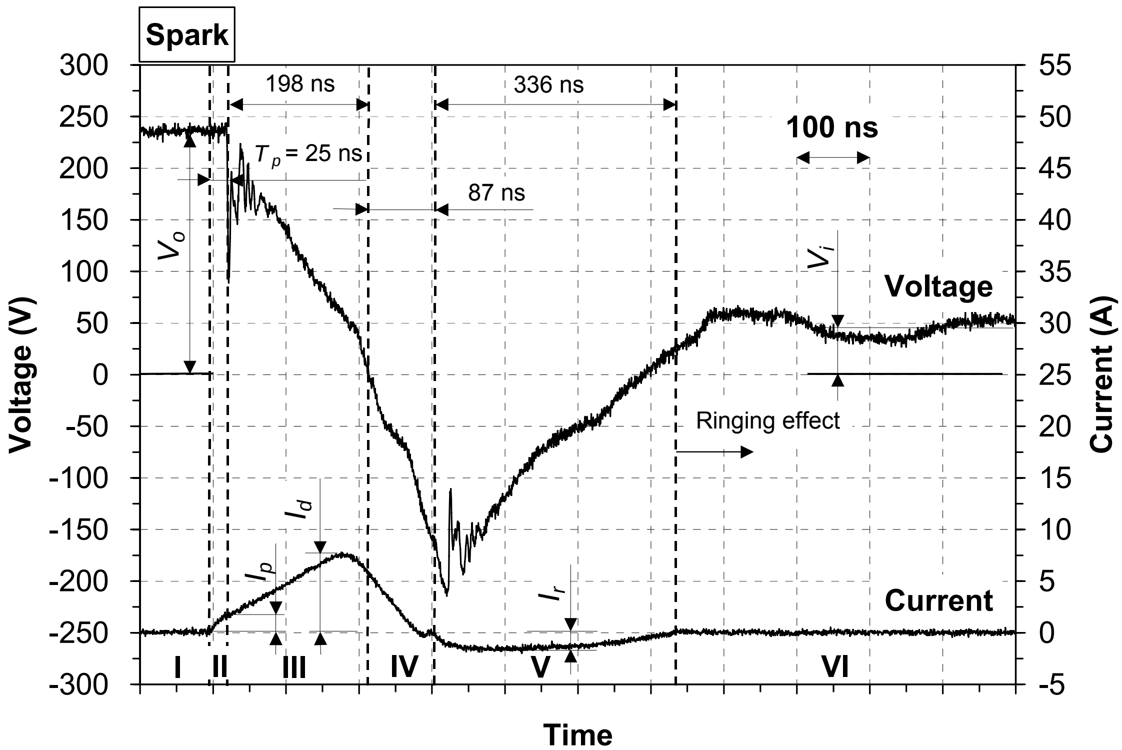

(a)

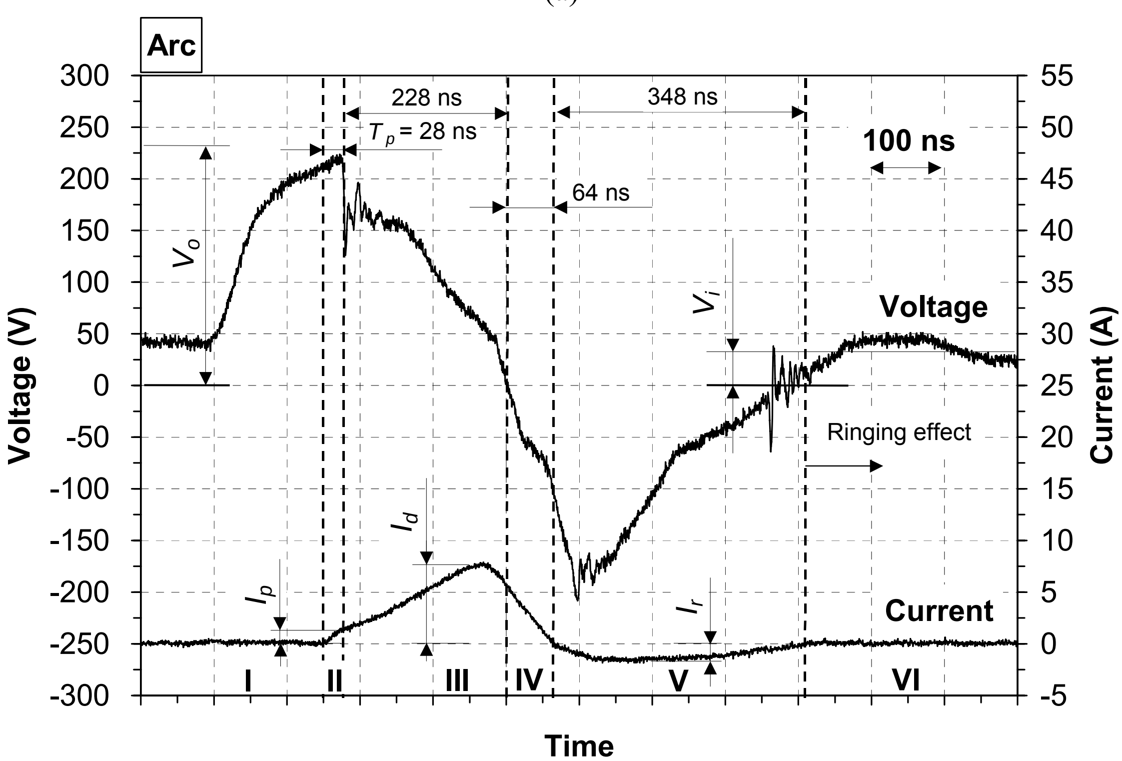

(b)

Figure 2.7. Sample EDM pulses in Stage 3: (a) spark and (b) arc (125 µm diameter wire electrode).

2.3.3. Spark and arc pulses in Stage 1 (Electrode Dressing)

The negative polarity setup changes the shape of the waveform for both spark and arc pulses in Stage 1. A spark pulse is shown in Figure 2.8(a). To make the shape consistent for the comparison, the measured signal was multiplied by –1. The voltage V_o is low, 170 V. The output parameters in Periods II and III are about the same as the spark in Stages 1 and 3: T_p = 30 ns, I_p = 1.1 A, I_d = 8.3 A, and rate of voltage drop is –20.5 V/ns.

The most significant impact of negative polarity occurs after the voltage drops below zero. Instead of continuing to reduce to –150 V in Stage 2 (Figure 2.5) or –200 V in Stage 3 (Figure 2.7), the voltage reduces to only –70 V, marked by circle C in Figure 2.8(a), and starts to increase. The gradually increasing voltage results in a lower rate of current drop and elongates the time duration of Period IV, from less than 90 ns under positive polarity to 240 ns using the negative polarity. The effect of a polarity change on electrode wear has been studied (Her and Weng, 2001). The small debris generated is likely to be negatively charged and accelerate to impact and neutralize the positive charged tungsten electrode. This reduces the level of voltage below zero. The reverse current I_r is –1.7 A in Period V. The discharging time T_d is long, 1372 ns, more than twice of that in Stages 2 and 3. In Period VI, the interval voltage V_i is very low, only 8 V.

An arc pulse in Stage 1 is shown in Figure 2.8(b). Two peaks of current are recognized. The voltage rises to about 70 V in the end of Period II. Both I_p (0.2 A) and T_p (16 ns) are very small. Although the initial voltage drop in Period III was slow, only –0.6 V/ns, the voltage drops quickly to zero. Period III is also short, only 125 ns. The peak current does not happen in Period III as in other arc and spark pulses in Stages 2 and 3. In Period IV, the current reaches its first peak (2.0 A), marked as I_{d1}, as the voltage continues to drop. After the first peak in current, the voltage rises to 50 V in 120 ns and starts another discharge. The magnitude of second discharging current, denoted I_{d2}, is also about 2.0 A. The period of reverse current, Period V, still exists and I_r (–0.8 A) is very small. The time duration for an arc pulse with two discharges (T_d) is 1383 ns, about the same as that of the spark pulse in Stage I. In Period VI, the V_i is low, about 10 V.

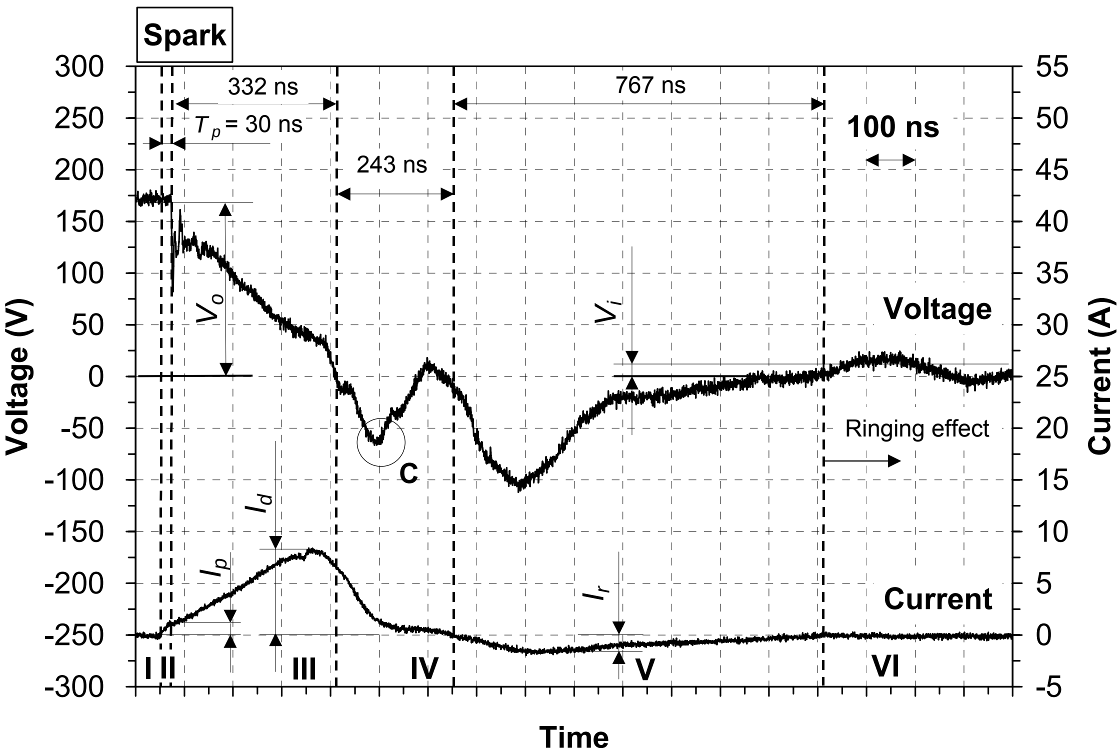

(a)

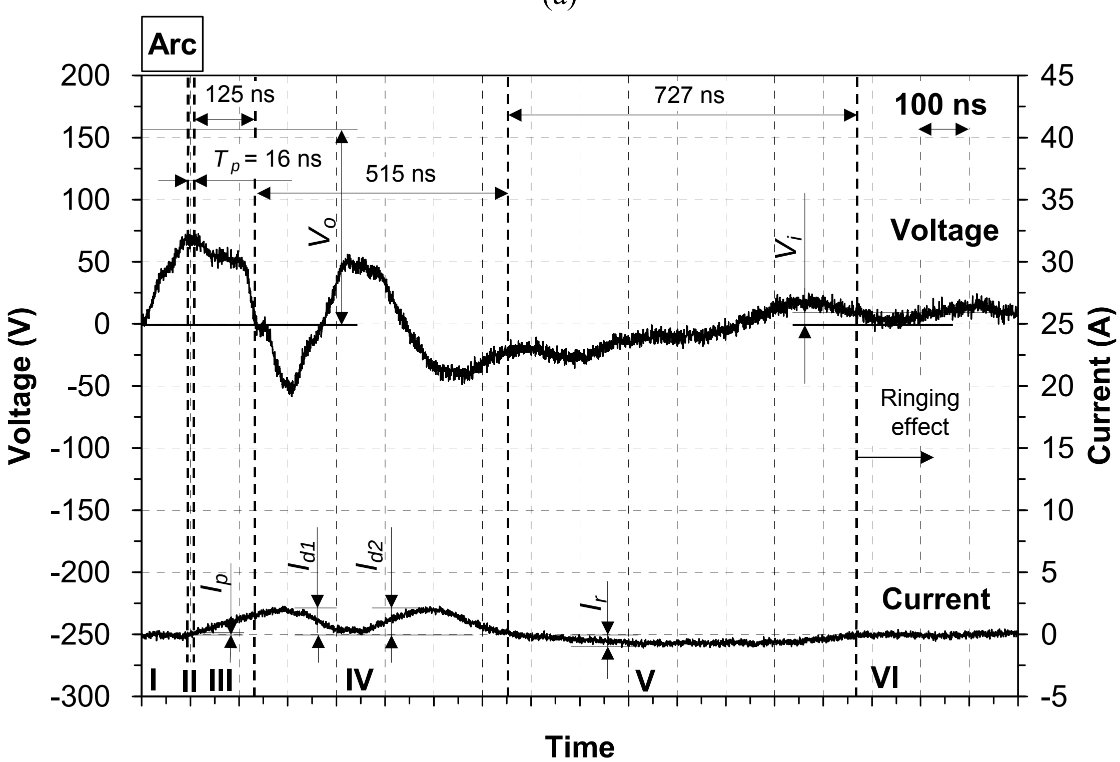

(b)

Figure 2.8. Sample EDM pulses in Stage 1: (a) spark and (b) arc (125 µm diameter wire electrode).

2.4. Pulse Rate and Electrode Feed Rate

The rate of spark, arc, and short pulses in Stages 1, 2, and 3 for 125 and 225 μm diameter wire electrodes are analyzed and the results are shown in Figure 2.9.

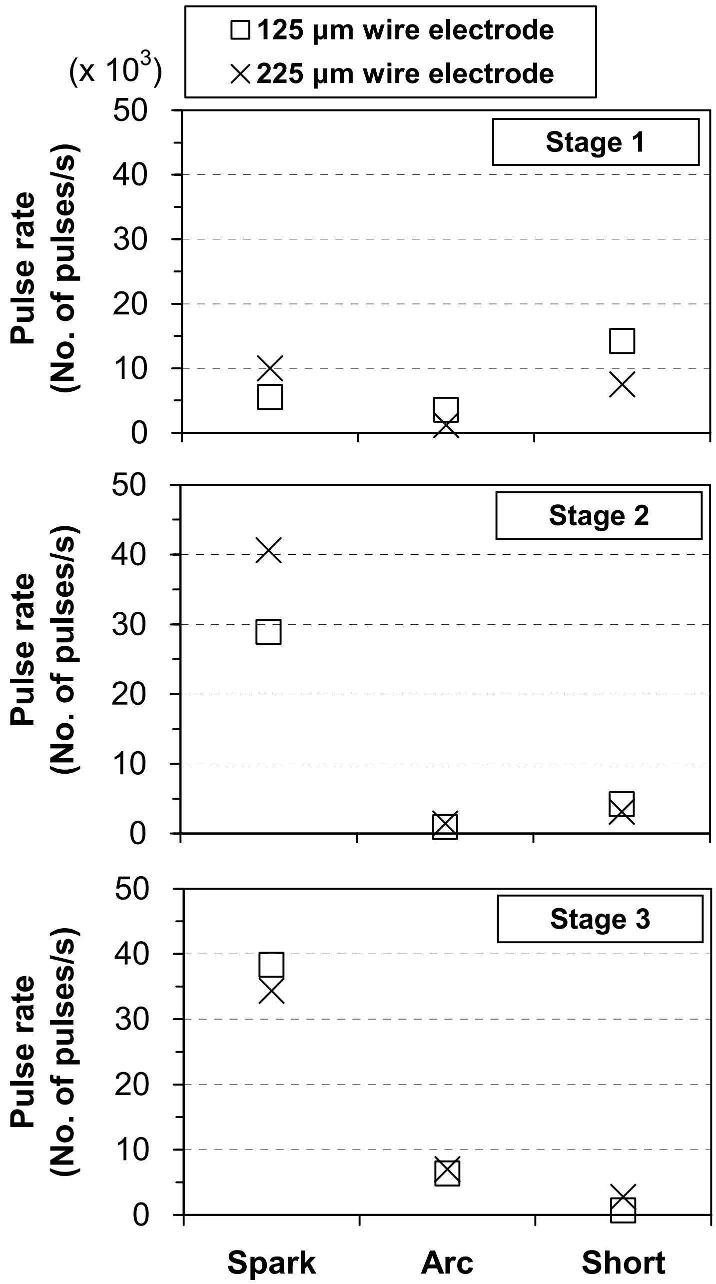

Figure 2.9. Rate of spark, arc, and short pulses for 125 and 225 μm wire electrodes in three EDM stages.

In Stage 1, due to the negative polarity setting used to increase electrode wear, high short pulse rate and low spark pulse rate are observed. The lack of spark pulses and frequent short pulses affect the efficiency of removing the work-material. The electrode feed rate is the slowest in Stage 1, as shown in Figure 2.10. The diameter of electrode wire has an effect on the feed rate. Although the 225 μm electrode has more frequent spark pulses and less frequent short pulses than that of the 125 μm electrode, as shown in Figure 2.10, the electrode feed rate is slightly faster for the 125 μm electrode. This is due to the fact that less volume of work-material is removed by the 125 μm electrode during EDM. Debris flushing was not a problem for 125 μm electrode.

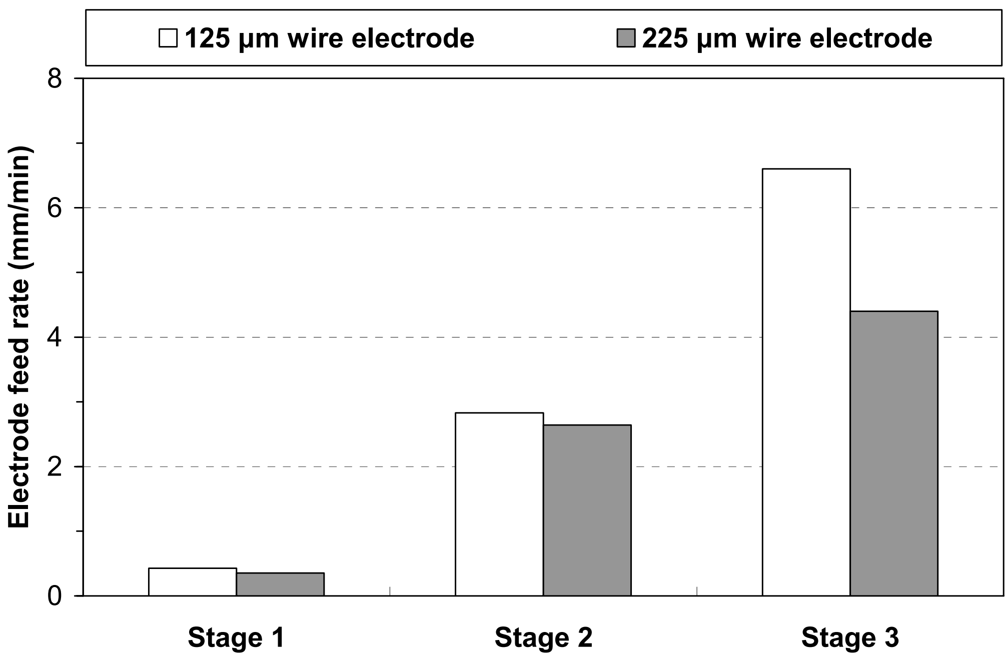

Figure 2.10. Feed rate for 125 and 225 μm wire electrodes in three EDM stages.

In Stage 2, as shown in Figure 2.9, the pulse rate for sparking is much higher than in Stage 1. The EDM process was adjusted to achieve a high spark pulse rate in this stage for fast material removal. The electrode feed rate, as shown in Figure 2.10, has increased to 2.8 and 2.6 mm/min for 125 and 225 μm electrode, respectively. Similar to Stage 1, the 225 μm electrode has more frequent spark pulses but a slower feed rate than the 125 μm electrode.

In Stage 3, the high V_o slightly reduces the spark pulse rate but significantly increases the electrode feed rate, particularly for the 125 μm electrode. Each spark pulse under high V_o has more energy, which removes more work-material and increases the gap width. This is important to create the desired reverse taper shape of spray hole with larger diameter inside the hole. Although a high V_o is helpful to increasing the electrode feed rate to 6.7 and 4.5 mm/min for 125 and 225 μm diameter wire, respectively, it deteriorates the roundness of the hole. All of these have been observed in an investigation (Kao and Shih, 2007a) to measure the form of spray holes under the same EDM setup in this study.

2.5. Concluding Remarks

In this study, a high speed oscilloscope with 0.5 ns sampling period was applied to investigate spark and arc pulses for a better understanding of the micro discharging process. Sample spark and arc pulses for three stages (electrode dressing, drilling, and penetration) of micro-hole EDM were analyzed.

A new phenomenon of pre-discharging current, a short time duration (less than 30 ns) current rise before the rapid voltage drop, was observed. The effect of electrode dressing using negative polarity was evidenced by SEM micrographs showing a blunted electrode tip. Negative polarity not only induced a high short pulse rate and elongated the discharging period, but also resulted in double discharges in arc pulses. When a wire electrode with larger diameter was used, a higher spark pulse rate was observed but it did not correspond to a high electrode feed rate.

Monitoring of voltage and current can assist in the selection and optimization of micro-hole EDM process parameters. Moreover, with the detail demonstration of nanosecond level interactions between the gap voltage and current, the EDM research can move further, while combining the knowledge of plasma physics, to the theoretical field, such as the study of nano-scale discharging mechanisms.

CHAPTER 3

ADAPTIVE FUZZY LOGIC CONTROLLER FOR MICRO-HOLE EDM

The fuzzy logic control, well known for its capability of handling highly nonlinear processes with only qualitative knowledge available (Reznik, 1997; Isermann, 1998), is able to adaptively control the EDM process using multiple input parameters and prevent the undesired arc and short circuit pulses by actively responding to the gap conditions (Rajurkar and Wang, 1997).

An adaptive, three-input fuzzy logic controller is developed in this study. Average gap voltage, deviation of spark ratio, and the change of deviation of spark ratio, are the three input parameters of this fuzzy logic controller. Servo motion commands are real time synthesized based on these input parameters, which not only represent the current EDM status but also indicate the trend of ongoing EDM conditions.

The design and tuning of fuzzy logic controller for micro-hole EDM are important because the computational time of fuzzy logic reasoning would grow significantly when the number of inference rules increases. Better EDM drilling efficiency can be achieved through a proper tuning process.

3.1. Review of the Fuzzy Logic Controller

The improvement of drilling time is one of the major technical challenges for micro-hole EDM drilling. The key to faster drilling speed is dependent on the generation of normal discharges and the minimization of abnormal discharges. Spark pulse is the normal discharge for efficient material removal. Arc and short circuit pulses are abnormal discharges, which increase the drilling time and are harmful to the machined surface (Kao and Shih, 2006). This study develops a fuzzy logic based EDM process controller to increase the spark and decrease the arc and short circuit pulses to improve the efficiency and drilling time in micro-hole EDM.

The proportional-integral-derivative (PID) and pulse width modulation (PWM) are two commonly used EDM process control method. The PID controller utilizes a predefined mathematical model to dynamically adjust the servo movement according to sensor feedback. The PWM controller adjusts the servo position by varying the duty cycle of input voltage pulses. However, the pulse generation in the EDM process is highly stochastic and complicated. The difficulty of using a mathematical model to precisely describe the EDM process renders the PID controller less competitive in preventing the undesired arc and short circuit pulses (Wang and Rajurkar, 1992; Rajurkar and Wang, 1997). PWM controller, relying on the variation of pulse duty cycles, lacks the EDM condition feedback and operates with a severe non-linearity known as the deadband, which degrades the controller performance significantly (Ko and Good, 2005).

Adaptive control of EDM process has been studied since the late 70s (Kruth et al., 1979; Snoeys et al., 1980; Rajurkar and Pandit, 1980; Wang and Rajurkar, 1990; Weck and Dehmer, 1992). The adaptive control strategy is able to detect and react to EDM status changes by continuously adjusting system responses based on the feedback information. Gain scheduling, which uses local linear controllers to collectively perform a global nonlinear process control by scheduling gains at different operating conditions (Shamma and Athans, 1992), is a common adaptive EDM process control method.

Artificial intelligence, such as neural networks and fuzzy logic, has been successfully applied to further advance the EDM process control (Ho and Newman, 2003; Mediliyegedara and Wijayakulasooriya; 2004). Fuzzy logic control is more popular in EDM research because it has faster response and higher stability (Karakuzu, 2000) and can more accurately model real world events by allowing the existence of uncertainty to simulate human reasoning (Reznik, 1997). The fuzzy logic controller (Boccadoro and Dauw, 1995; Zhang et al., 1997; Yan and Liao, 1998; Zhang et al., 2002; Kaneko and Onodera, 2004; Zhang, 2005) has demonstrated the capability to adaptively control the EDM process by handling highly nonlinear processes with only qualitative knowledge (Reznik, 1997; Isermann, 1998) and reduce the drilling time by minimizing the arc and short circuit pulses (Rajurkar and Wang, 1997).

In addition to handling the nonlinearity, an ideal EDM process controller should be able to receive and analyze multiple input parameters from the feedback loop to synthesize more accurate and objective servo commands. Fuzzy logic controllers with single and multiple input parameters have been investigated for die-sinking and wire EDM. For example, the frequency of arc and short circuit pulses has been utilized as the single-input parameter (Kaneko and Onodera, 2004). The lack of information and limitations of the single-input fuzzy logic controller have been studied (Kao and Shih, 2007c; Kao and Shih, 2007d; Kao and Shih, 2007e). Two-input fuzzy logic controllers have been investigated that use error of gap voltage and its change rate (Zhang et al., 1997), servo position error and its change rate (Zhang et al., 2002), pulse time ratio error and its change rate (Zhang, 2005), or the ignition delay and percentage of abnormal discharges (Boccadoro and Dauw, 1995). Three-input fuzzy logic controller for wire EDM has been developed using the spark frequency error, abnormal spark ratio error and its change rate (Yan and Liao, 1998). These three input parameters for wire EDM control focus on counting and identification of EDM pulses but neglect the variation of average gap voltage V_g, which is important for micro-hole EDM drilling and needs to be ideally maintained at a constant value for a stable drilling process. One of the goals in this research is to develop a three-input fuzzy logic controller including V_g as an input parameter.

The design and development of the fuzzy logic controller is presented in Sec. 3.2. The importance of fuzzy logic controller tuning is explained in Sec. 3.3. Conclusions are discussed in Sec. 3.4.

3.2. Design and Development of the Fuzzy Logic Controller

3.2.1. Input and output parameters

The fuzzy logic control allows the existence of uncertainty in handling parameter values (Reznik, 1997). This is achieved by using linguistic variables, which are associated with different levels of linguistic values, to map a specific numerical value with uncertainty, the so-called fuzziness. The schematic diagram of a typical fuzzy logic controller is shown in Figure 3.1. Three major parts of a fuzzy logic controller are: fuzzifier, inference engine, and defuzzifier. The fuzzifier determines the fuzziness of each input parameter via the membership functions, which map an input parameter from the universe of discourse (the input domain) to a fuzzy value between 0 and 1. The inference engine then, based on the input fuzzy values, triggers the If-Then inference rules and synthesizes output fuzzy values. The defuzzifier maps output fuzzy values back to the output domain to generate the output parameters.

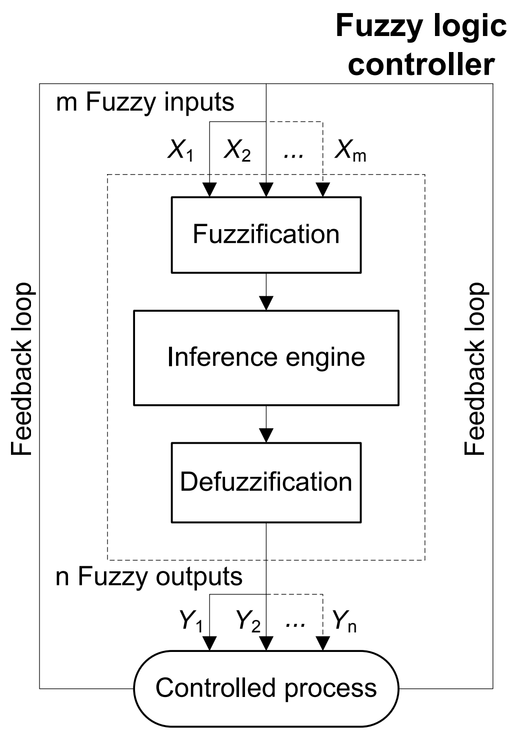

Figure 3.1. Schematic diagram of a typical fuzzy logic controller.

In this study, Mamdani's inference method (Reznik, 1997), a commonly used fuzzy logic methodology, is utilized as the kernel of the fuzzy logic controller. The fuzzy logic controller has three input parameters: the average gap voltage, V_g, deviation of spark ratio, ΔR_s, and change of deviation of spark ratio, $\delta(\Delta R_s)$. These three parameters enable the fuzzy logic controller be adaptive to the rapid-changing EDM processes by real time identification of the current EDM status and the trend of ongoing EDM conditions. An adaptive fuzzy logic controller with three input parameters, error of sparking frequency, error of abnormal spark ratio, and change of error of abnormal spark ratio, has been developed for wire EDM (Yan and Liao, 1998). These three input parameters focus on counting and identification of EDM pulses but neglect the variation of V_g, which should be ideally maintained at a constant value for the stable EDM drilling. As a result, V_g as well as ΔR_s and $\delta(\Delta R_s)$ are used in this study to develop the three-input fuzzy logic controller for micro-hole EDM.

The fuzzy logic controller generates output parameters for servo motion commands, which are synthesized through the inference engine based on the feedback information. The servo motor receives commands and feeds the electrode accordingly.

Three linguistic values, as shown in Figure 3.2, are associated with ΔR_s and $\delta(\Delta R_s)$: Positive (PO), Zero (ZE), and Negative (NE). Servo motion can be specified by the servo speed v and servo displacement d. There are five linguistic values associated with v: Forward Fast (FF), Forward (FO), Dwell (DW), Backward (BA), and Backward Fast (BF). The linguistic value, Dwell, is used to describe the transition between Forward and Backward. For d, there are also five linguistic values: Very Large (VL), Large (LA), Medium (ME), Small (SM), and Very Small (VS). Triangular membership functions are selected for the input and output parameters of the fuzzy logic controller, as shown in Figure 3.2.

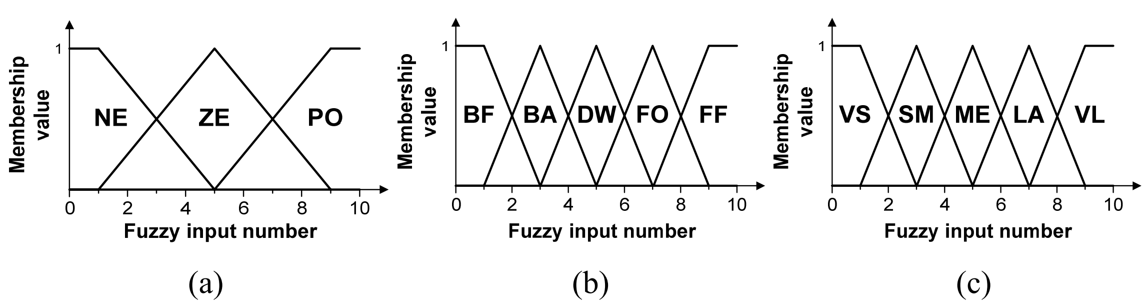

Figure 3.2. Membership functions for fuzzy logic parameters: (a)ΔR_s and $\delta(\Delta R_s)$, (b) v, and (c) d.

3.2.2. Fuzzy logic inference engine

The average gap voltage V_g is used to identify the current EDM status by comparing its value with the open circuit voltage V_o. The voltage ratio of V_g/V_o, designated as R_v, is an index indicating the stability of EDM conditions during each sampling duration. In the fuzzy logic inference engine, the value of R_v is used to distinguish six EDM status (Open Circuit, Good, Fair, Bad, Dual State, and Short Circuit), as presented in Figure 3.3, and call sub-programs, which have a unique set of inference rules for the associated EDM status.

For conditions of Open Circuit, Dual State, and Short Circuit, each associated sub-program is implemented with the predefined If-Then rules without using the fuzzy logic inference engine because solutions to the three conditions are relatively straightforward. In Open Circuit, the set of rules is designed to command the servo stage to move forward to reduce the gap distance and induce discharges. In Short Circuit, the set of rules commands the stage to move backward to widen the gap distance. In Dual State, if there is no arc pulse detected, the stage is commanded to move forward; otherwise, the stage will move backward.

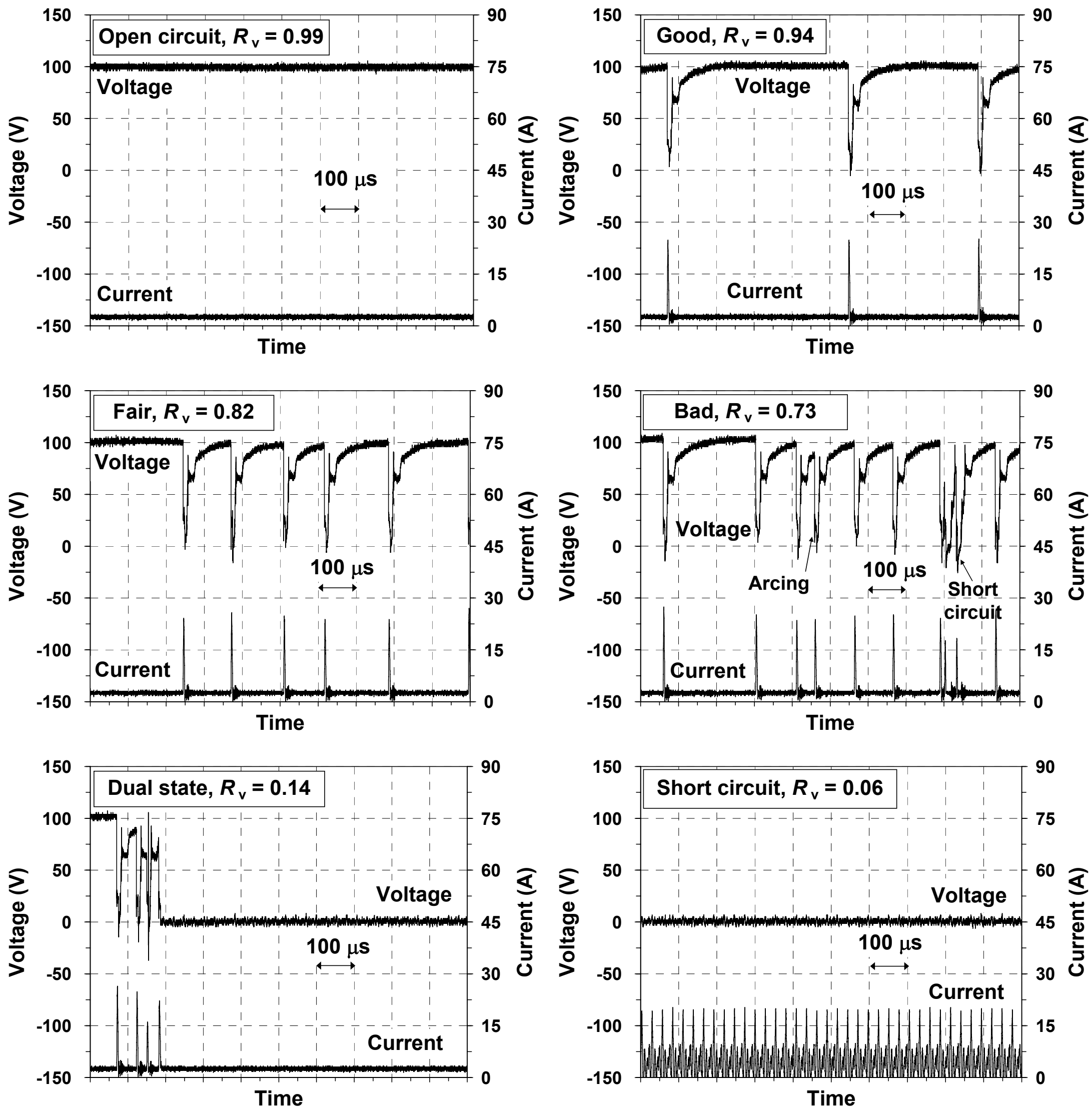

Figure 3.3. Sample pulse trains for six levels of EDM status (open circuit voltage V_o = 100 V).

Three examples of fuzzy inference rules are shown here:

- *If* R_v is Good and ΔR_s is Positive and $\delta(\Delta R_s)$ is Positive, *then* v is Forward Fast and d is Very Large.
- *If* R_v is Fair and ΔR_s is Positve and $\delta(\Delta R_s)$ is Zero, *then* v is Dwell and d is Small.
- *If* R_v is Bad and ΔR_s is Negative and $\delta(\Delta R_s)$ is Negative, *then* v is Backward Fast and

d is Very Large.

These fuzzy inference rules use values of ΔR_s and $\delta(\Delta R_s)$ to calculate the weight, between 0 to 1, to indicate how much this rule is related to the given input parameters. Membership functions of output parameters are scaled by the weights and aggregated for the synthesis of v and d. In this study, the area of aggregated membership functions is discretized as singletons, a commonly used technique in fuzzy logic (Reznik, 1997), to reduce the computational effort (Isermann, 1998). The output fuzzy values of v and d are calculated using the centroid method (Reznik, 1997) and then defuzzified to real values of speed and displacement used as inputs for the servo motor.

3.3. Fuzzy Logic Controller Tuning

The design and tuning of fuzzy logic controllers are crucial to effective real time process control because the computational time for fuzzy logic reasoning grows significantly with the complexity of inference engines (Chiu and Togai, 1988; Chiueh, 1991). Longer computational time will delay the controller response and results in poorer performance. For micro-hole EDM, the EDM status can change rapidly because the pulse duration in micro-hole EDM is very short, usually less than 1 μs. To maintain stable EDM status, the computational time of fuzzy logic reasoning needs to be sufficiently short to generate timely servo responses. As a result, the architecture of the fuzzy logic controller needs to be optimally designed for the micro-hole EDM process to achieve the best control performance. This requirement necessitates the tuning of fuzzy logic controller. The performance of fuzzy logic controller can be tuned by optimized hardware resource allocations (Li and Gatland, 1996). Software based tuning is not yet reported for the micro-hole EDM process. A systematic and software based approach to tune the performance of the fuzzy logic controller is developed in this study for more efficient micro-hole EDM process.

3.4. Concluding Remarks

The architecture of the adaptive fuzzy logic controller was presented in this chapter. The importance of fuzzy logic tuning was discussed. Implementation and experimental validation of the fuzzy logic controller on two platforms will be presented in Chapter 4.

CHAPTER 4

IMPLEMENTATION AND VALIDATION OF ADAPTIVE FUZZY LOGIC CONTROLLER FOR MICRO-HOLE EDM

The fuzzy logic micro-hole EDM controllers are implemented and evaluated in two platforms for comparison and validation. Platform 1 is a Gromax micro-hole EDM machine with PWM controller. Platform 2 is a production micro-hole EDM drilling machine using gain scheduling controller, made by Ann Arbor Machine Company (AAM).

4.1. Platform 1: Gromax Micro-Hole EDM Machine

4.1.1. Overview

Configuration of the fuzzy logic EDM control system in Platform 1 is shown in Figure 4.1. The test platform for the fuzzy logic based micro-hole EDM control system is a Gromax MD20 micro-hole EDM machine. Major components of the fuzzy logic micro-hole EDM control system are a real time data acquisition system built upon a programmable digital oscilloscope, a PC-based adaptive fuzzy logic controller, and a precision piezoelectric stage.

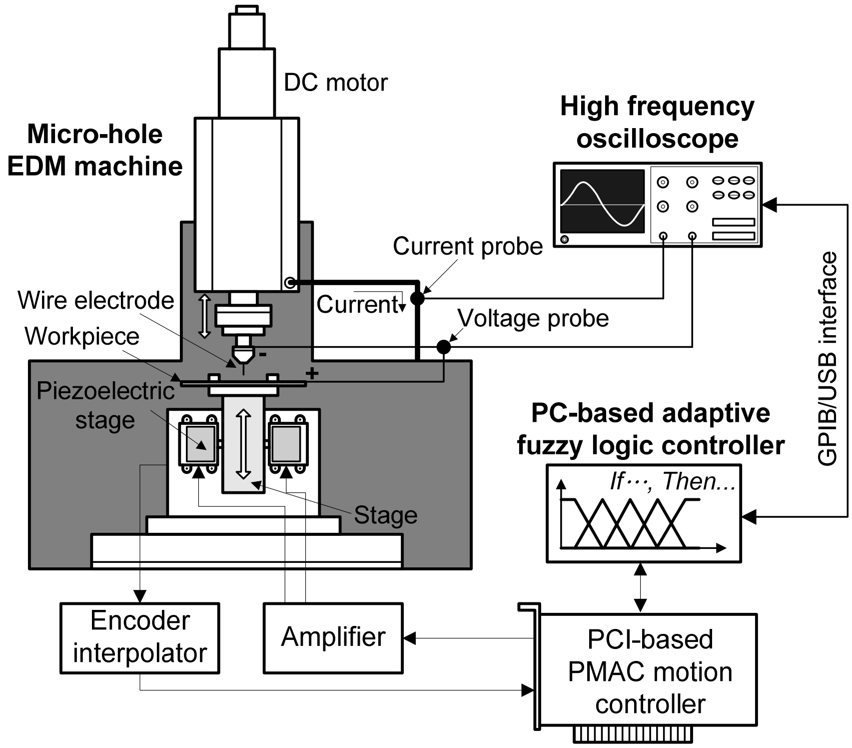

Figure 4.1. Configuration of the fuzzy logic micro-hole EDM control system.

These components in Platform 1 are analogous to the building blocks of an intelligent machine (Albus, 1992), as shown in Table 4.1. The intelligent machine system, as defined by Albus (1992), is capable of analyzing the past, perceiving the present, and planning for the future through integrating functional elements, knowledge representations, and flow information in a coherent and efficient way (Evans et al., 2002). Such system requires the integration of real time software and precision mechanisms (Nunes et al., 2000).

This fuzzy logic based EDM control system is developed for Platform 1 to enhance the micro-hole EDM drilling performance. The wire electrode is moved by a PWM-controlled DC servo motor, which has coarse movement and limited speed. The workpiece is actuated by a piezoelectric stage, which has better dynamic response and more precise, μm-level movement than the DC servo motor. The combination of DC servo motor for electrode and piezoelectric stage for the workpiece determines the EDM gap condition

The implementation of adaptive fuzzy logic controller, tuning of the piezoelectric stage, and setup of the data acquisition system, is first discussed. The micro-hole EDM drilling performance with and without the fuzzy logic EDM control system is compared. Experiments investigating effects of single and multiple input parameters, ignition delay threshold value, and maximum servo displacement and speed on micro-hole EDM drilling, are presented. DOE study of the correlation between EDM parameters and drilling time and the optimal EDM parameter search using DOE analysis are discussed.

Table 4.1. Analogy between the intelligent machine system (Albus, 1992) and the fuzzy logic EDM control system.

Elements of intelligent machine system	Components of fuzzy logic EDM control system
Sensors	Data acquisition system
Sensory processing	Fuzzification
World model/database	Fuzzy logic rules
Value judgment	Fuzzy inference kernel
Behavior generation	Defuzzification
Actuators	Piezoelectric stage

4.1.2. Data acquisition system

The data acquisition is based on an Agilent Infiniium 54833A digital oscilloscope, which has the real time data processing and storage capability. An Agilent 10076A 250 MHz 100:1 high voltage probe and an Agilent 1147A 50 MHz AC/DC current probe are used to monitor the gap voltage and current. The signal sampling rate is 1 MHz. The gap voltage and current sampling duration, T, is 1 ms. This setup gives sufficient sampling rate without sacrificing the data processing speed. The Agilent Standard Instrument Control Library (SICL), an application development tool, is applied to perform the data communication between the desktop and the oscilloscope by way of a GPIB/USB interface. The update frequency through the GPIB/USB interface is 25 to 30 Hz to synthesize the servo displacement and speed of the piezoelectric stage.

Sample voltage and current waveforms in 1 ms sampling duration are shown in Figure 4.2. The number represents EDM pulses. Three parameters, the average gap voltage V_g, number of detected arc pulses N_a, and total pulse number N_t, are measured in each sampling duration to access the EDM condition. In Figure 4.2, V_g = 83.3 V, N_a = 4, and N_t = 9.

4.1.3. Adaptive fuzzy logic controller

A schematic diagram of the fuzzy logic controller implemented for the Gromax EDM machine is shown in Figure 4.3. The fuzzy logic controller has three input parameters: the average gap voltage, V_g, deviation of spark ratio, ΔR_s, and change of deviation of spark ratio, $\delta(\Delta R_s)$.

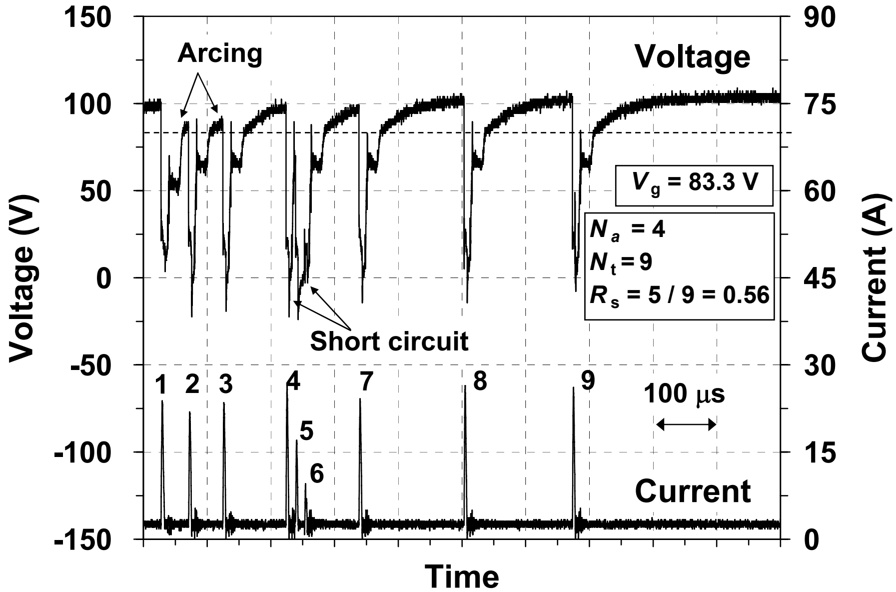

Figure 4.2. Measured voltage and current and corresponding parameters in a 1 ms sampling duration *T*.

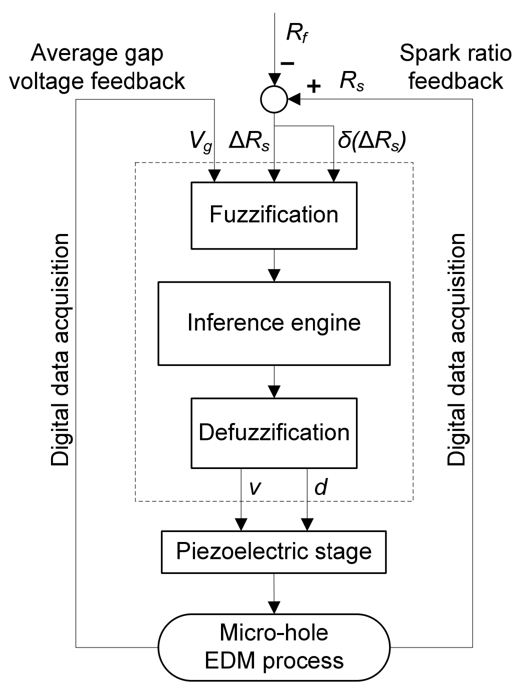

Figure 4.3. Schematic diagram of the adaptive fuzzy logic controller for Gromax EDM machine.

The fuzzy logic controller generates two output parameters, the servo command speed v and servo command displacement d, that are synthesized based on the feedback from the data acquisition system, to drive the piezoelectric stage. The maximum servo command speed, designated as v_{max}, is the upper bound of the synthesized speed and empirically set to be 1.8 mm/s. The maximum servo command displacement, designated as d_{max}, is the upper bound of the synthesized displacement and empirically set to be 2 μm. Triangular membership functions are selected for the input and output parameters of the fuzzy logic controller.

For conditions of Good, Fair, and Bad, the fuzzy inference rules, as summarized in Table 4.2, are applied.

Table 4.2. Fuzzy inference rules of the fuzzy logic controller for Gromax EDM machine.

R_v is Good		Electrode speed, v			Electrode displacement, d		
		$\delta(\Delta R_s)$			$\delta(\Delta R_s)$		
		PO	ZE	NE	PO	ZE	NE
ΔR_s	PO	FF	FF	FO	VL	LA	LA
	ZE	FF	FF	DW	LA	LA	ME
	NE	FO	DW	BA	ME	ME	SM

R_v is Fair		Electrode speed, v			Electrode displacement, d		
		$\delta(\Delta R_s)$			$\delta(\Delta R_s)$		
		PO	ZE	NE	PO	ZE	NE
ΔR_s	PO	FO	DW	BA	LA	SM	ME
	ZE	DW	DW	BA	SM	ME	ME
	NE	BA	BA	BF	ME	LA	VL

R_v is Bad		Electrode speed, v			Electrode displacement, d		
		$\delta(\Delta R_s)$			$\delta(\Delta R_s)$		
		PO	ZE	NE	PO	ZE	NE
ΔR_s	PO	BA	BA	BF	ME	ME	LA
	ZE	BA	BF	BF	ME	LA	VL
	NE	BF	BF	BF	LA	VL	VL

4.1.4. The piezoelectric stage

The stage is driven by two piezoelectric motors (Nanomotion HR4), each of which contains a piezoelectric ceramic beam to perform the high frequency (39.6 kHz) elliptic oscillation to actuate the stage. A polyimide plate, due to its electrical insulation capability, is placed between the workpiece holder and the stage to isolate the discharging current loop from the piezoelectric motors. The piezoelectric stage is actuated by a 24 V DC power source and commanded by a Delta Tau PMAC multi-axis motion controller. The position of piezoelectric stage is interpolated by a linear encoder with 50 nm resolution.

The dynamic response of the piezoelectric stage is optimized using the Delta Tau interactive PID tuning software. The bandwidth of the piezoelectric stage is about 150 Hz for two sinusoidal inputs (50 and 10 μm amplitude), as shown in Figure 4.6. For displacement less than 5 μm, a precise sinusoidal movement is not possible because such small amplitude is beyond the motion synthesis capability of the controller. As a result, the ramp response analysis is conducted for the case of d_{max} = 2 μm and v_{max} = 1.8 mm/s. For the continuous ramp response test, the time lag is about 0.5 ms and the ramp movement is executed with high fidelity. Figure 4.7 shows the following error, which is the command position minus the actual position, demonstrates a regular pattern for each ramp movement and has an average value less than 0.1 μm. These test results indicate that the piezoelectric stage is able to perform rapid and precise position control.

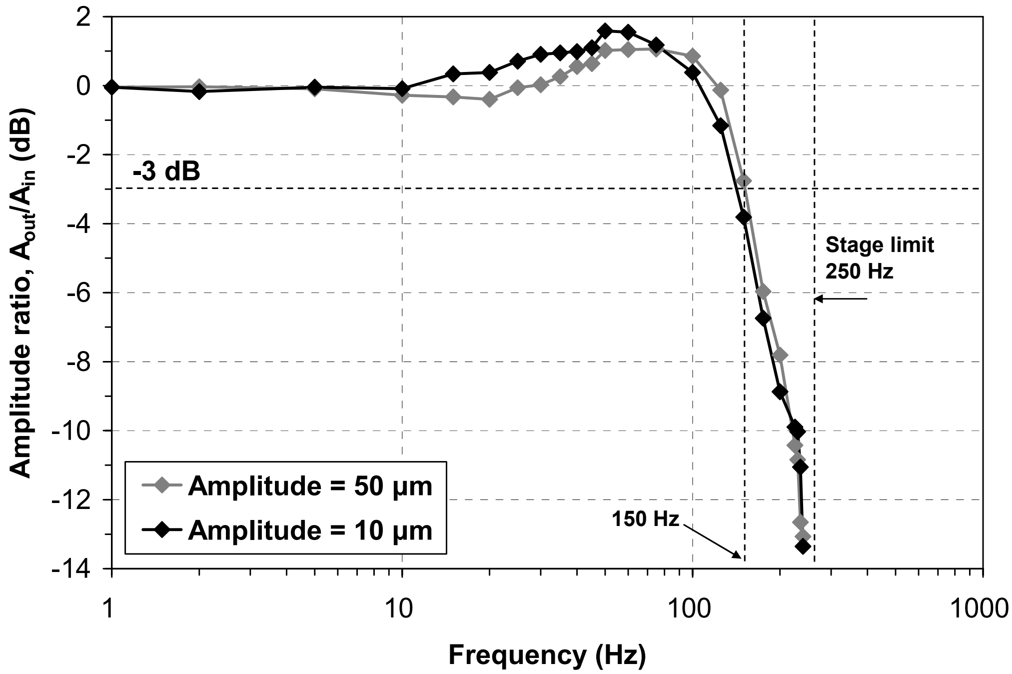

Figure 4.6. Bandwidth of the piezoelectric stage with two sinusoidal inputs.

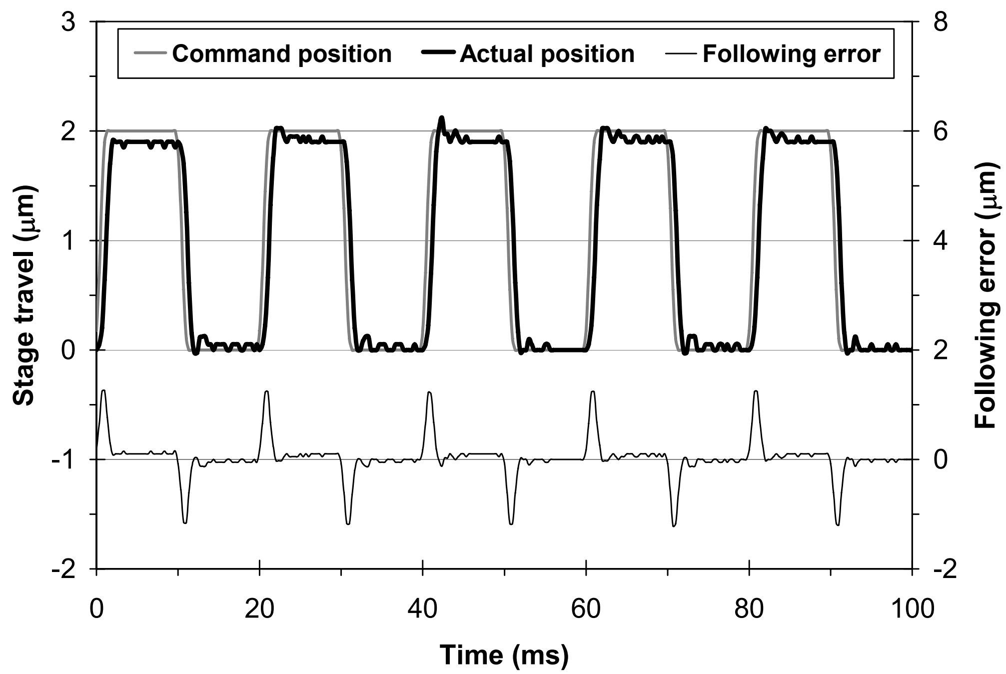

Figure 4.7. Continuous position ramp response of the piezoelectric stage at 50 Hz (Travel = 2 µm, velocity = 1.8 mm/s).

4.1.5. Characterization of EDM conditions

For the Gromax EDM machine, the classification of EDM status and identification of EDM pulses are discussed in the following two sections.

4.1.5.1. Classification of EDM status

In Platform 1, $T = 1$ ms and $V_o = 100$ V. Six levels of R_v, as discussed in Sec 3.2.2, are experimentally identified based on the analysis of measured voltage and current pulse trains:

- Open Circuit, $0.98 \le R_v$: There is no discharge occurred and the gap voltage is maintained around the open circuit level.
- Good, $0.85 \le R_v < 0.98$: Discharge occurs regularly with constant peak value of discharge current.
- Fair, $0.75 \le R_v < 0.85$: Discharges become dense.
- Bad, $0.30 \le R_v < 0.75$: Discharges occur more frequently and the discharge current becomes irregular due to the arc and short circuit pulses.
- Dual State, $0.10 \le R_v < 0.30$: It is the combination of zero gap voltage (off state) and some localized discharges.
- Short Circuit, $0 \le R_v < 0.10$: The electrode touches the workpiece and the gap voltage is almost zero.

4.1.5.2. Identification of EDM pulses

For the Gromax EDM machine, the ignition delay, t_d, defined as the time duration of high voltage maintained for subsequent discharging, is used to characterize EDM pulses. Spark pulses usually have a long t_d to accumulate discharge energy for dielectric breakdown. For arc and short pulses, t_d is relatively short because the current can flow across the discharge gap without the dielectric breakdown due to bridges formed by remaining debris or plasma channels from previous discharges. The comparison of t_d for the spark, arc, and short pulses of a sample pulse train is shown in Figure 4.8. A specific time interval is used as the ignition delay threshold value, designated t_{dt}, to characterize the spark, arc, and short pulses. The value of t_{dt} is initially set to be 80 μs, same as the preset pulse interval time, t_0, by empirical estimation. In the ideal case, each EDM pulse should have consistent t_0. Any pulse with t_d less than the preset t_0 is identified as an arc pulse. The t_d of each sampled pulse is measured by the oscilloscope using a built-in measuring function, which identifies the time duration of each EDM pulse. Pulses with t_d longer than t_{dt} are recognized as spark pulses, whereas pulses with t_d shorter than t_{dt} are identified as arc pulses.

In the sampling duration T, N_a is the number of arc pulses and N_t is the number of total pulses. The spark ratio, R_s, is defined as:

$$R_s = (N_t - N_a) / N_t \tag{4.1}$$

An example of N_a = 4, N_t = 9, and R_s = 0.56 in a 1 ms sample duration is presented in Figure 3.2. When R_s = 1, no arc pulse is detected in the sampling duration. Low R_s means frequent occurrence of arc pulses and implies an unstable EDM condition.

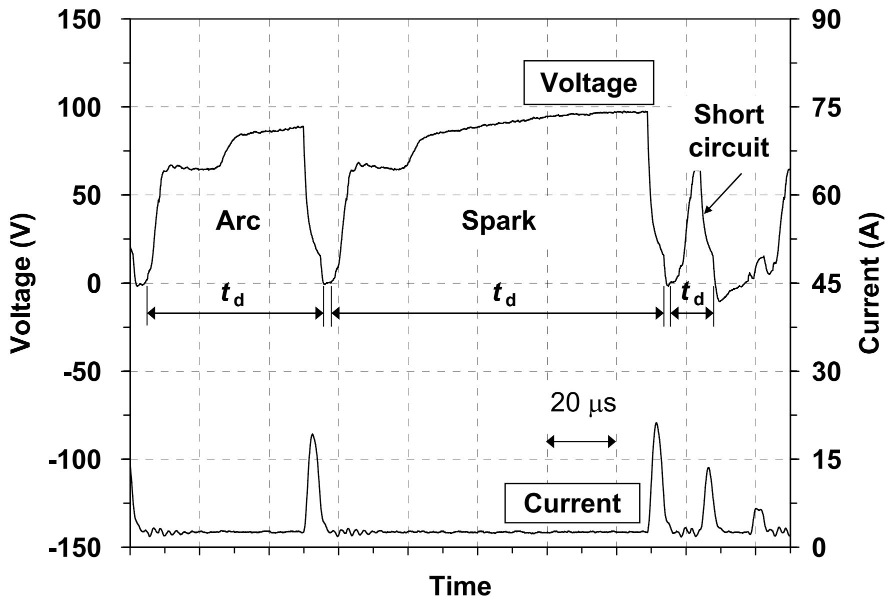

Figure 4.8. Classification of EDM pulses by ignition delay t_d.

The difference between R_s and a reference value, R_f, is used to evaluate the EDM condition. R_f is the desired R_s value for a stable EDM process, and ΔR_s measures the deviation between the desired and actual values. Large, negative ΔR_s means very low spark ratio and the electrode needs to quickly move away from the workpiece to restore a normal EDM status. The deviation of spark ratio, designated as ΔR_s, is defined as:

$$\Delta R_s = R_s - R_f \tag{4.2}$$

For Platform 1, $R_f = 0.7$, which is experimentally estimated from the EDM pulse train analysis. The change of ΔR_s from the previous sampling time t_{k-1} to current sampling time t_k is denoted as $\delta(\Delta R_s)$.

$$\delta(\Delta R_s) = \Delta R_s(t_k) - \Delta R_s(t_{k-1}) = R_s(t_k) - R_f - [R_s(t_{k-1}) - R_f] = R_s(t_k) - R_s(t_{k-1}) \tag{4.3}$$

$\delta(\Delta R_s)$ is the change of deviation of spark ratio and an effective index to observe the trend of EDM conditions.

4.1.6. Experimental procedures

For the Gromax EDM machine, four sets of micro-hole EDM experiments, pulse train analysis, parameter analysis of the fuzzy logic controller, DOE analysis and optimal search, are performed to investigate the fuzzy logic control for micro-hole EDM. The workpiece is 1.0 mm thick AISI 1010 steel. The wire electrode diameter is 100 μm. The gap voltage is 100 V, discharge current is 20 A, pulse interval time t_0 is 80 μs, and discharge duration t_e is 5 μs.

4.1.6.1. Pulse train analysis

The goal of pulse train analysis is to compare the drilling performance with and without the fuzzy logic EDM control. When the fuzzy logic EDM control is enabled, the piezoelectric stage is set active to assist the DC motor servo by real time adjusting the discharge gap distance. When the fuzzy logic EDM control is disabled, the piezoelectric stage is set inactive and the entire EDM drilling process is carried out by the DC motor servo. The gap voltage and current are extracted from the EDM pulse trains to study the distribution of spark, arc, and short pulses. The drilling time and number of arc pulses are used to evaluate the EDM drilling performance.

4.1.6.2. Parameter analysis of the fuzzy logic controller

The fuzzy logic controller compares the drilling time with one and three input parameters, analyzes the value of t_{dt}, and investigates the influence of d_{max} and v_{max}. For the single input fuzzy logic controller, R_v is selected as the input parameter. For the three-input fuzzy logic controller, R_v, ΔR_s, and $\delta(\Delta R_s)$, are used. Seven levels of t_{dt}, 5, 40, 80, 150, 250, 400, and 1000 μs are selected to study the effect of t_{dt} on arc pulses and drilling time. The influence of d_{max} and v_{max} is studied by testing at three levels of d_{max}, 2, 4, and 8 μm, with v_{max} = 1.8 mm/s and four levels of v_{max}, 0.6, 1.2, 1.8, and 2.4 mm/s, with d_{max} = 2 μm.

4.1.6.3. DOE analysis of fuzzy logic control parameters

The DOE analysis is applied to study the correlation between fuzzy logic control parameters, t_{dt} and v_{max}, and the drilling time. The central composite response surface methodology is selected in this study. The design contains 6 center points (3 cube and 3 axial) with axial ratio α = 1.414 (MINITAB User Manual Release 14 for Windows, 2003).

As shown in Table 3.3, 13 experiments with three replicates are performed for the two-parameter (t_{dt} and v_{max}) DOE analysis. The t_{dt} varies from 5 to 400 μs while v_{max} changes from 0.6 to 2.4 mm/s. The EDM drilling time is averaged from three replicates for analysis.

A quadratic surface represented by t_{dt} and v_{max} is generated by the DOE analysis. The DOE optimizer (MINITAB User Manual Release 14 for Windows, 2003) is used to find the optimal t_{dt} and v_{max} setup for the fastest micro-hole EDM drilling. Experiments of 9 repeated micro-hole drilling are conducted to validate this optimal setup.

Table 4.3. DOE experiment setup and associated EDM drilling time.

Experiment number	t_{dt} (μs)	v_{max} (mm/s)	Average EDM drilling time (s)
1	342	0.86	10.5
2	203	1.50	8.87
3	400	1.50	11.3
4	203	1.50	10.5
5	63	2.14	8.45
6	63	0.86	8.45
7	203	1.50	10.5
8	203	1.50	11.9
9	203	0.60	12.9
10	203	2.40	12.4
11	203	1.50	10.8
12	342	2.14	12.6
13	5	1.50	13.7

4.1.7. Experimental results and discussions

4.1.7.1. Pulse train analysis

Representative pulse trains of gap voltage and current in EDM drilling with and without fuzzy logic control are shown in Figure 4.9. Without fuzzy logic EDM control, as shown in Figure 4.9(a), frequent irregular discharges are generated, regardless of the predefined t_0 and t_e, due to the inferior discharge gap condition. The short circuit is very significant because the PWM-controlled DC motor servo does not have either the sufficient EDM status feedback or an effective algorithm to generate adequate and precise servo movement to maintain a stable EDM drilling process. With three-input fuzzy logic EDM controller and piezoelectric stage, as shown in Figure 4.9(b), the discharge gap distance can be better controlled. Almost no short circuit is observed and arc pulses are quickly suppressed to enable a stable and fast EDM drilling process with regular discharges.

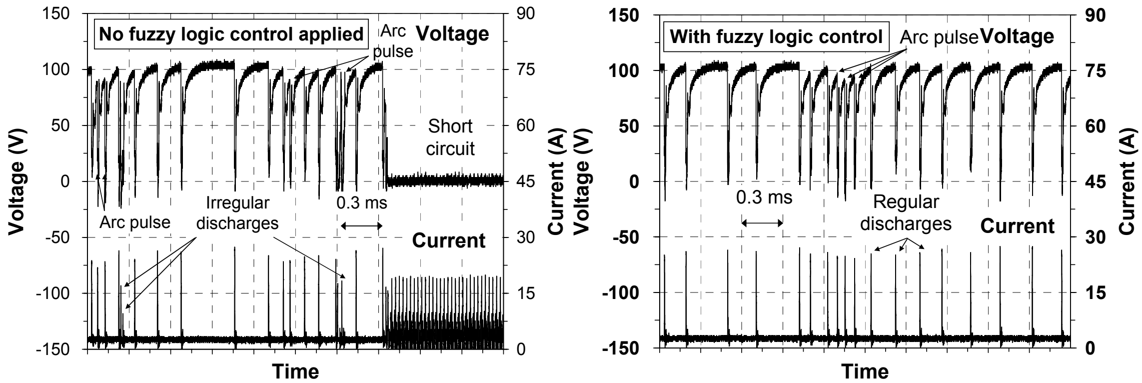

(a) (b)

Figure 4.9. Gap voltage and current of the EDM pulse train: (a) no fuzzy logic control applied and (b) with the fuzzy logic EDM control (three-input type, d_{max} = 2 μm, v_{max} = 1.8 mm/s, and t_{dt} = 80 μs).

The improvement of EDM drilling performance via the maintenance of regular discharges and the prevention of frequent short circuits is experimentally validated by comparing the drilling time and number of arc pulses during each 1 ms sampling duration. As shown in Figure 4.10, the EDM drilling time is shortened from 15.7 to 10.7 s and the number of arc pulses is also greatly reduced with the fuzzy logic EDM control. It should be noted that this improvement is limited by the slow computational speed of the built-in PC in the oscilloscope, which limits the data sampling frequency to only 25 to 30 Hz. If a faster data processing speed can be achieved using the digital signal processor, the EDM drilling time can be further reduced. Nevertheless, this pulse train analysis shows the advantage of fuzzy logic EDM control for micro-hole EDM.

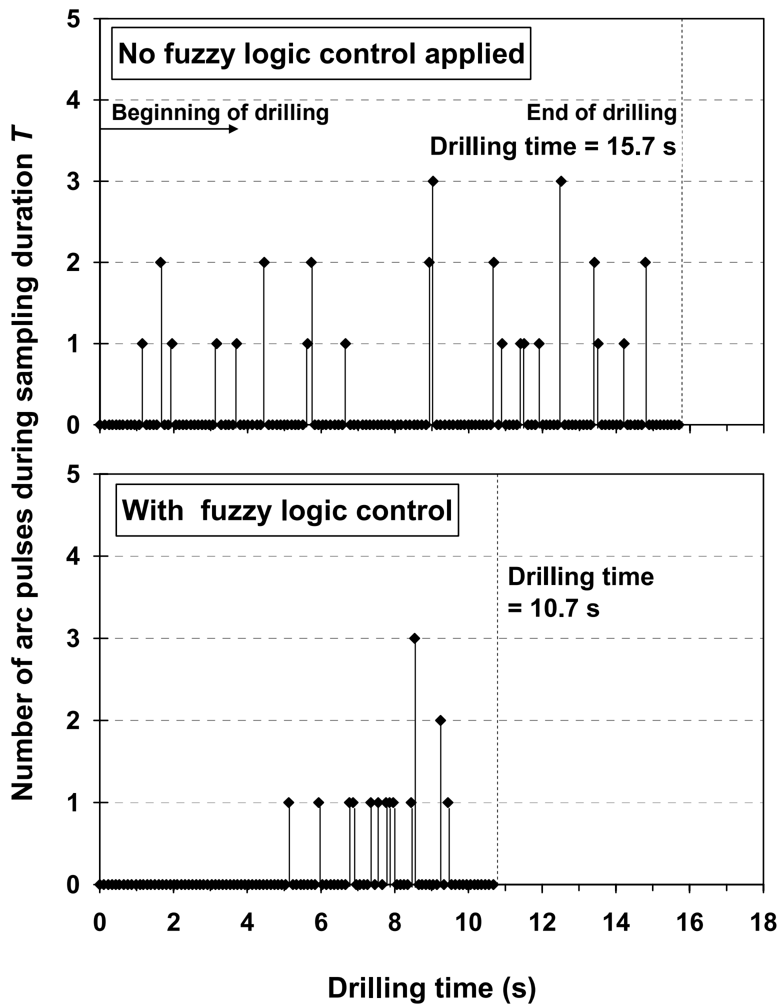

Figure 4.10. Effects of the fuzzy logic EDM control on arc pulse and EDM drilling time (three-input type, d_{max} = 2 μm, v_{max} = 1.8 mm/s, and t_{dt} = 80 μs).

4.1.7.2. Effect of single and multiple input parameters

As illustrated in Figure 4.11, the fuzzy logic controller using three-input parameters (R_v, ΔR_s, and $\delta(\Delta R_s)$) has shorter cycle time (21% reduction) and less arc pulses than that using one input parameter (R_v). The single-input fuzzy logic controller is prone to be biased. The multi-input fuzzy logic controller has more reference information available for servo command synthesis.

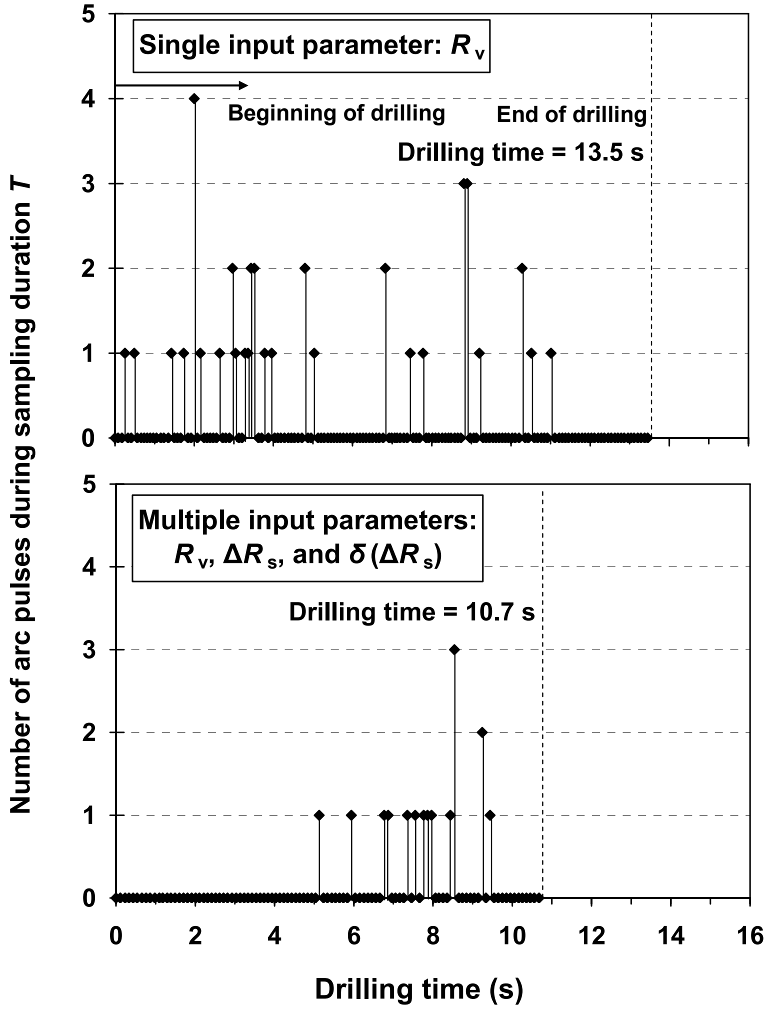

Figure 4.11. Effects of single and multiple input parameters on arc pulses and drilling time (d_{max} = 2 μm, v_{max} = 1.8 mm/s, and t_{dt} = 80 μs).

During the discharge gap distance adjustment, proper commands for the piezoelectric stage depend on not only the current EDM status but also the past EDM pulses. ΔR_s and $\delta(\Delta R_s)$ incorporate the information of past EDM pulses to improve the accuracy of servo command synthesis. For example, the future EDM status may become worse as indicated by the negative ΔR_s and $\delta(\Delta R_s)$ but still be identified as Good if only the R_v is used for EDM status identification. In comparison, the single-input fuzzy logic controller using R_v as the input parameter neglects the trend of EDM status and consequently has a higher possibility of generating inadequate servo movement, which results in more arc pulses and longer drilling time.

4.1.7.3. Parameter analysis of the fuzzy logic controller

Effect of t_{dt}

The selection of t_{dt} influences the detection of arc pulses, as discussed in Sec. 4.1.3.2. The drilling time and the number of arc pulses in each sampling duration at five levels of t_{dt} are shown in Figure 4.12. When t_{dt} is too small, such as 5 and 40 μs, very few arc pulses are detected because only pulses with very narrow time span can be identified as arc pulses. Based on the fuzzy inference rules, very few arc pulses represent a stable EDM condition. The fuzzy controller will synthesize a corresponding forward movement to the workpiece for the piezoelectric stage. The excessive forward movements, without properly identifying existing arc pulses, causes more frequent arc pulses unidentified by the fuzzy logic controller. As a result, the gap condition is deteriorated and drilling time is increased.

When t_{dt} is too large, such as 250 and 1000 μs, more pulses will be mistakenly identified as arc pulses, even for genuine sparks. Under such high arc pulse density condition, the fuzzy logic controller synthesizes a fast backward movement to flush the discharge gap. The frequent backward movements of the piezoelectric stage increase the drilling time. At t_{dt} = 1000 μs, the EDM drilling time (19.8 s) is more than doubled, compared to 9.50 s for t_{dt} = 80 μs.

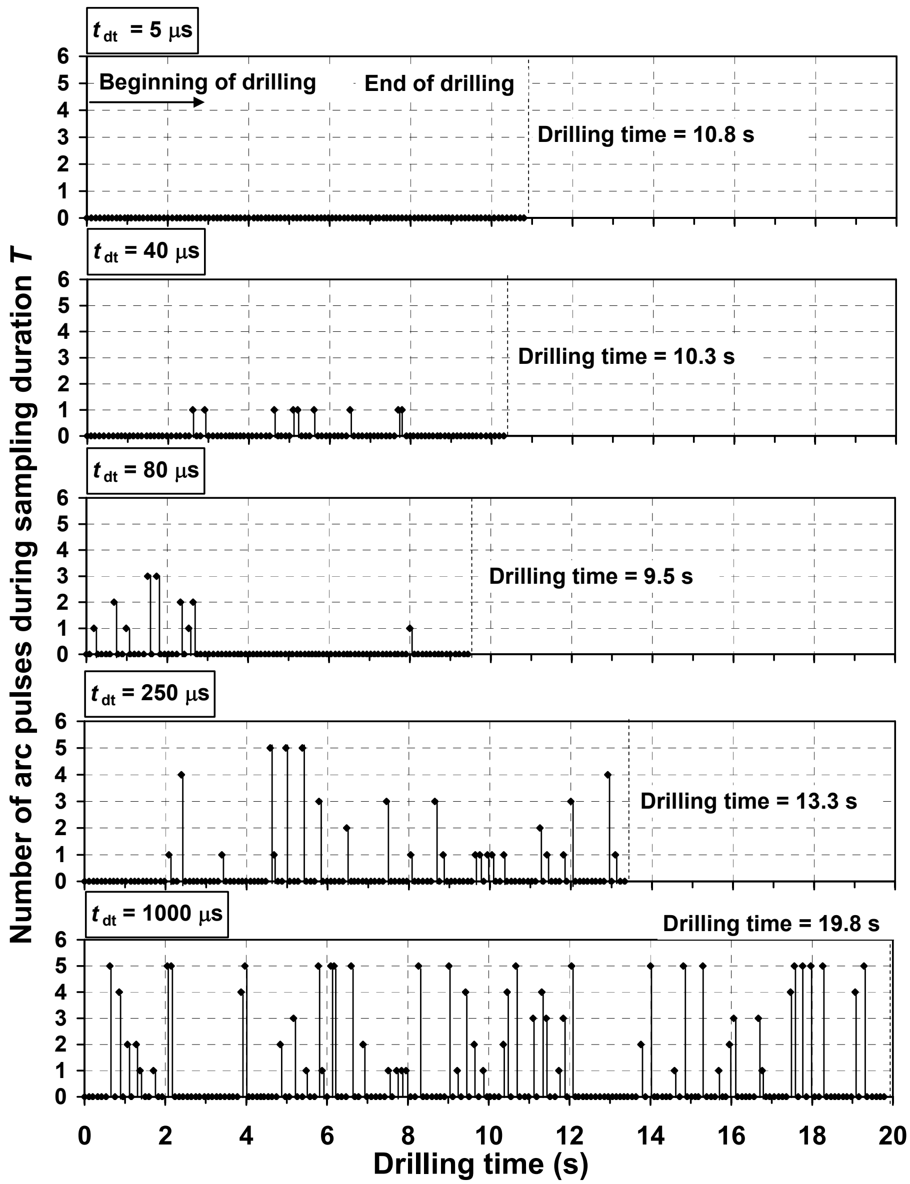

Figure 4.12. Arc pulses and drilling time under different t_{dt} (three-input type, d_{max} = 2 μm, v_{max} = 1.8 mm/s).

The t_{dt} should be selected within a specific region to achieve minimum EDM micro-hole drilling time. The selection of t_{dt} is further discussed in Sec. 4.1.7.4 using the DOE analysis and optimal search.

Influence of d_{max}

The position of the piezoelectric stage in each sampling duration (T) during drilling at 2, 4, and 8 μm of $d_{\max}$ is shown in Figure 4.13. The drilling starts from the zero position of piezoelectric stage. Positive position means the piezoelectric stage is moving the workpiece away from the advancing electrode to maintain proper discharge gap condition for a stable EDM process. This indicates that the PWM-controlled DC servo motor feeds the electrode toward the workpiece too aggressively. The EDM drilling time increases monotonically with $d_{\max}$.

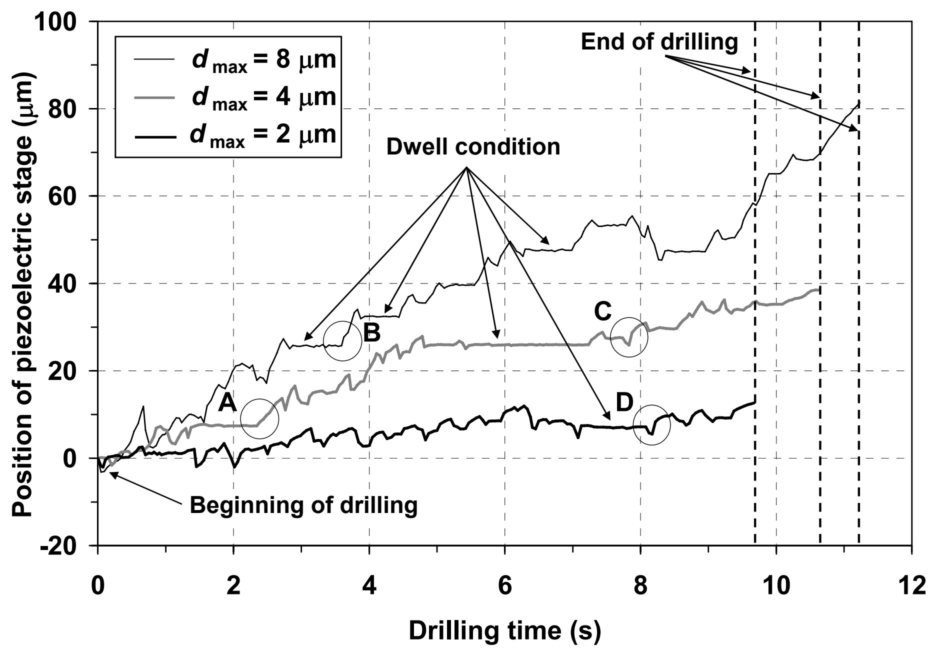

Figure 4.13. Movements of piezoelectric stage under three levels of d_{max} = 2, 4 and 8 μm (three-input type, v_{max} = 1.8 mm/s, and t_{dt} = 80 μs).

At the start of drilling, the piezoelectric stage moves toward the electrode for all levels of $d_{\max}$ according to the preset fuzzy rules under the circumstance of open circuit. After a short time, about 0.3 s, the piezoelectric stage begins to move away from the advancing electrode because of the frequent arc and short circuit pulses generated at the early stage of EDM drilling, where the electrode just touches the workpiece and starts discharging. It is observed that with larger d_{max}, the piezoelectric stage moves farther away from the electrode and has longer dwell condition. The dwell condition is primarily synthesized under a fair EDM condition with ΔR_s and $\delta(\Delta R_s)$ assigned the Zero linguistic value, as listed in Table 4.2.

When d_{max} is large, the away-from-the-electrode movement of piezoelectric stage caused by unstable EDM conditions may increase the discharge gap more than necessary. The discharge gap is narrow down later by the feeding of electrode, which will induce discharges first and maintain a stable EDM condition for a while before the feeding of electrode becomes too aggressive and turns the stable EDM condition into an unstable one. Usually the Dwell condition is followed by a sudden and significant away-from-the-electrode movement of piezoelectric stage because of the collapse of a stable EDM condition, as marked by A and B in Figure 4.13. Two exceptions, marked as C and D, were observed in which small overshoots occur at the end of dwell condition. This is because the piezoelectric stage does not stay absolutely still in dwelling. The piezoelectric stage drifts with very small oscillation amplitude, which can generate a better EDM condition identified by the fuzzy controller and induce the toward-the-electrode movement of piezoelectric stage. More frequent dwell condition also contributes to a longer drilling time: 9.7 s for d_{max} = 2 μm, 10.6 s for d_{max} = 4 μm, and 11.2 s for d_{max} = 8 μm.

Influence of v_{max}

The variation of drilling time under different v_{max} is relatively flat and not as significant as that under different d_{max}, as shown in Figure 4.14. This is because the generation of discharges is very sensitive to the gap distance (Kao and Shih, 2007b), which is only about several μm. However, unlike d_{max}, the EDM drilling time does not increase monotonically with v_{max}. Smaller v_{max} results in slower stage movement and causes a slower response in drilling. Larger v_{max} contributes to faster stage movement, which is beneficial to quickly restore the normal discharge gap condition but is prone to cause the short circuit in the forward movement. Therefore, like t_{dt}, an optimal v_{max} exists in the selected v_{max} region (0.6 to 2.4 mm/s) for the minimum EDM drilling time. This leads to the DOE based optimal search for the t_{dt} and v_{max} in fuzzy logic control parameters to minimize the micro-hole EDM drilling time.

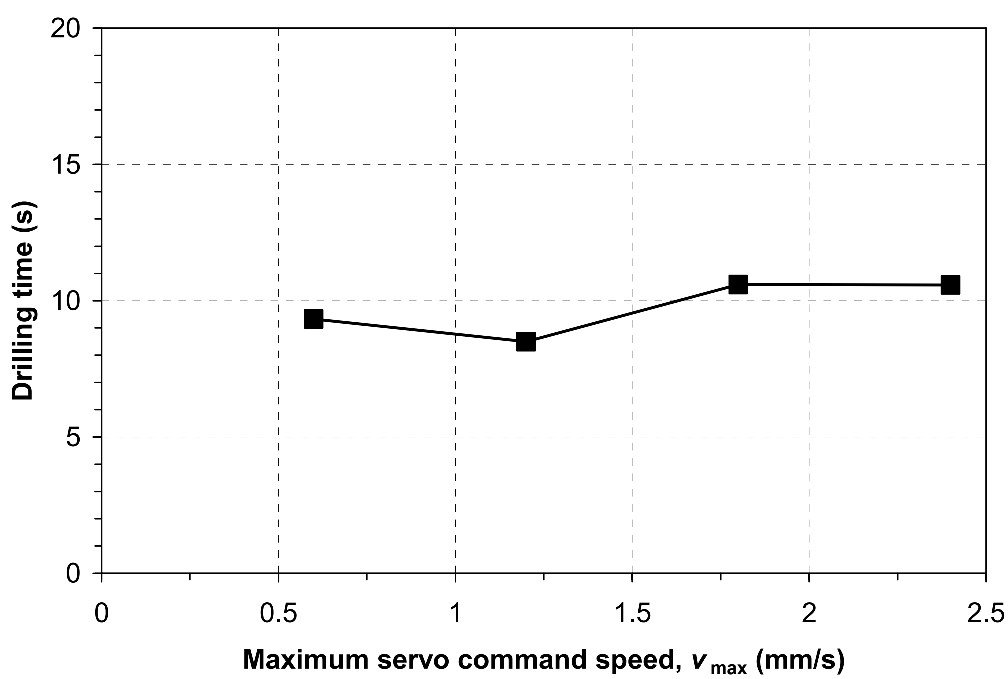

Figure 4.14. Effects of v_{max} on EDM drilling time (v_{max} = 0.6, 1.2, 1.8, and 2.4 mm/s).

4.1.7.4. DOE analysis of fuzzy logic control parameters

The DOE analysis of t_{dt} and v_{max} on the EDM drilling time generates a quadratic surface F, which is mathematically represented as $F(t_{dt}, v_{max})$ based on DOE experiment results.

$$F(t_{dt}, v_{\max}) = 13.7 - 0.0130t_{dt} - 3.08v_{\max} + 1.59\times10^{-5}t_{dt}^2 + 0.74v_{\max}^2 + 6.06\times10^{-3}t_{dt}v_{\max} \quad (3.4)$$

The value of F at specific t_{dt} and v_{max} is the EDM drilling time. A 3D visualization of F is illustrated in Figure 4.15. When t_{dt} and v_{max} are either very small or very large, i.e. at four corners of the quadratic surface, the corresponding F increases. The distribution of F suggests the existence of an optimal F value. As shown in Figure 4.15, the DOE analysis finds the minimum F = 10.52 s at t_{dt} = 62.0 μs and v_{max} = 1.82 mm/s.

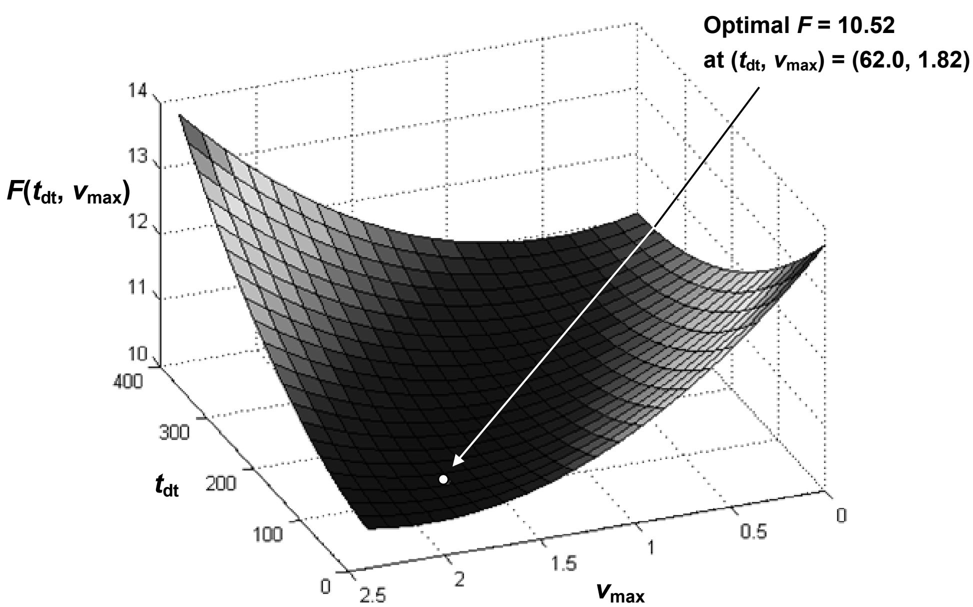

Figure 4.15. DOE generated surface $F(t_{dt}, v_{max})$ and the locations of optimal F by DOE analysis.

Cycle time results of 9 repeated EDM hole drilling experiments using the optimal t_{dt} and v_{max} with and without fuzzy logic control are shown in Figure 4.16. Without the fuzzy logic EDM control, the average drilling time is long, about 15.1 s with with standard deviation of 5.85 s. When the fuzzy logic EDM control is implemented, the average drilling time is reduced to 9.94 s with much less standard deviation of 0.69 s. It is also noted that the average drilling time, 9.94 s, under the fuzzy logic EDM control is very close to the estimated 10.52 s by the DOE analysis. The stability, consistency, and efficiency of micro-hole EDM process is greatly improved with the fuzzy logic EDM control.

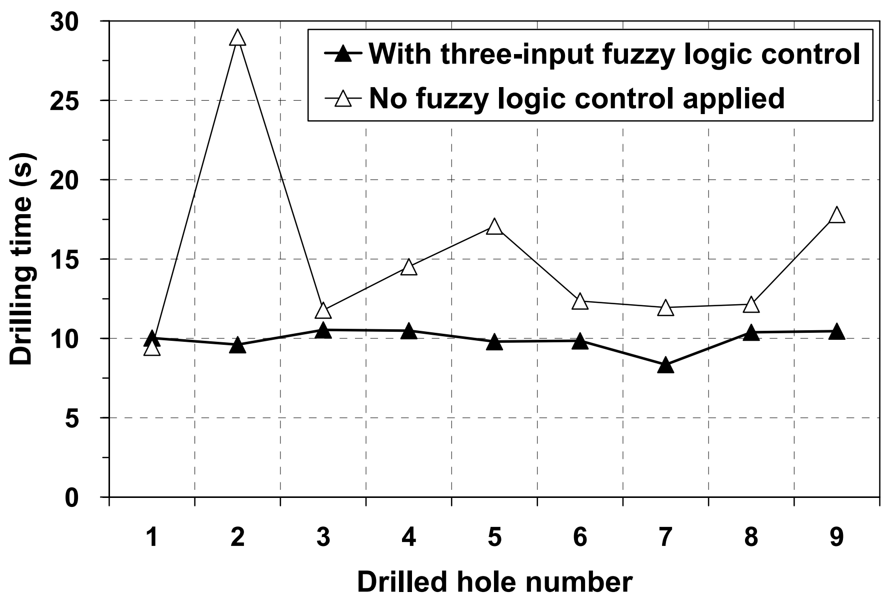

Figure 4.16. Experimental results of fuzzy logic EDM control at the optimal t_{dt} and v_{max} (three-input type, d_{max} = 2 μm, v_{max} = 1.82 mm/s, and t_{dt} = 62 μs).

4.2. Platform 2: AAM Micro-Hole EDM Machine

4.2.1. Overview

The design and tuning of the adaptive fuzzy logic controller are conducted on a micro-hole EDM machine made by AAM at Chelsea, Michigan. The electrode feed is performed by a DC servo motor, which is controlled by a Texas Instrument TMS320F2812 DSP. The machine has an onboard sensor system to monitor and record the EDM status, including the servo position and the number of spark and total pulses. The onboard EDM sensor system is controlled by an Altera Acex 1K field programmable gate array (FPGA) and synchronized with the DSP at an interrupt request (IRQ) frequency of 1000 Hz to update the servo motion command. In Platform 2, the computation cycle time of fuzzy logic reasoning needs to be tuned to less than 1 ms, which is determined by the 1000 Hz IRQ.

The number of spark pulses and total pulses in each sampling duration is acquired by the onboard EDM sensor and used to calculate the spark ratio R_s, defined as the number of spark pulses divided by the number of total pulses (Kao and Shih, 2007c; Kao and Shih, 2007d; Kao and Shih, 2007e). R_s is between 0 to 1. $R_s = 1$, when all pulses in the sampling duration are sparks and $R_s = 0$ when all pulses in the sampling duration are the arc and short circuit pluses. The R_s evaluates and represents the efficiency of EDM process in each IRQ period.

The adaptive fuzzy logic controller is compared with the gain scheduling controller of Platform 2. The software based tuning of fuzzy logic controller is presented to balance the computational capability of the controller and the level of data precision.

In this section, the design of adaptive fuzzy logic controller and experimental procedures are first presented. Results of the software based tuning and comparison with an existing gain scheduling EDM controller are discussed. Effects of fuzzy input parameter selection are compared. Finally, deep micro-hole (2.3 mm thick workpiece with 150 µm diameter electrode) and small diameter micro-hole (75 µm diameter electrode with 1.14 mm thick workpiece) EDM drilling are investigated to demonstrate advantages and adaptability of the fuzzy logic controller to different EDM configurations.

4.2.2. Fuzzy logic controller development and tuning process

4.2.2.1. Gain scheduling controller

Gain scheduling is the process control strategy currently used in Platform 2. The gain scheduling controller is specifically designed for general purpose injector spray holes. This controller has been developed and adjusted with years of practice in industrial applications.

This controller uses the gap voltage error, ΔV_g, the difference between the actual and a preset gap voltage, as the input parameter to schedule six operating conditions for servo motion synthesis. Each operating condition has a specific rule to adjust the servo speed. The servo speed is updated for each IRQ. The sign of ΔV_g is used to indicate the status of discharge gap distance. When ΔV_g is negative, meaning the discharge gap is narrowing, the electrode feed speed is reduced. If the value of reduction is higher than the current electrode feed speed, then the electrode is moved away from the workpiece. When ΔV_g is positive, the feed speed is increased in the direction toward the workpiece. The rule of adjusting servo speed depends on the operating condition, which is determined by comparing the ΔV_g to a preset value called breakpoint. Two quantities called breakpoint gain and reverse gain, both experimentally derived, are used for servo speed adjustment based on the difference between ΔV_g and the breakpoint, which is classified into six levels, negative big, negative small, zero, positive small, positive big, positive very big. Each level corresponds to an operating condition and both gains are adjusted in proportion to the difference value. For this gain scheduling controller, breakpoint gain is used for conditions of negative small and zero and reverse gain for all the other four conditions.

For each IRQ, the servo speed for next IRQ is updated by calculating a proper offset value and adding to the current servo speed. The sign of ΔV_g is used to indicate the status of discharge gap, the distance between the electrode and workpiece, and accordingly adjust the servo moving direction and speed. When ΔV_g is negative, meaning the discharge gap is narrowing, the speed offset would be negative to slow down the servo motion. If the speed offset is negative and larger than the current servo speed, then the servo speed for next IRQ would be negative and the servo will move away from the workpiece in next IRQ. When ΔV_g is positive, the speed offset would be positive to accelerate the servo motion toward the workpiece.

4.2.2.2. Fuzzy logic controller

The adaptive fuzzy logic controller, coded in C programming language, has the schematic diagram shown in Figure 4.17. The value of V_g is used to calculate the R_v for the identification of current EDM status (Kao and Shih, 2007c; Kao and Shih, 2007d; Kao and Shih, 2007e). The range of six R_v levels are experimentally determined:

- Open Circuit, $0.95 \leq R_v$.

- Good, $0.90 \le R_v < 0.95$.
- Fair, $0.70 \le R_v < 0.90$.
- Bad, $0.40 \le R_v < 0.70$.
- Dual State, $0.05 \le R_v < 0.40$.
- Short Circuit, $0 \le R_v < 0.05$.

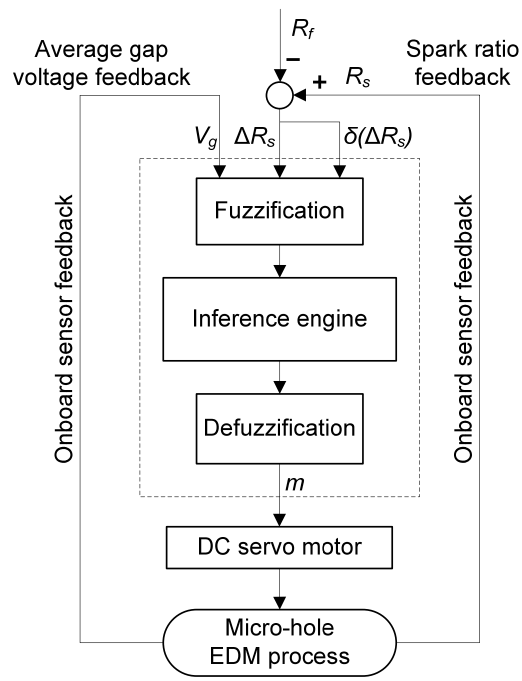

Figure 4.17. Schematic diagram of the adaptive fuzzy logic controller for AAM EDM machine.

Numbers of spark and total pulses during each IRQ period are updated by the onboard sensors and utilized to calculate the spark ratio R_s. The deviation of R_s from a preset value, R_f, is defined as the deviation of spark ratio, denoted as ΔR_s. R_f is the desired R_s value for a stable EDM process. ΔR_s measures the deviation between the desired and actual values. Large, negative ΔR_s means very low spark ratio and the electrode needs to quickly move away from the workpiece to restore the normal EDM status. For Platform 2, R_f, is experimentally determined as 0.8. ΔR_s is a potential input parameter for the fuzzy logic controller.

Another fuzzy logic input parameter is the change of ΔR_s from the previous sample duration, denoted as $\delta(\Delta R_s)$, which is used to indicate the trend of EDM status (Yan and Liao, 1998). In summary, three fuzzy input parameters, the average gap voltage V_g, ΔR_s, and $\delta(\Delta R_s)$, are available to synthesize the servo motion command, m, which is sent to the DC servo control and determines the speed and moving direction of the electrode.

Three linguistic values are associated with ΔR_s and $\delta(\Delta R_s)$: Positive (PO), Zero (ZE), and Negative (NE), as shown in Table 4.4.

Table 4.4. Fuzzy inference rules of the fuzzy logic controller for AAM EDM machine.

Good	Servo motion type, m		
	$\delta(\Delta R_s)$		
ΔR_s	PO	ZE	NE
PO	FF	FF	FO
ZE	FF	FO	FO
NE	FO	FO	DW
Fair	Servo motion type, m		
	$\delta(\Delta R_s)$		
ΔR_s	PO	ZE	NE
PO	FF	FO	FO
ZE	FO	FO	FO
NE	FO	DW	BA
Bad	Servo motion type, m		
	$\delta(\Delta R_s)$		
ΔR_s	PO	ZE	NE
PO	FO	FO	DW
ZE	FO	DW	DW
NE	DW	DW	BA

There are five linguistic values for *m,* Forward Fast (FF), Forward (FO), Dwell

(DW), Backward (BA), and Backward Fast (BF), which specify the direction and speed of servo motion. Dwell is used to describe the transition between Forward and Backward. A complete list of fuzzy inference rules for three EDM conditions, Good, Fair, and Bad, is summarized in Table 4.4. For computational efficiency, triangular membership functions are selected for input and output parameters and the area of aggregated membership functions is discretized as singletons. The discretization level l has substantial effects on the EDM drilling time and will be discussed in next section. Centroid method is applied to calculate output fuzzy value of m.

4.2.2.3. The tuning process

Tuning the fuzzy logic controller based on the data precision and discretization level is applied in Platform 2 to improve fuzzy logic reasoning speed. As summarized in Table 4.5, three major fuzzy logic controller data are the input parameter, output parameter, and linguistic variables. The input parameters can be coded using the regular floating point or the double precision floating point, denoted as *Float* and *Double*, respectively. The output parameters can be coded using the *Double* or integer (*Int*). The linguistic variables can be coded using *Int* and character (*Char*). *Float* and *Double* have 32 and 64 bits of data storage and represent the compromise on computational time and data precision. The *Int* has 16 bits of data storage. The *Char* is a string represented by a sequence of *Int*-based characters (Kernighan and Ritchie, 1988).

Discretization level l determines the resolution of membership functions, as shown in Figure 4.18. Higher l increases the resolution of fuzzy values at the penalty of computational time.

Table 4.5. Variable types and discretization level of three fuzzy logic controller tests.

		Test type		
		High data precision, high discretization level	Medium data precision, high discretization level	Medium data precision, low discretization level
Controller data	Input parameters	*double*	*float*	*float*
	Output parameters	*double*	*int*	*int*
	Linguistic variables	*char*	*int*	*int*
Discretization level		40	40	10
Computational time (ms)		4	1.5	0.7

double: Double precision floating point
char: Character
float: Floating point
int: Integer

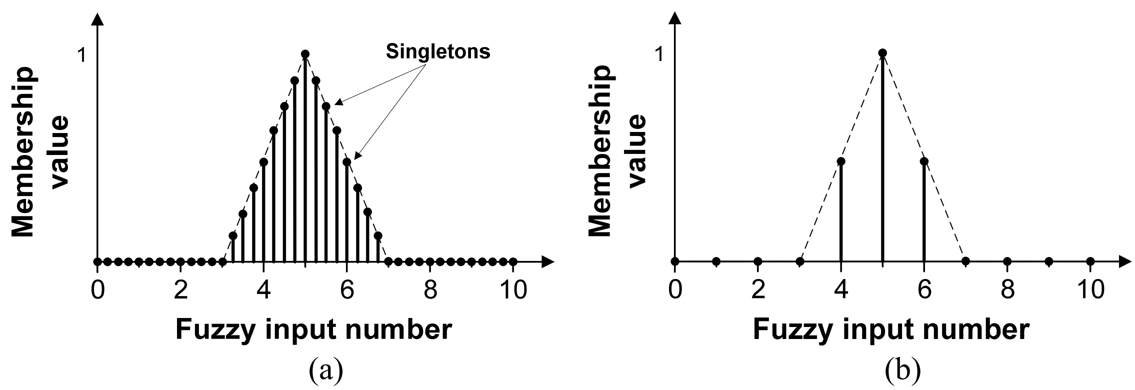

Figure 4.18. Discretization level *l* of membership functions: (a) high (*l* = 40) and (b) low (*l* = 10).

Proper selection of variable type and discretization level is important to the performance of fuzzy logic controller. In Platform 2, as shown in Table 2, three tests (i) high data precision and high discretization, (ii) medium data precision and high discretization, and (iii) medium data precision and low discretization, are conducted to tune the fuzzy logic controller.

4.2.3. Experiment design

Six sets of experiments, denoted as Exp. I to Exp. VI, are conducted. The workpiece for micro-hole EDM is hardened AISI 52100 steel disk. The thickness of workpiece is 1.14 mm in all experiments except for Exp. V which is 2.28 mm to study the deep micro-hole drilling. The diameter of the wire electrode is 150 μm in all experiments except Exp. VI, which uses the 75 μm diameter electrode to investigate the small diameter micro-hole drilling. The deionized water flush rate is 63 cm^3/min for all experiments.

The setup and purpose of Exps. I to VI are:

- *Exp. I. DOE analysis of EDM parameters for gain scheduling controller*: The DOE analysis searches the optimal setup of the discharge duration t_e, pulse interval time t_0, and open circuit voltage V_o based on the gain scheduling controller. The DOE utilizes the central composite response surface methodology with 6 center points (3 cube and 3 axial) and 1.414 axial ratio (MINITAB User Manual Release 14 for Windows, 2003).
- *Exp. II. Tuning of the fuzzy logic controller*: Three tuning tests in Table 2 are conducted.
- *Exp. III. Selection of fuzzy input parameters*: Five tests, three with single-input (V_g, ΔR_s, and $\delta(\Delta R_s)$), one with two-input (V_g and ΔR_s,), and one with three-input (V_g, ΔR_s, and $\delta(\Delta R_s)$) are conducted to study the effects of type and number of fuzzy input parameters on micro-hole drilling time.
- *Exp. IV. DOE analysis of EDM parameters for fuzzy logic controller*: Based on the

tuning process and the number of input parameters that yield the lowest drilling time, the DOE analysis is applied on the fuzzy logic controller to find the optimal t_e, t_0, and V_o that will yield the shortest drilling time.

- *Exp. V. Deep micro-hole EDM drilling*: The drilling time and waveforms of gap voltage and current for drilling the 2.28 mm deep hole are compared for the gain scheduling and fuzzy logic controllers.
- *Exp. VI. Small diameter micro-hole EDM drilling*: The DOE analysis is again applied to find the optimal t_e, t_0, and V_o setup. The drillng time and waveforms of gap voltage and current using the 75 μm diameter wire electrode are studied for the gain scheduling and fuzzy logic controllers.

4.2.4. DOE analysis of EDM parameters for gain scheduling controller (Exp. I)

Input values of t_e, t_0, and V_o and drilling time results of the 20 DOE tests are listed in Table 4.6. The range of input is 0.1 to 0.8 μs for t_e, 1 to 10 μs for t_0, and 180 to 220 V for V_o. Because only four t_0 values, 0.1, 0.2, 0.4, and 0.8 μs, are available for the EDM machine, the statistically determined optimal t_e is replaced by the closest value of available t_e. Each test is repeated three times and associated drilling time is averaged for analysis.

Table 4.6. DOE experiment setup for EDM parameter optimization using 150 and 75 μm diameter electrodes.

DOE test number	t_e (μs)	t_0 (μs)	V_o (V)	Average EDM drilling time (s)		
				150 μm		75 μm (Exp. VI)
				(Exp. I)	(Exp. IV)	
1	0.8	9	214	61	66	70
2	0.8	2	214	94	104	143
3	0.4	6	200	28	30	88
4	0.4	6	220	24	26	93
5	0.8	9	186	32	32	114
6	0.2	9	186	29	30	119
7	0.4	6	180	25	26	105
8	0.4	9	214	28	30	70
9	0.8	2	186	101	95	158
10	0.4	6	200	23	25	72
11	0.2	2	214	71	69	100
12	0.4	10	200	37	38	65
13	0.4	6	200	25	25	98
14	0.8	6	200	25	26	91
15	0.1	6	200	24	25	100
16	0.4	1	200	116	119	187
17	0.2	2	186	108	93	164
18	0.4	6	200	27	27	97
19	0.4	6	200	24	26	96
20	0.4	6	200	24	27	84

The response surfaces generated by the DOE are shown in Figure 4.19. An optimal value exists in the selected range. Using the MINITAB optimizer (MINITAB User Manual Release 14 for Windows, 2003), the expected optimal drilling time is 20 s at t_e = 0.268 μs, t_0 = 4.64 μs, and V_o = 200.0 V. Based on these values, the setup for gain scheduling controller is t_e = 0.2 μs, t_0= 5 μs, and V_o = 200 V. EDM micro-hole drilling experiments are conducted at this setup.

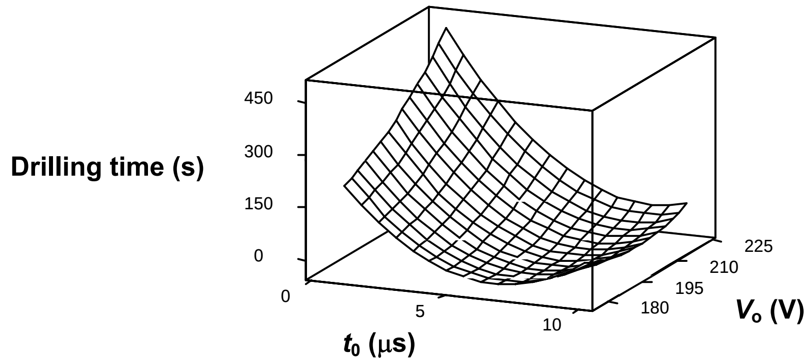

(a)

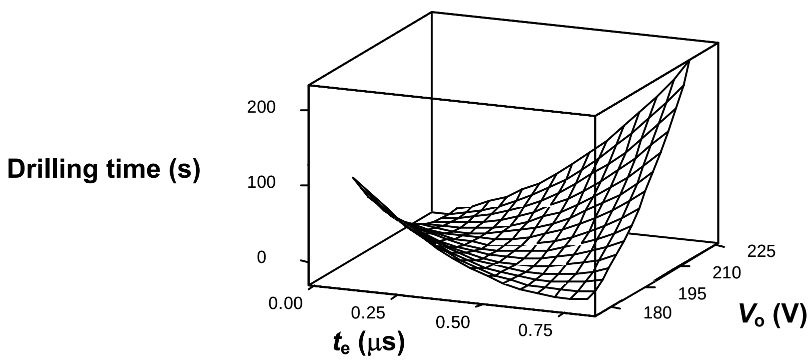

(b)

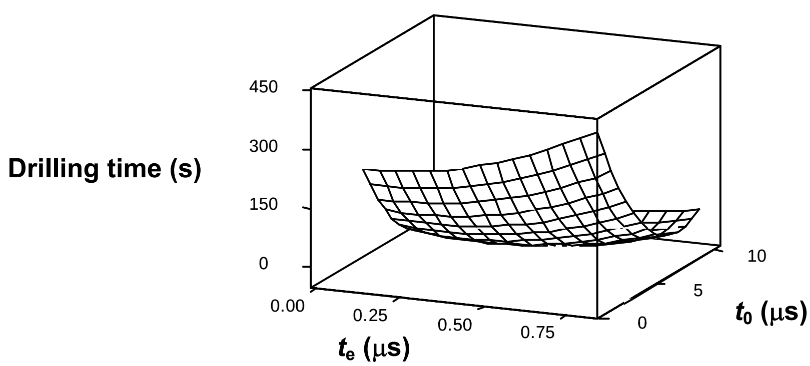

(c)

Figure 4.19. Response surfaces generated by the DOE analysis for 1.14 mm thick AISI 52100 using 150 μm diameter electrode: (a) t_0 and V_o (b) t_e and V_o, and (c) t_e and t_0.

The measured drilling time of 21 s, that is lower than the shortest drilling time, 23 s, in test 10 of the DOE in Table 4.6. This further validates the DOE approach and optimal setup. The optimal EDM parameter setup for t_e, t_0, and V_o is applied in Exps. II, III, and V.

The servo position and spark ratio R_s vs. drilling time of the gain scheduling controller is shown in Figure 4.20. The spark ratio is low, close to 0, in the first 0.8 s of drilling. After the initial unstable EDM period, the drilling process is relatively efficient and R_s ranges from 0.75 to 1, with occasionally drops to 0.5 or 0. In the last 2.7 s before the end of drilling, marked by A in Figure 4.6, the R_s value reduced significantly due to the difficulty of debris flushing. The drilling speed becomes very slow, which can be recognized by the nearly flat servo position curve in A.

After the sharpened electrode tip (see Figure 1.3) penetrates the workpiece, the electrode still needs to move forward for a specific distance to generate a complete hole with consistent diameter (Kao and Shih, 2006). This is marked as the electrode penetration in the final steep slope of the servo position curve.

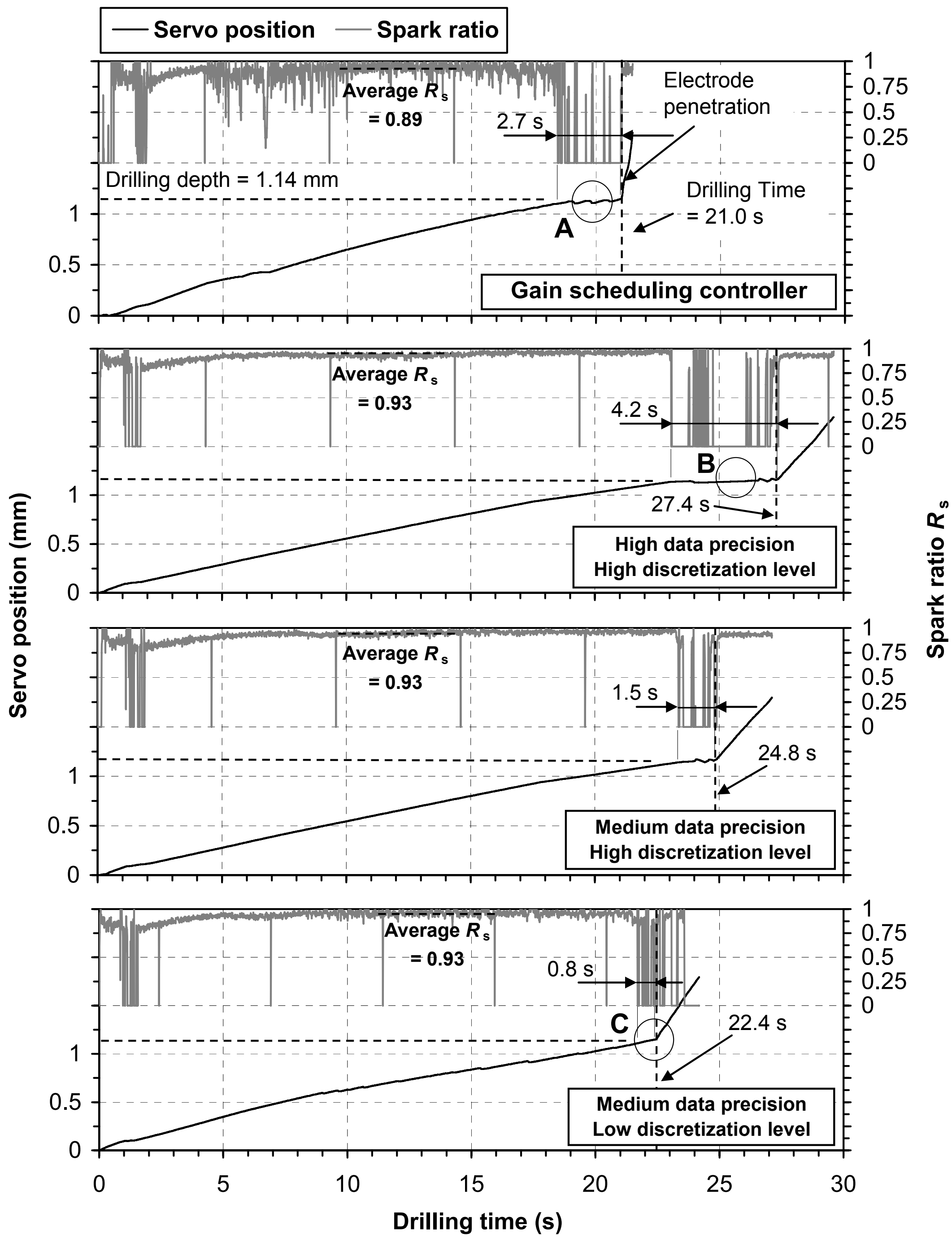

Figure 4.20. Comparison of servo position and spark ratio under gain scheduling controller and fuzzy logic controllers from three tuning tests.

4.2.5. Tuning of the fuzzy logic controller (Exp. II)

4.2.5.1. Effects of the computation time

Using the high data precision and high discretization level in Table 4.5, the fuzzy logic controller has good data resolution but long computational time, average about 4 ms, much longer than the 1 ms IRQ period. This makes the DSP wait longer for the servo command update from the fuzzy logic controller. This computational delay results in slow servo responses and renders this controller less capable. It is evidenced by the long, 27.4 s drilling time, as shown in Figure 4.20.

The medium data precision and high discretization level setup, the average computational time is reduced to 1.5 ms. The drilling time is reduced to 24.8 s. This illustrates the importance of computational time in fuzzy logic control. The average R_s is better, improved to 0.93.

The high data precision and low discretization level setup is tested but the average computational time is longer than 1 ms. A conservative approach using medium data precision and low discretization level is thus studied. The average computation time is reduced to 0.7 ms by lowering the discretization level from 40 to 10, as shown in Table 4.5. This is below the 1 ms IRQ period and ensures that almost all the servo commands can be updated on time. The drilling time is 22.4 s, which is comparable to, but still slightly longer than, the 21.0 s of the gain scheduling controller. A DOE analysis is conducted to find the optimal setup of V_g level, R_f, and l for the fuzzy logic controller but cannot further reduce the drilling time.

There are three major findings from the comparison of this three tuning test results with the gain scheduling controller. First, the gain scheduling is a good control strategy and has shorter drilling time compared to the tuned fuzzy logic controller for this specific EDM configuration. The major benefit of fuzzy logic controller is on the capability to handle different EDM configurations. This will be demonstrated later in Secs. 4.2.8 and 4.2.9 on the deep micro-hole and small diameter micro-hole drilling. Second, experimental results show that data precision will affect the computational time and consequently the drilling time and R_s. Last, the tuned fuzzy logic controller is more stable. The duration of unstable R_s at end of drilling is only 0.8 s, as shown by C in Figure 4.20, for the tuned fuzzy logic controller, much shorter than the 2.7 s for the gain scheduling controller. This will be proven later as critical to deep micro-hole drilling in Sec. 4.2.8.

4.2.5.2. EDM pulse train analysis

Representative pulse trains for gain scheduling controller and the three fuzzy logic controllers are shown in Figure 4.21. EDM discharges using the gain scheduling controller are dense and clustered, as marked by D and E. Clustered discharges may induce arc pulses and thus the pulse interval time t_0 is automatically extended, up to about 60 μs, by the gain scheduling controller to restore the normal EDM condition in the discharge gap. The dense and clustered discharges contribute to higher MRR at the penalty of more frequent arc pulses and its associated surface damage.

For the fuzzy logic controller with high data precision and high discretization level, long duration of open circuit is observed. The servo system is waiting during the long open circuit for the next command. This delay is due to long computational time. For the fuzzy logic controller with medium data precision and high discretization, due to the reduced computational time, the long open circuit is rare. But clustered discharges are not as frequent as those in the gain scheduling controller.

For the fuzzy logic controller with medium data precision and low discretization level, the discharge is uniformly distributed but without the cluster spark and arc pulses as in the gain scheduling controller. The challenge for fuzzy logic controller is on how to generate more frequent spark pulses for higher MRR, a topic for future research.

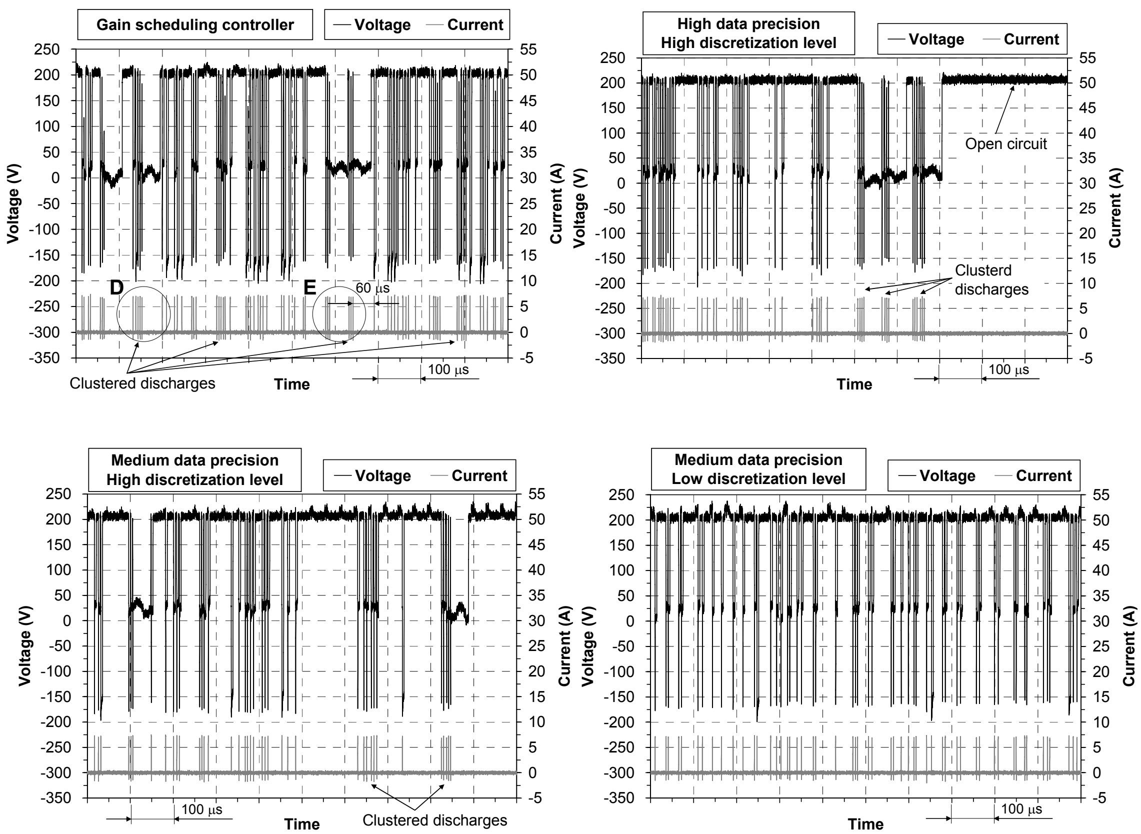

Figure 4.21. Representative gap voltage and current waveforms for gain scheduling controller and fuzzy logic controller in micro-hole EDM drilling.

4.2.6. Selection of fuzzy input parameter (Exp. III)

The servo position, R_s, and drilling time for three single-input parameter fuzzy controllers, V_g, ΔR_s, and $\delta(\Delta R_s)$, are presented in the top three graphs in Figure 4.22.

Based on the drilling time, V_g has the best performance, 27.2 s, among three cases of single input parameter. This confirms our earlier assessment that the V_g should be maintained at a constant value and is an important fuzzy logic input parameter for micro-hole EDM drilling. In comparison, ΔR_s is less effective (28.3 s) and $\delta(\Delta R_s)$, if used alone, is the least effective input parameter (30.5 s). When $\delta(\Delta R_s)$ is used alone, the oscillation of R_s at the start of drilling, as marked by F in Figure 4.22, is very significant, about 5 s. This is because at the early drilling stage, R_s changes rapidly and $\delta(\Delta R_s)$ is not capable of synthesizing correct servo motion.

When V_g and ΔR_s are used together for the two-input fuzzy controller, with the benefit of an additional parameter ΔR_s for servo motion synthesis, the drilling time is reduced from 27.2 s to 25.6 s. The three-input fuzzy controller using V_g, ΔR_s, and $\delta(\Delta R_s)$ has the shortest EDM drilling time, 22.5 s.

The selection of fuzzy input parameters has no significant effect on the spark ratio R_s, which is almost the same, about 0.93, for the five fuzzy controller designs in Exp. III.

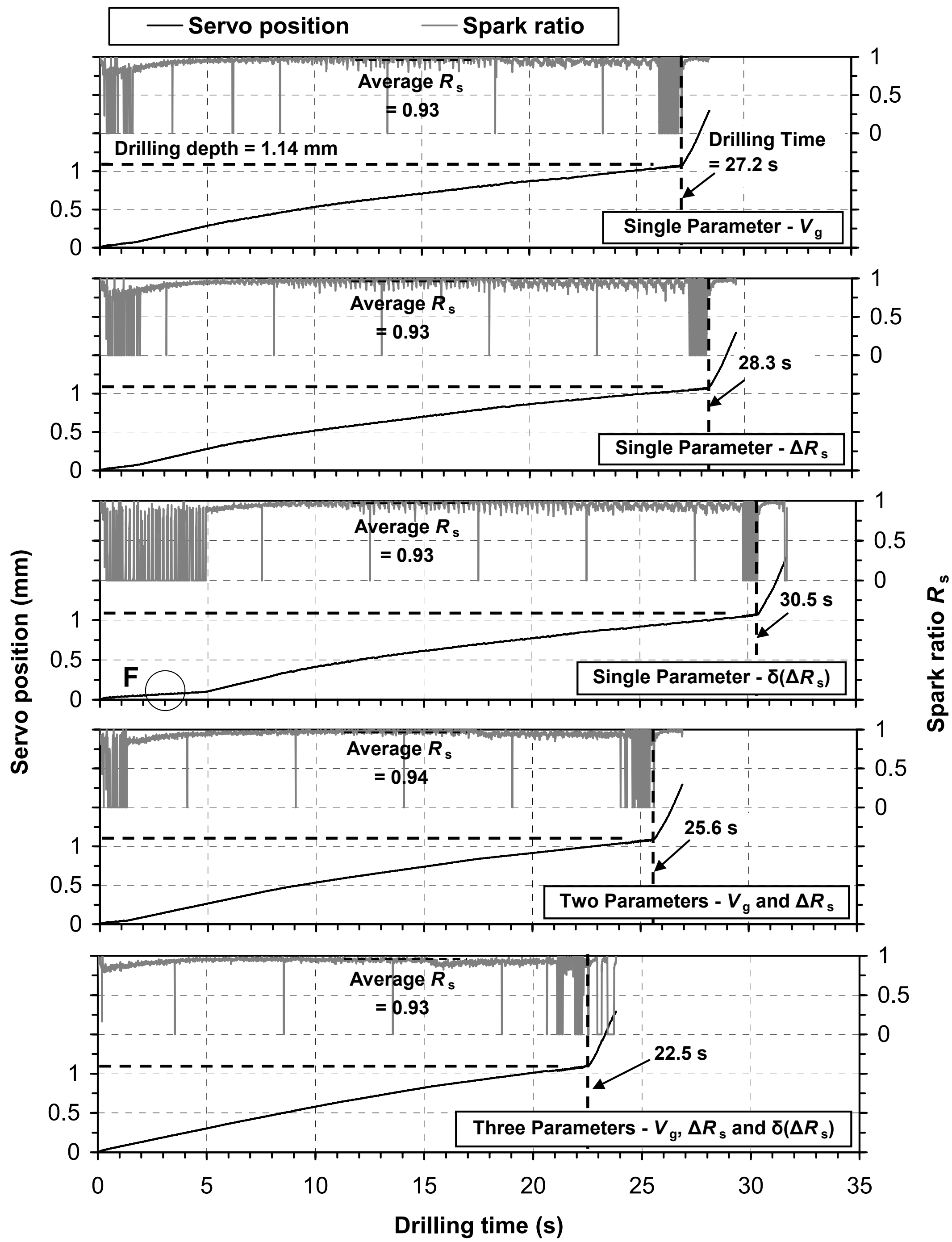

Figure 4.22. Effects of fuzzy input parameter selection (using the tuned fuzzy logic controller).

4.2.7. DOE analysis of EDM parameters for fuzzy logic controller (Exp. IV)

Drilling time results of DOE analysis to search the optimal t_e, t_0, and V_o setup for the three-input fuzzy logic control with medium data precision and low discretization level is presented in Table 4.6. The MINITAB optimizer finds that, under the setup of t_e = 0.162 μs, t_0 = 4.90 μs, and V_o = 207.6 V, the drilling time is expected to be 21 s. Experiments were conducted under this setup and the average drilling time is slightly longer, 22.5 s, which is about the same as that with the original setup t_e = 0.2 μs, t_0 = 5.0 μs, and V_o = 200 V obtained in Exp. I. The DOE analysis is not successful to further reduce the drilling time by varying the EDM setup. Therefore, the original setup of t_e = 0.2 μs, t_0 = 5.0 μs, and V_o = 200 V is used in the following deep micro-hole drilling experiment.

4.2.8. Deep micro-hole EDM drilling (Exp. V)

The servo position and spark ratio of 2.28 mm deep micro-hole EDM drilling using the gain scheduling and fuzzy logic controllers are shown in Figure 4.23. The gain scheduling controller cannot complete the deep micro-hole drilling. After 131 s, the electrode has moved only 1.6 mm. The fuzzy logic controller can successfully complete the deep micro-hole drilling in 105 s. It is much longer than the 21-22 s cycle time for drilling the 1.14 mm thick workpiece.

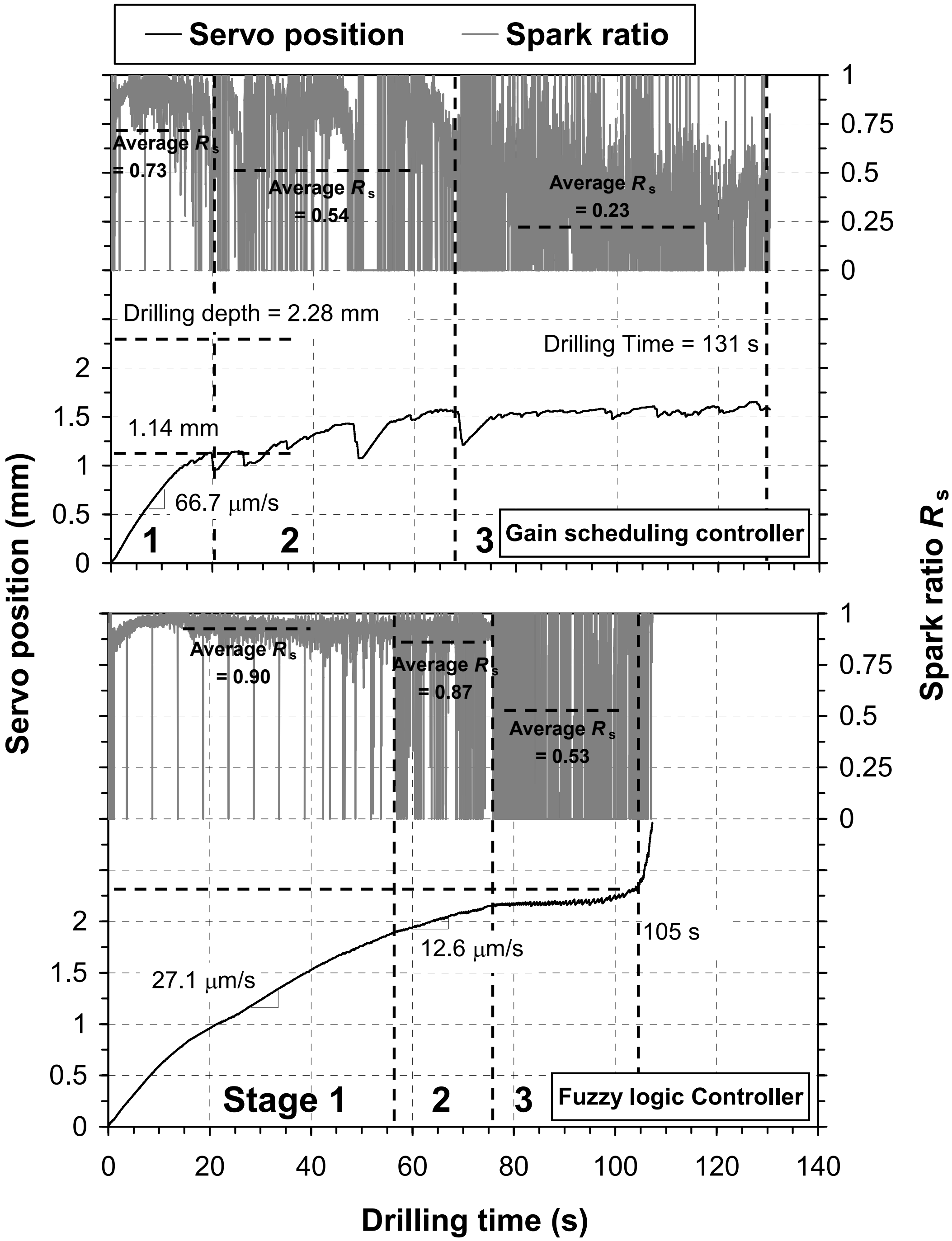

Figure 4.23. Deep micro-hole EDM drilling under gain scheduling controller and fuzzy logic controller.

For gain scheduling controller, the drilling to the 1.1 mm servo position is fast. It took about 20 s, which is comparable to the drilling time in Exp. I. After this threshold position the drilling process becomes unstable with occasionally large, up to 0.4 mm, backward motion away from the workpiece. On the contrary, the fuzzy logic controller is able to maintain a steady drilling speed to about 2.1 mm servo position. The drilling speed then decreases significantly but continues to perform drilling at a slower pace till the penetration. The failure of gain scheduling controller and the very long drilling time under fuzzy logic controller is primarily due to the difficulty of debris flushing, a challenge for deep micro-hole EDM drilling.

The deep micro-hole drilling process can be classified based on the level of R_s into three stages, designated as Stage 1, 2, and 3 in Figure 9. In Stage 1, both gain scheduling and fuzzy logic controllers can perform fast and stable EDM drilling. The R_s and average drilling speed (represented by the slope of the servo position vs. time curve) are maintained at a high level, 0.73 and 66.7 μm/s for the gain scheduling and 0.90 and 27.1 μm/s for the fuzzy logic controller, respectively. In Stage 2, R_s becomes unstable and changes rapidly between 0 and 1 for both controllers. The gain scheduling controller (R_s = 0.54) cannot maintain a steady servo motion toward the workpiece. For the fuzzy logic controller (R_s = 0.87), a slow (12.6 μm/s average speed) but steady servo motion is maintained in Stage 2. In Stage 3, the gain scheduling controller (R_s = 0.23) performs poorly and is unable to drill. For the fuzzy logic controller (R_s = 0.53), the servo motion exhibits smaller amplitude of back-and-forth oscillation, which lasts for about 30 s before the electrode penetrates.

Representative gap voltage and current waveforms of Stages 1, 2, and 3 are shown in Figure 4.24. Waveforms under the fuzzy logic controller are more uniform with less arc pulses than the gain scheduling controller in Stage 1. In Stage 2, for the gain scheduling controller, continuous arc and short circuit pulses due to difficulty of debris flushing are shown in Figure 4.24(a). Long, periodical open circuit pulses are observed for the fuzzy logic controller due to the frequent electrode retraction away from the workpiece for debris flushing. In Stage 3, as shown in Figure 4.24(b), the gain scheduling controller generates severe arc and short circuit pulses with virtually no spark for material removal. The fuzzy logic controller generates many long open circuits and a few sparks, which are enough to continue and complete the deep micro-hole drilling.

This experiment shows that the fuzzy logic controller is more adaptive to different micro-hole EDM drilling configurations.

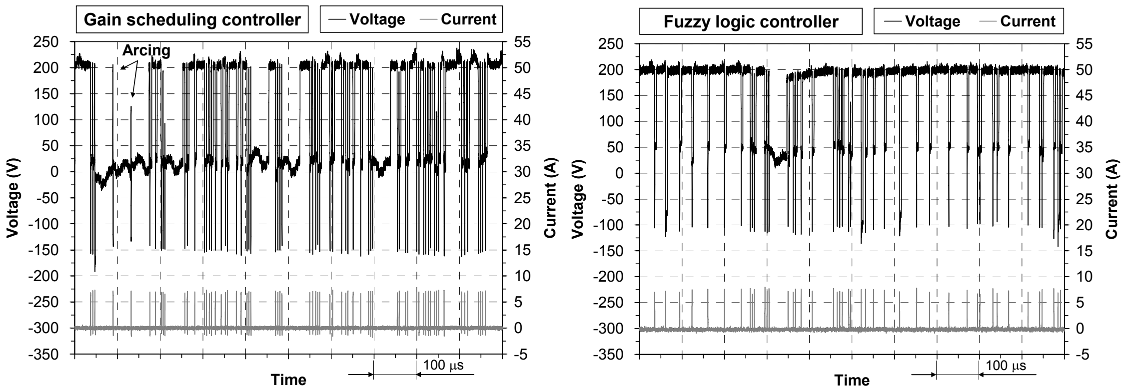

(a)

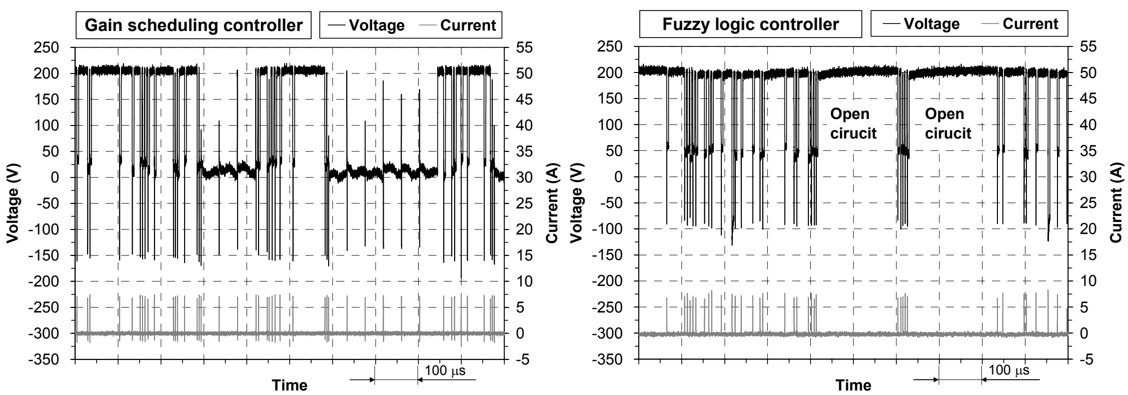

(b)

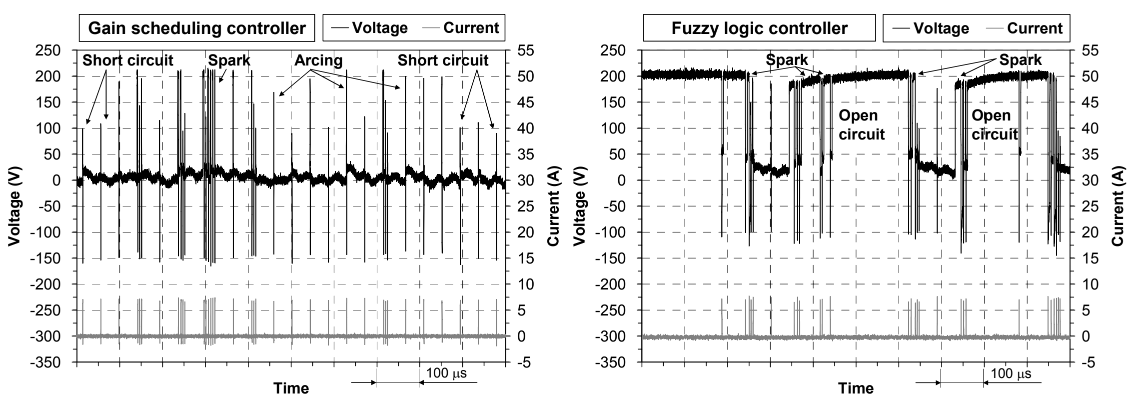

(c)

Figure 4.24. Representative waveforms of different stages in deep micro-hole EDM drilling under gain scheduling controller and fuzzy logic controller: (a) Stage 1, (b) Stage 2, and (c) Stage 3.

4.2.9. Small diameter micro-hole EDM drilling (Exp. VI)

The 75 μm diameter electrode significantly changes the EDM condition due to its thin size. DOE analysis is conducted to search the optimal t_e, t_0, and V_o setup for the fuzzy logic controller in small diameter micro-hole EDM drilling. The experiment setup and drilling time result of the 20 DOE tests are listed in Table 4.6. Three response surfaces generated by the DOE analysis are shown in Figure 4.25. The MINITAB analysis of optimal EDM setup is t_e = 0.4 μs, t_0= 8 μs and V_o = 200 V with the expected drilling time of 65 s, which is slightly longer than the experiment results (57 s in Figure 4.26).

The servo position and spark ratio of small diameter micro-hole EDM drilling are shown in Figure 4.26. Using the gain scheduling controller, the drilling time is 165 s. This is much longer than the 21 s cycle time for drilling the same thickness workpiece using the 150 μm diameter wire electrode. The servo position to penetrate the workpiece is 1.56 mm, much longer than the 1.14 mm thickness. This is due to the severe electrode wear, which is estimated to be 0.42 μm. Electrode wear, the difference between the workpiece thickness and the servo position at penetration, is small using the 150 μm diameter electrode. But for the 75 μm diameter electrode, the electrode wear is very significant due to high heat concentration and the lack of heat capacity at the tip of thin wire electrode. The worn electrode material becomes floating debris, which in turn increases the difficulty of flushing and makes the small diameter micro-hole EDM drilling difficult.

For fuzzy logic controllers, the drilling time is 57 s, much shorter than that of the gain scheduling controller (165 s) but still longer than the 22 s for drilling same thickness workpiece using 150 μm diameter electrode. The electrode wear, 0.41 mm, is about the same as that in gain scheduling controller. For both controllers, the drilling speed is reduced as the electrode advances deeper, due to the difficulty of flushing.

The small diameter micro-hole drilling process can also be classified by the R_s level into Stages 1, 2, and 3. In Stage 1, the R_s value is low and drilling speed is slow compared to those for 150 μm diameter wire electrode. Gap voltage and current waveforms for the gain scheduling controller in Stage 1, as shown in Figure 4.27(a), has a long sequence of short circuits (> 1 ms) with long open circuit followed by a cluster of discharges. This waveform pattern repeats for the gain scheduling controller in Stage 1. The fuzzy logic controller performs better, with higher average R_s value (0.37) and, as illustrated in Figure 4.27(b), has less frequent open circuit and more often sparks than the gain schedule controller.

In Stage 2, the drilling speed is maintained at an approximately constant value, 22.3 μm/s and 38.8 μm/s for the gain scheduling and fuzzy logic controller, respectively. Waveforms in Stage 2 are show in Figure 4.28. For the fuzzy logic controller, higher drilling speed results from more uniform and frequent spark pulses, as evidenced by the higher level of average R_s (0.83) in Figure 4.26.

In Stage 3, drilling using the gain scheduling controller becomes very slow, at 5.7 μm/s speed, due to inefficient debris flushing. Repeated short circuits, similar to Figure 4.27(a), are common and desired sparks are sporadically generated, as indicated by the low average R_s (0.27) and speed (5.7 μm/s). For the fuzzy logic controller, a much faster speed, 20.1 μm/s, is maintained in Stage 3 due to the better control to reduce short circuits.

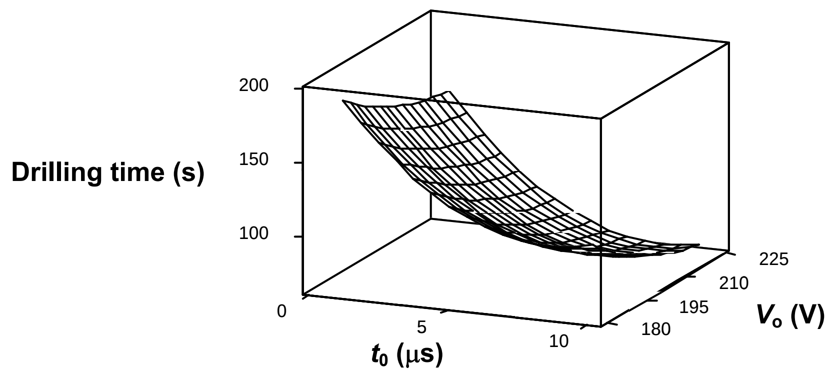

(a)

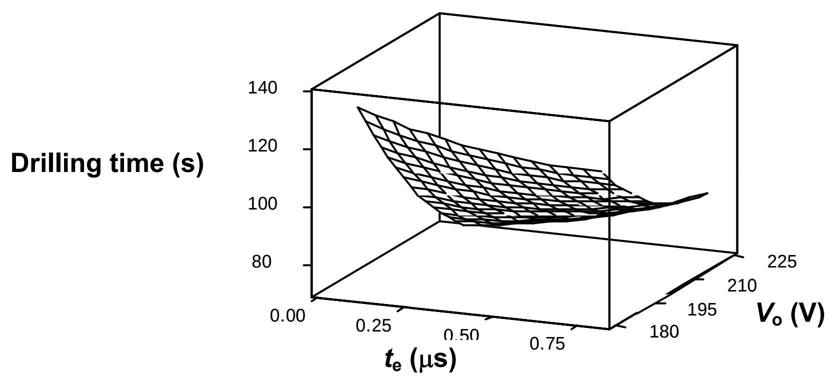

(b)

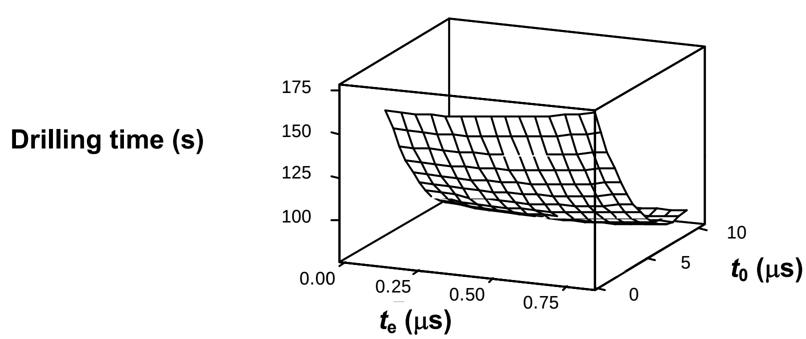

(c)

Figure 4.25. Response surfaces generated by the DOE analysis for 1.14 mm thick AISI 52100 using 75 μm diameter electrode: (a) t_0 and V_o (b) t_e and V_o, and (c) t_e and t_0.

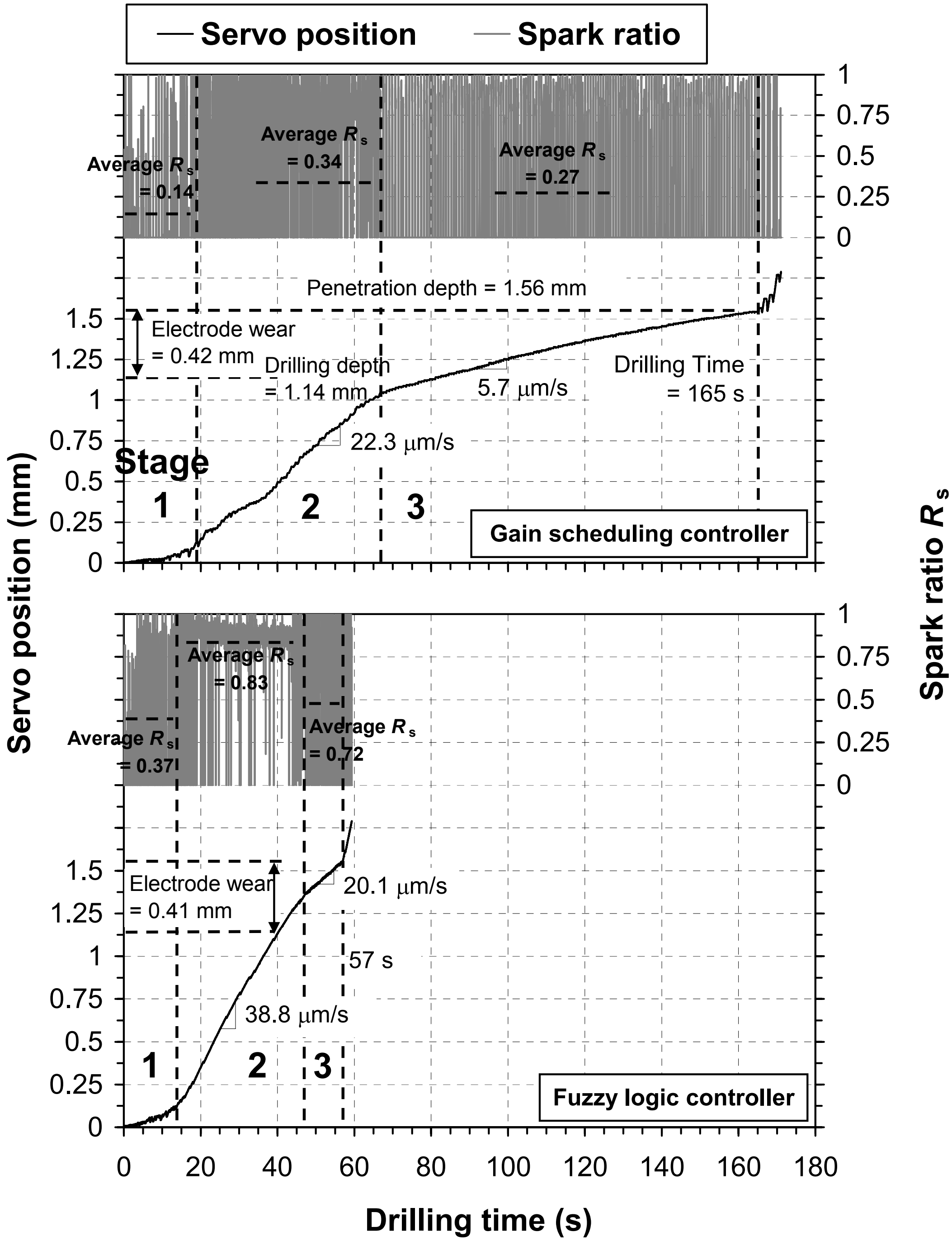

Figure 4.26. Small diameter micro-hole EDM drilling using 75 μm diameter electrode under gain scheduling controller and fuzzy logic controller.

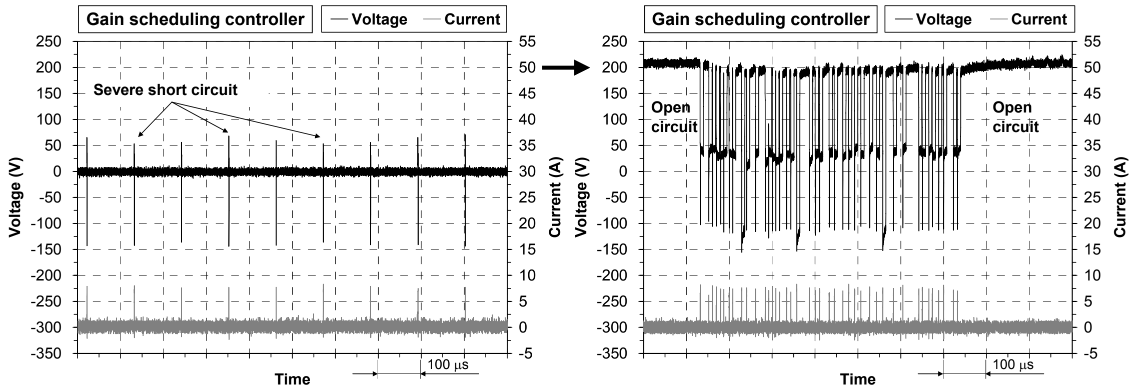

(a)

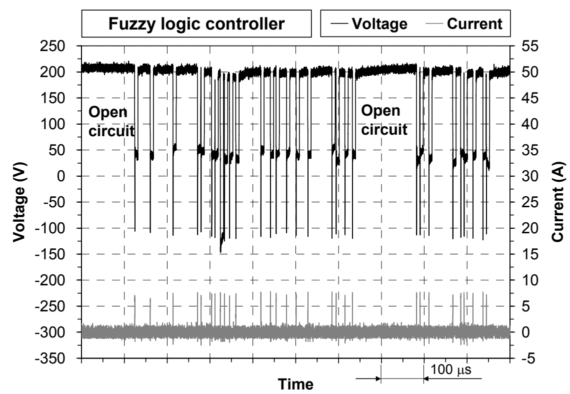

(b)

Figure 4.27. Representative waveforms of Stage 1 in small diameter micro-hole EDM drilling: (a) gain scheduling controller and (b) fuzzy logic controller.

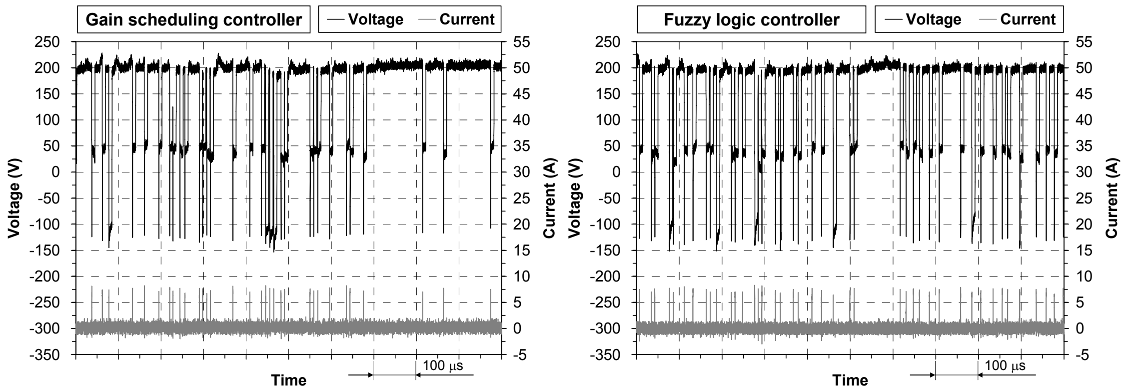

Figure 4.28. Representative waveforms of Stage 2 in small diameter micro-hole EDM drilling under gain scheduling controller and fuzzy logic controller.

4.3. Concluding Remarks

The adaptive fuzzy logic controller using three input parameters V_g, ΔR_s, and $\delta(\Delta R_s)$, demonstrated better EDM performance, in terms of drilling time, stability, and consistency, for Platform 1 and was more adaptive, as compared with the gain scheduling controller of Platform 2, to different EDM configurations.

For Platform 1, the EDM drilling efficiency was greatly improved with the proposed EDM control system integrating an adaptive fuzzy logic controller, a precision piezoelectric stage, and a digital data acquisition system. Effects of ignition delay threshold value t_{dt}, as well as maximum servo command displacement d_{max} and speed v_{max}, were quantitatively studied. The correlation between t_{dt} and v_{max} and associated effects on the EDM drilling time were studied through the DOE analysis. The optimal fuzzy logic control parameters were searched using DOE analysis and validated experimentally. Experiments conducted on Platform I showed that the discharge gap distance could be precisely controlled by the proposed fuzzy logic control system to suppress unwanted arc pulses and assure a smooth and stable EDM drilling process.

For Platform 2, the fuzzy logic controller demonstrated to be advantageous in deep micro-hole and small-diameter micro-hole EDM drilling due to its adaptability to different EDM configurations. The gain scheduling controller, specifically designed for general purpose diesel fuel injector spray holes, performed brilliantly with lower drilling time than the fuzzy logic controller but was not adaptive to other micro-hole drilling conditions. Proper tuning process to decrease the computational time by balancing the data precision and discretization level for fuzzy logic controller had been quantified. Three tuning tests were performed and effectively improve the drilling time from 27.4 to 22.4 s through the reduction of average computational time from 4 to 0.7 ms.

A study of single and multiple input parameters for fuzzy logic controller was conducted for both platforms. Multi-input fuzzy logic controller outperformed the single-input fuzzy logic controller because more reference information was available to generate adequate and objective servo commands.

The intelligent control systems could be considered as online, real time expert systems (Isermann, 1998). Based on the current configuration, the fuzzy logic EDM control system can be further developed by adding online optimization modules to enable the self-learning ability, or by building a database to store various type of micro-hole EDM drilling process information for offline user queries.

The reason gain scheduling controller could achieve faster drilling speed was the ability to generate more discharges in a unit time. The clustered spark and arc discharges, identified through the waveform analysis of measured gap voltage and current, were regarded as a feature of the gain scheduling controller and the key to fast EDM drilling speed. How to generate and control the cluster discharges using the fuzzy logic controller is a topic for future research.

Electrode wear was very significant in small diameter micro-hole EDM drilling. Debris flushing was very difficult due to the large amount of floating debris in the discharge gap. The efficient debris flushing for small diameter micro-hole EDM drilling needs advanced studies.

CHAPTER 5

CONCLUSIONS AND FUTURE WORK

This research advances the state-of-the-art micro-hole EDM drilling. Sub-ns monitoring and analysis of EDM pulses, adaptive fuzzy logic EDM process control and its application on deep and small diameter micro-hole EDM drilling, form measurement of micro-holes and gage R&R study, and the multi-stage EDM drilling for negative tapered micro-holes are developed.

5.1. Major Contributions

Major contributions are made in three research areas:

<u>EDM process monitoring</u>

- Sub-ns level monitoring was conducted to investigate spark and arc pulses for a better understanding of the micro discharging process. Nanosecond level interactions between the gap voltage and current were demonstrated in detail. A new phenomenon of pre-discharging current, a short time duration (less than 30 ns) current rise before the rapid voltage drop, was observed.

- The effect of electrode dressing using negative polarity was evidenced by SEM micrographs showing a blunted electrode tip, which was then utilized in the multi-stage EDM drilling to fabricate negative tapered micro-holes.
- A *RLC* circuit, derived from the inductance of the voltage probe jumper cable and parasitic capacitance and resistance of the wire electrode, was proposed to model the ringing effect generated at the end of discharges.

<u>Adaptive fuzzy logic control for micro-hole EDM</u>

- An advanced three-input fuzzy logic based micro-hole EDM control system was developed through the integration of an adaptive fuzzy logic controller, a precision piezoelectric stage, and a digital data acquisition system. The EDM drilling time was reduced through the precise discharge gap distance control by the fuzzy logic EDM control system.
- Experimental results validate that the three-input fuzzy logic controller outperformed the single- and two-input fuzzy logic controllers because more reference information is available to generate adequate and objective servo commands.
- The design and tuning of adaptive fuzzy logic controller for micro-hole EDM drilling were conducted on a commercial EDM machine. The computational time of fuzzy logic reasoning was experimentally confirmed as the major key to the controller performance and greatly improved by proper tuning methods, which achieved a balance between the fuzzy data precision and computational time.

- Average gap voltage V_g was an important parameter to the fuzzy logic controller and when used together with deviation of spark ratio ΔR_s and change of deviation of spark ratio $\delta(\Delta R_s)$ for the three-input fuzzy controller, contributed to the shortest drilling time compared with the single-input and two-input fuzzy logic controllers.
- The proposed fuzzy logic controller was more adaptive to different EDM conditions, as evidenced in experiments of deep micro-hole (2.3 mm thick workpiece with 150 μm diameter electrode) and small diameter micro-hole (75 μm diameter electrode with 1.14 mm thick workpiece) EDM drilling.

Form measurement of micro-holes and multi-stage EDM drilling

- Geometric (cylindricity, roundness, straightness, and taper) and dimensional (diameter) characteristics of typical 160 μm diameter micro-holes were measured in this research. Capable tolerance specifications for micro-holes were derived from the gage R&R study using the multi-sensor CMM.
- A multi-stage micro-hole EDM drilling technique, incorporating the pilot hole drilling and electrode dressing, was developed in this research. This EDM drilling technique could effectively and consistently fabricate 1.14 mm deep negative tapered micro-holes with inlet and outlet diameter difference larger than 15 μm.

This research showed that the three-input fuzzy logic controller was more adaptive than PWM and gain scheduling controllers and could effectively reduce the EDM drilling cycle time with better process stability and consistency. The multi-stage EDM drilling was proposed to generate negative tapered micro-holes and validated by the form measurement. This research, however, is not complete and future challenges will be discussed in the next section.

5.2. Recommendations for Future Study

Future researches can be conducted on minimizing the ringing effect, which is important to the reduction of drilling time, and the real time diagnosis of micro-hole EDM process to enhance the EDM drilling efficiency. The application of sub-ns EDM process monitoring can combine with plasma physics to study the nano-scale discharging mechanisms.

This study is a foundation for the development of intelligent control systems as well as real time expert systems. Based on the current configuration, the fuzzy logic EDM control system proposed in Chap. 3 can be further developed by adding online optimization modules to enable the self-learning ability, or by building a database to store various type of micro-hole EDM drilling process information for offline user queries.

Clustered discharges, generated by the gain scheduling controller, have been identified in this study as the key to faster drilling speed. How to generate and control the cluster discharges using the fuzzy logic controller is a topic for future research. For small diameter micro-hole EDM drilling, the severe electrode wear drastically increases the drilling time. Advanced researches are necessary to enhance the efficiency of small diameter micro-hole EDM drilling for HCCI and other technologies developed for future diesel engine fuel systems.

Besides diesel engine injector spray holes, micro-hole EDM has high potential for the fabrication of biomedical devices, such as the μm-level channels for microfluidics

(Sasaki et al., 2005) and surface texturing for implants (Lu and Leng, 2005). This research will be further expanded to biomedical applications of the micro-hole EDM.

All the recommended future researches can broaden the knowledge scope of, and further enhance the understanding for, micro-hole EDM drilling.

APPENDICES

Appendix A

Form Measurement of Micro-Holes

The form measurement and gage repeatability and reproducibility (R&R) of micro-hole using a coordinate measuring machine (CMM) with the combination of optical and contact sensors were conducted in this study. The micro-holes, about 160 μm in diameter and 0.9 mm in depth, were fabricated using EDM process for diesel fuel injectors. The shape and size of micro-holes are important for the desired spray pattern, fuel economy, and exhaust emission of diesel engines. In this study, the setup of measurement machine and procedure to determine the contact points are presented. Five form characteristics, the cylindricity, diameter, roundness, straightness, and taper, of the micro-hole are analyzed from measurement points. The gage repeatability and reproducibility test was conducted to determine the micro-hole form measurement capability and to calculate the tolerance specifications for each characteristic that the CMM is capable to measure. An example to quantify the change in shape of the micro-holes before and after the abrasive flow machining (AFM) was presented.

A.1. Introduction

Micro-holes, small holes with diameter less than 0.5 mm (Masuzawa et al., 1993), have a wide range of applications, including ink-jet printer nozzles, orifices for bio-medical device, cooling vents for gas turbine blade, and diesel fuel injector spray holes. Micro-holes can be fabricated by the EDM (Masuzawa et al., 1989), laser drilling (Giedl et al., 2003), electrochemical machining (Ahmed and Duffield, 1989), or conventional drilling (Iwata and Moriwaki, 1981). The micro-hole for diesel engine fuel injector, as illustrated in Figure A.1, is a representative of a high volume production application. The size, shape, orientation, flow rate, and surface roughness of the injector micro-hole are important to the spray pattern, fuel atomization and combustion, and emission of the diesel engine (Adler, 1994). This research investigates the form measurement of 0.16 mm diameter fuel injector micro-holes.

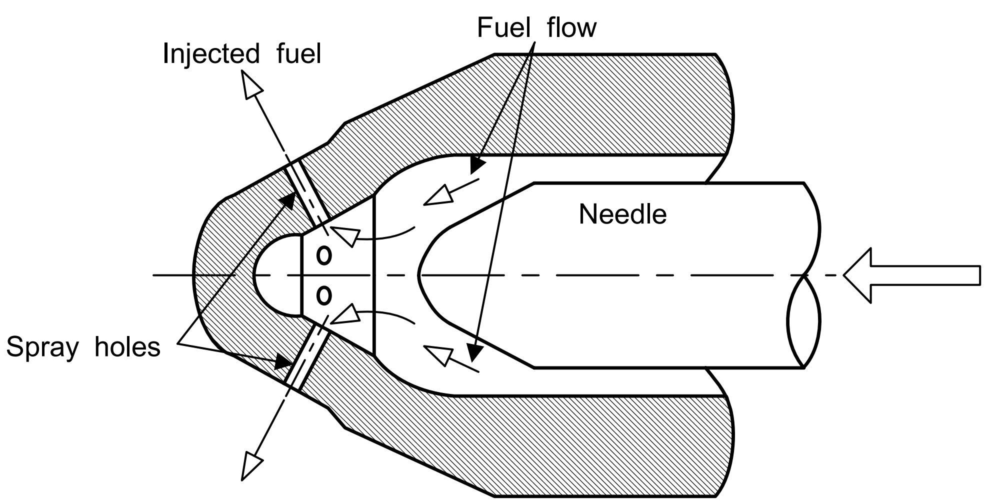

Figure A.1. Schematic diagram of diesel fuel injector micro-holes of an injector nozzle, a needle, and fuel flow.

EDM is the current production method to machine micro-holes for diesel engine fuel injector (Hebbar, 1992; Morita et al., 2000). A wire electrode is fed through a wire guide, which is made of ceramic for wear resistance, to drill a hole. Sparks at the tip of the wire electrode remove the work-material and, subsequently, wear the electrode to create rounded tip. The EDM micro-hole drilling process for diesel injector was developed in the early 1970s when the heat-treatment process was utilized to increase the material strength for high pressure fuel injection and emission reduction. Due to the stringent diesel emission regulations (Johnson, 2003; Holt, 2004), the form measurement of injector micro-hole has become an important quality control tool that bridges product design and manufacturing for diesel engine emission reduction.

Accurate form measurements of micro-holes are difficult due to the small diameter and high aspect ratio. State-of-the-art injector micro-holes for on-highway truck diesel engines are usually 150 to 200 μm in diameter and 1 mm in depth. Conventional CMM and vision-based systems are not capable for form measurements of the micro-hole (Masuzawa et al., 1993; Kim et al., 1998; Yamamoto et al., 2000). The micro-holes are currently evaluated using a destructive method (Diver et al., 2004) to cut hole cross-sections and/or the plastic molding to make a replica of micro-holes (Hebbar, 1992). Both methods provide limited information on the form accuracy and dimension of micro-holes.

New micro-hole measurement methods were developed in 1990s. The vibroscanning method, developed by Masuzawa's research group at University of Tokyo, utilized the vibration of a thin probe to detect the contact and measure the form accuracy of micro-holes (Masuzawa et al., 1993). More advanced vibroscanning methods were developed to measure the workpiece made of non-conductive materials (Kim et al., 1998;

Yamamoto et al., 2000; Masuzawa et al., 1997; Kim et al., 1999; Pourciel et al., 2001; Lebrasseur et al., 2002; Pourciel et al., 2003). Another method applies the combination of contact and non-contact (optical) sensors in a CMM. This multi-sensor technology, developed by Werth GmbH (Christoph, 2004), is studied in this research for micro-hole measurement. The micro-hole shape measurement, gage repeatability and reproducibility (R&R), and effect of abrasive flow machining (AFM) on the shape and size of micro-holes are investigated.

Giedl et al. (2003) has classified the shape of micro-hole: negative taper, positive taper, and rounded flow entry (flow inlet), as shown in Figure A.2. In EDM drilling, if the process parameters remain the same throughout the drilling, the hole will have positive taper due to the wear of wire electrode. Advanced micro-hole EDM adjusts the process parameters in different stages to control the hole shape (Kao and Shih, 2006). At the start of drilling, the negative polarity (anode for the wire electrode and cathode for the workpiece) is applied to blunt or flatten the tip of electrode sharpened after micro-hole drilling. This is called electrode dressing.

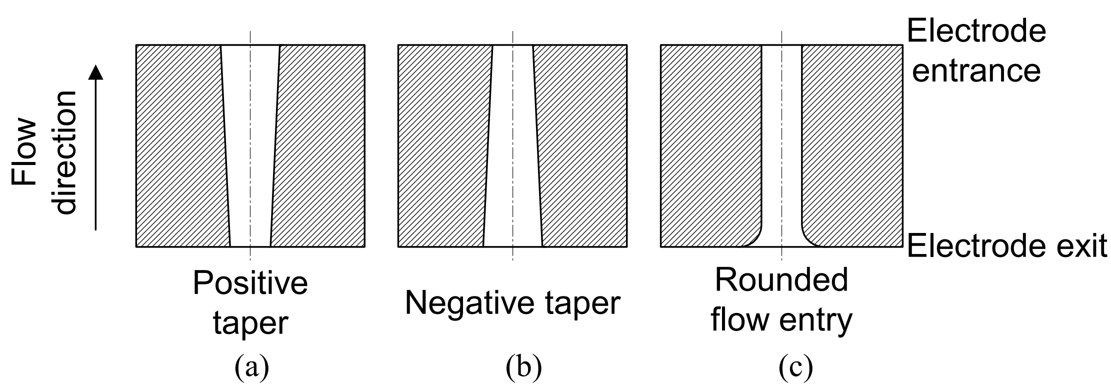

Figure A.2. Classification of shape of a micro-hole for the fuel injector: (a) positive taper, (b) negative taper, and (c) rounded flow entry.

Figures A.3(a) and (b) show the tip of a 125 μm diameter tungsten electrode after the micro-hole drilling and electrode dressing, respectively. A flat end electrode can reduce the positive taper of the drilled hole. Near the end of micro-hole drilling, the gap voltage is increased to enlarge the gap width inside the micro-hole to enable the generation of negative taper, as shown in Figure A.2(b). The rounded flow entry, as shown in Figure A.2(c), can be achieved using the AFM, which flows abrasive media through the micro-hole under high pressure to round the inlet edge of the micro-hole (Perry, 1986; Stackhouse, 1993; Loveless et al., 1994). Both negative tapered hole and rounded flow entry have proven to improve the diesel fuel flow and atomization characteristics and can reduce engine exhaust emissions (Giedl et al., 2003; Diver et al., 2004). The CMM measurement provides a quantitative method to specify and evaluate the effect of AFM on micro-hole geometry.

(a)

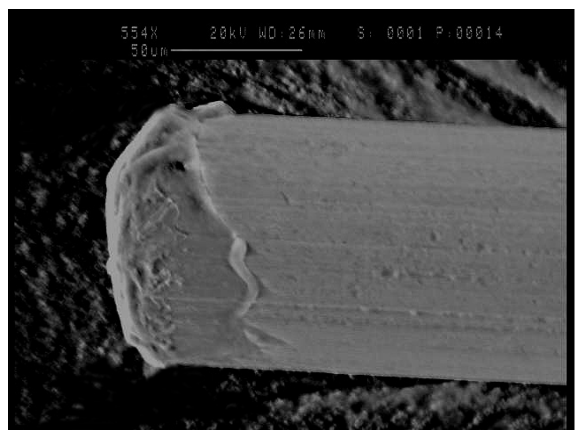

(b)

Figure A.3. SEM micrographs of the tip of tungsten wire electrode: (a) sharpened electrode tip after EDM Stage 2 and (b) blunted electrode tip after EDM Stage 1 (diameter of wire electrode: 125 μm).

In this appendix, the measurement machine setup is first presented. The EDM process parameters and measurement procedure for micro-hole are then discussed. Measurement results for form and dimension accuracy of micro-hole are then analyzed.

Gage R&R of micro-hole characteristics are discussed. Finally, the effect of AFM on the shape and size of micro-hole is demonstrated.

A.2. Measurement Machine Setup

A.2.1. Measurement machine

Measurements of injector micro-holes were conducted in a Werth VideoCheck HA 400 CMM. Figure A.4 shows the schematic diagram of the CMM measurement setup using a glass-fiber probe with a ball end tip and a charge coupling device (CCD) optical sensor to measure the ball position.

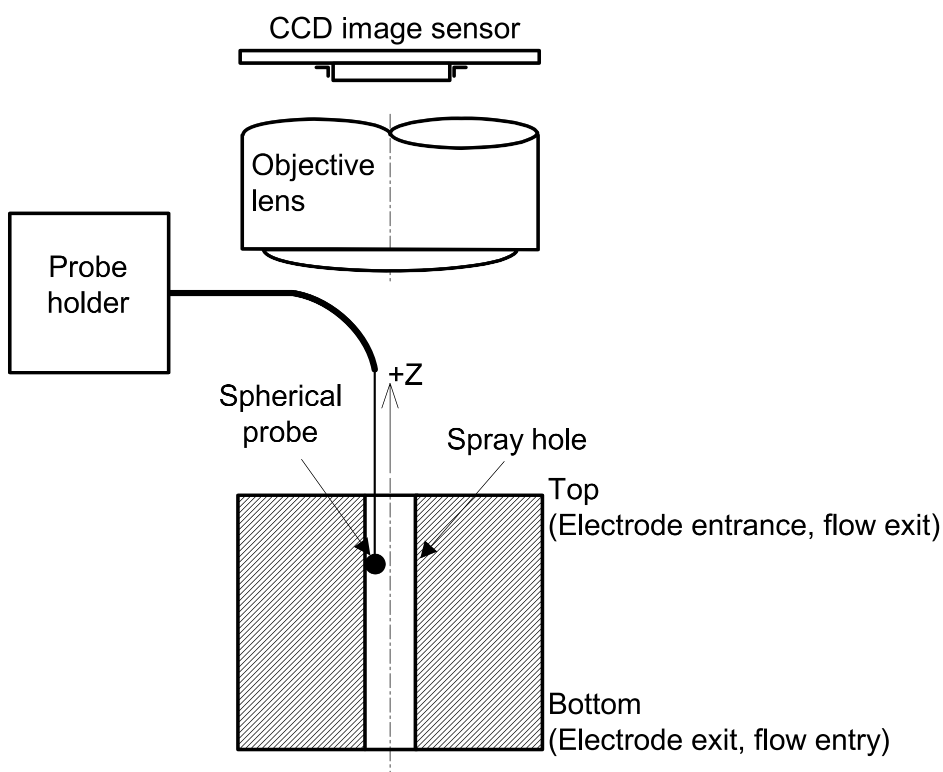

Figure A.4. Micro-hole measurement using the combination of optical and contact sensors in a CMM.

An overview of the experimental setup is shown in Figure A.5(a). The probe is made of glass and its tip has a spherical ball of 74 μm diameter. The ball is connected to a 25 μm diameter and 1.5 mm long glass fiber shank. Connecting to the glass fiber is the 20 mm long tapered glass shank which gradually increases the diameter from 25 to about 200 μm. This is illustrated in the close-up view of the nozzle tip and the glass probe in Figure A.5(b). The ball end tip of the probe in Figure A.5(b) is inside the micro-hole.

Three light sources are available from the inside, top, and bottom of the micro-hole. The light can be transmitted through the glass to illuminate the inside of the micro-hole. On the top is the light around the objective lens. Inside the nozzle, a 1 mm diameter metal tube with a reflective mirror at the tip delivers the light to the bottom of the hole.

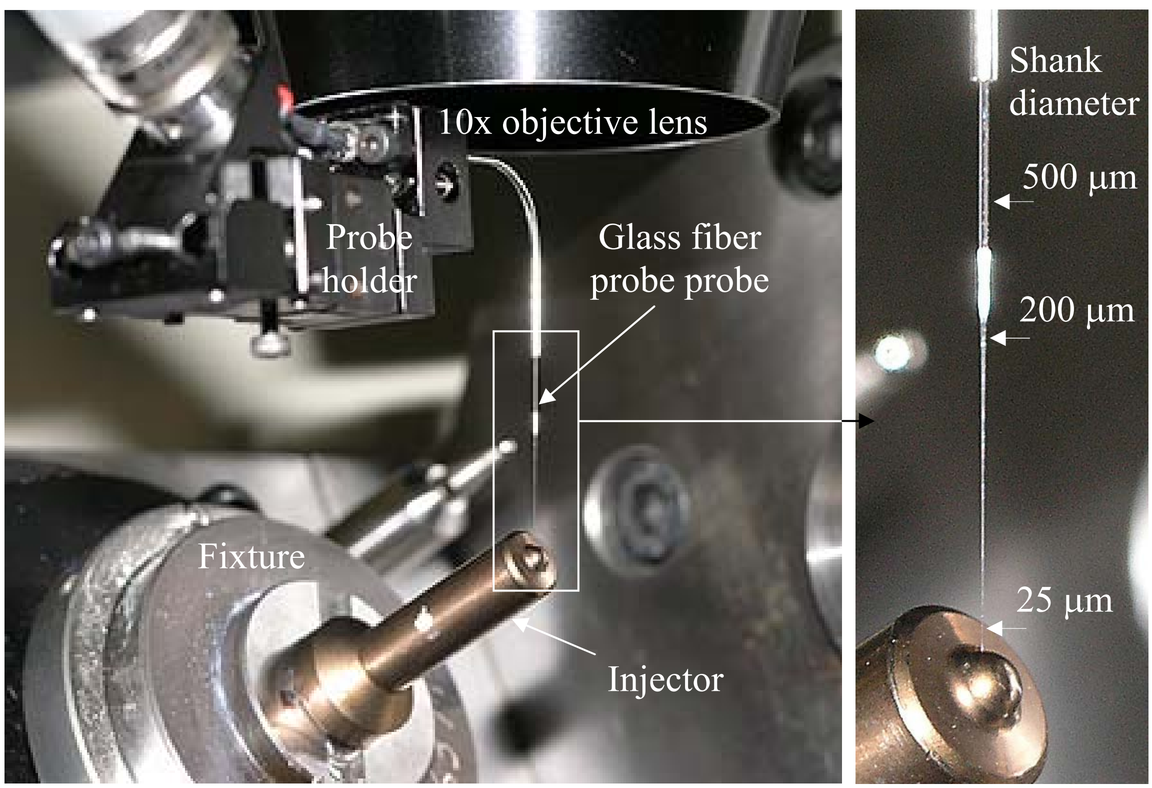

Figure A.5. Setup of micro-hole measurement: (a) overview of the nozzle, probe, and optical lens and (b) close-up view for the glass fiber probe.

The CMM has three axes. The injector with micro-holes is carried by the X and Y axes. The probe is moved up and down by the Z axis. All axes have 0.1 μm resolution and are moved by either the manual or computer-control mode.

A specially designed fixture, which can orient the micro-hole by three mutually perpendicular and computer controlled axes, is used to hold the injector.

A.2.2. Machine setup

Three setup procedures are performed: (1) align the axis of probe to the Z axis of CMM, (2) align the axis of hole to the axis of probe, and (3) identify the top datum circle of the hole.

A precision ring with mirror-polished taper inner surface is used as an artifact to align the axis of probe to the Z-axis of CMM. The ring is placed on a fixture, which aligns the axis of ring to the Z-axis. Orientation of the probe is adjusted by two rotational axes to avoid the interference between the probe shank and the inner surface of tapered ring, as shown in Figure 6(a). The taper and mirror-surface of the ring are important features to identify the interference if it does occur. If the shank touches the surface first, the view of the probe's ball tip and its mirrored image on the polished ring inner surface will separate. The interference check is evaluated at four positions, 90° apart from each other, around the circumference of the ring inner surface.

After the probe is aligned to the Z-axis of CMM, the ball tip is moved inside the micro-hole, as shown in Figure 6(b), to align the axis of hole to the axis of probe. The micro-hole in the injector is oriented to avoid the interference of the probe shank and micro-hole at four positions, 90° apart from each other, around the circumference of micro-hole. Since the difference of the radius between the ball and shank in the probe tip is only 25 μm, the hole is well aligned if no interference of the shank and the hole is achieved.

After the injector and micro-hole are aligned, the probe is moved to touch the top of the hole to identify the top circle of the hole as the datum for Z direction. A fine movement of the probe along the Z-axis is performed to find the edge of the hole, as shown in Figure 6(c). If the ball is above the edge of the hole, as shown by the probe on the left in Figure 6(c), the whole ball can be observed and the position of the probe needs to be lowered in the Z-axis. This procedure is repeated in 12 positions, 30° apart from each other, around the circumference of the top edge of the hole to find the Z-axis datum location. This position is set as the zero for Z-axis in the subsequent measurement.

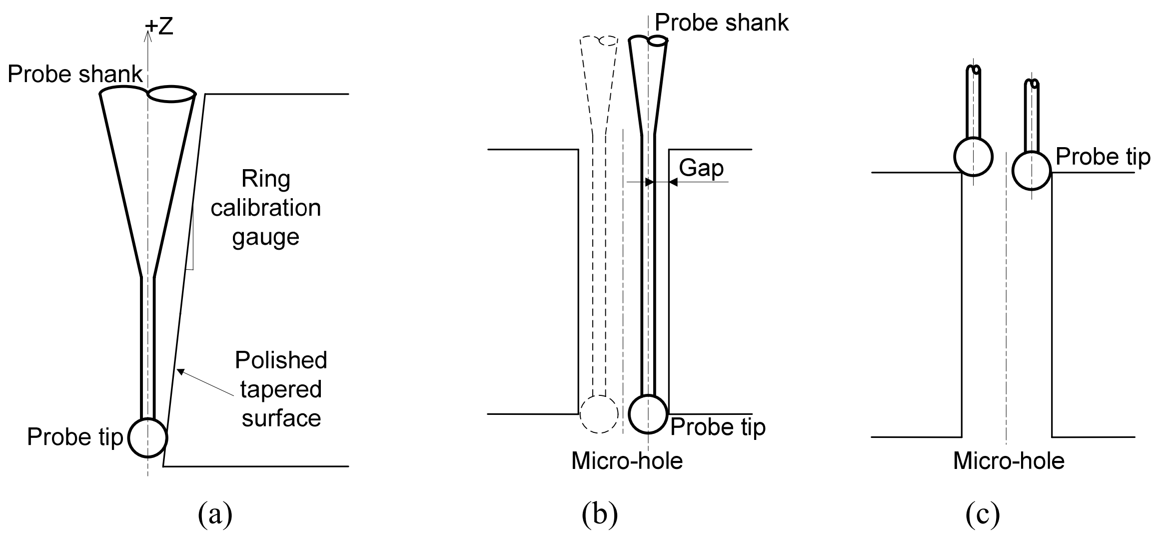

Figure A.6. Three setup procedures: (a) align the probe to the CMM machine Z axis, (b) align the micro-hole to the calibrated probe, and (c) locate the top datum circle and reference point of the micro-hole.

A.2.3. Determining the coordinates of contact points

The contact point between the ball tip of the probe and the hole surface cannot be detected by the CCD image sensor. Figure A.7(a) shows the image captured by the CCD when the probe is positioned near the center of the hole. When the probe is moved to contact the hole surface, as shown in Figure A.7(b), only a portion of the ball near the hole center is visible. The image processing software is utilized to define a rectangular box, as shown in Figure A.7(b), to enclose the arc region of the ball to find its center position and radius.

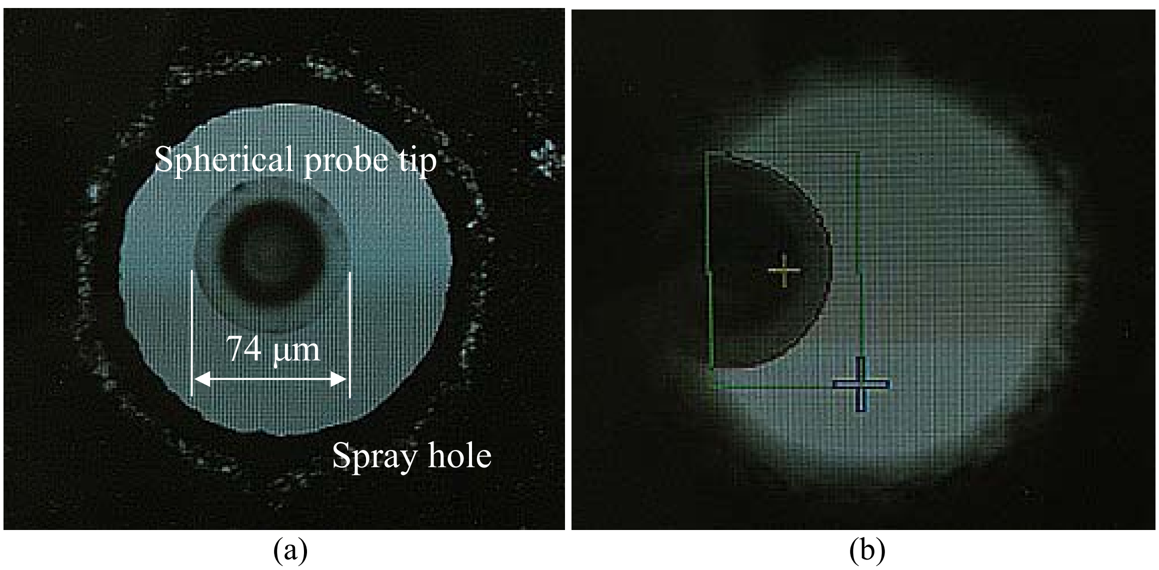

Figure A.7. The measurement of a micro-hole by the spherical probe tip: (a) the spherical probe tip inside a micro-hole and (b) the spherical probe tip in contact with the micro-hole and the user-defined rectangle for arc identification.

Mathematically, as shown in Figure A.8, the point P1 can be found using the CMM. The probe is contacted with the hole at 12 locations, 30° apart from each other, under the same Z position. The centers of the probe tip in the next two contact locations are marked as P_2 and P_3. Sequentially, the probe center from P_4 to P_{12} can be measured. Using the information of P_1 to P_{12}, the center of the circle O can be found. The vector from the center O to the contact point C_1 is derived using the following equation.

$$\overrightarrow{OC_1} = (r + |\overrightarrow{OP_1}|)\frac{\overrightarrow{OP_1}}{|\overrightarrow{OP_1}|} \tag{A.1}$$

where r is the radius of the probe tip. The contact points C_2 to C_{12} can be found following the same procedure.

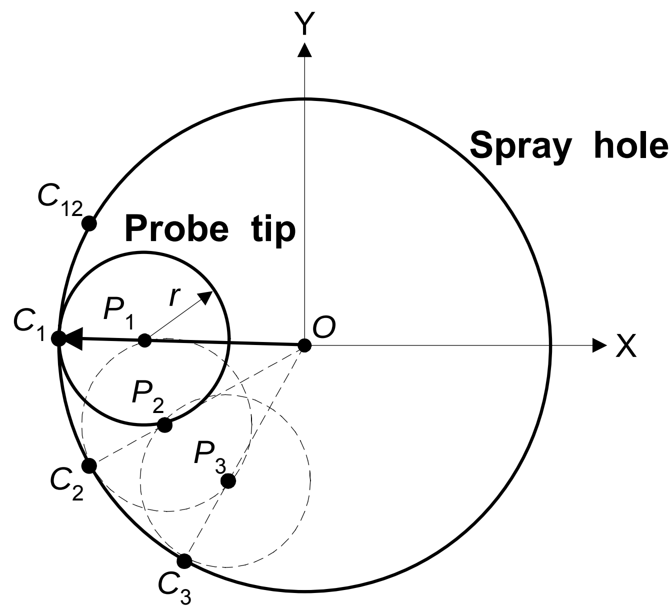

Figure A.8. Determination of the contact point between the micro-hole surface and the probe tip.

The contact points on circles at different Z positions are measured to create an array of contact points to represent the micro-hole.

A.3. Micro-Hole Preparation and Measurement Procedure

A.3.1. Fabrication of injector micro-holes

The micro–holes, about 0.9 mm deep and 160 μm in diameter, were drilled using 127 μm diameter tungsten wire electrode. The EDM process parameters vary at three drilling depths, denoted as Stage 1, 2, and 3. Table A.1 lists key EDM process parameters of three Stages.

Stage 1 is used for electrode dressing. Negative polarity and low gap voltage were applied to blunt the sharp electrode tip, as illustrated in Figure A.3, in the first 0.1 mm of drilling depth, denoted as *D*. Most of the drilling, with *D* from 0.1 to 0.76 mm, was completed in Stage 2 using the positive polarity and moderate gap voltage (200 V). The gap voltage was increased to 260 V in Stage 3 to enlarge the gap width between the electrode and workpiece. This setup generates the negative taper, as illustrated in Figure A.2(b). Three micro-holes, machined under identical EDM process setup, were used in this measurement study.

Table A.1. Process parameters of three Stages in micro-hole EDM.

Stage	1	2	3
Function	Electrode dressing	Drilling	Penetration
Drilling depth, *D* (mm)	0.10	0.762	1.20
Electrode travel relative to the hole depth (%)	11	73	16
Gap voltage, V_g (V)	160	200	230
Polarity	Negative	Positive	Positive

A.3.2. Procedures for measurement

As shown in Figure A.9, the micro-hole was measured using 12 contact points in 12 sections in the Z-axis direction. Positions of these 12 contact points, marked by 1 to

12, in the injector nozzle are illustrated in Figure A.9(a). Point 4 is the closest and point 3 is the farthest to the injector. Four sections are selected in each Stage. As shown in Figure A.9(b), the spacing in Z direction of the adjacent sections is about 30 μm in the Stage 1 region, machined using negative polarity for electrode dressing. The spacing between adjacent sections increases to 130 μm in Stage 2 and about 50 μm in Stage 3. For each hole, 144 points were measured. These measured points were analyzed to find the form characteristics of micro-holes.

For gage R&R study, the experiment and data analysis were implemented based on standard procedures developed for measurement system analysis (Measurement Systems Analysis Reference Manual, 1990). Three micro-holes were selected for gage R&R study. For the repeatability study, after setting up the reference position for a micro-hole, four repeated measurements were conducted without removing the injector from the fixture. For the reproducibility study, the number of measurement groups is set to two, i.e., the same procedure of three micro-holes with four measurements was repeated twice. In total, 3456 (=3x2x4x144) contact point measurements were conducted in this study.

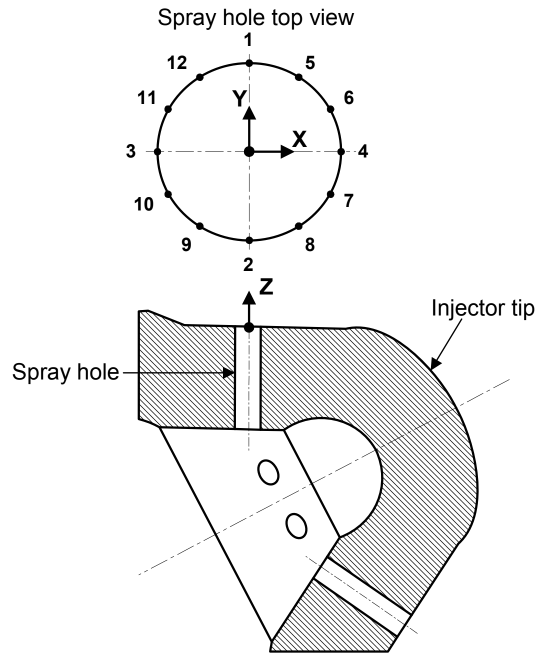

(a)

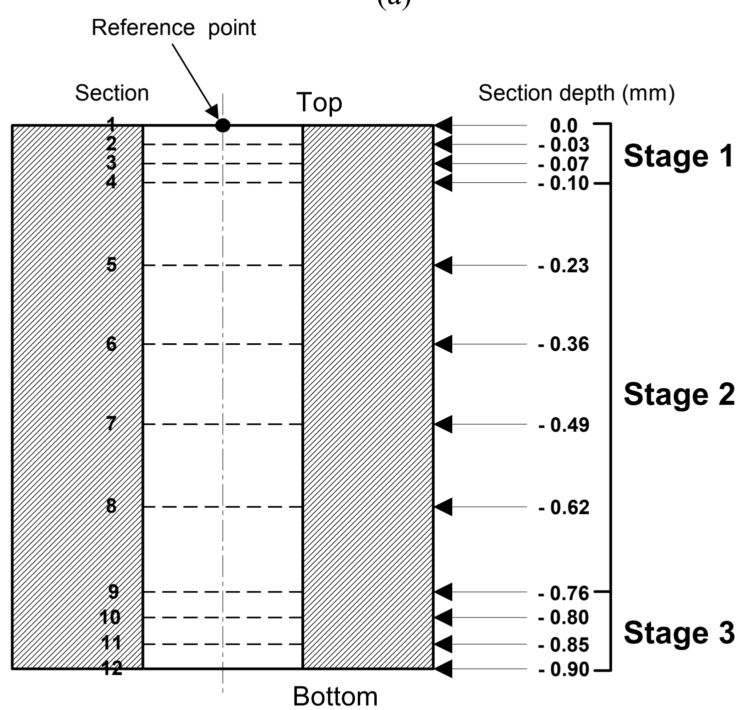

(b)

Figure A.9. Shape measurement of micro-holes: (a) orientation of coordinate system and locations of selected measurement points and (b) depths of different sections according to the three EDM Stages.

A.3.3. Characteristics of micro-holes

Five features, cylindricity, diameter, roundness, taper, and straightness, are used to characterize the micro-holes.

- *Cylindricity*: The cylindricity is defined as a tolerance zone bounded by two coaxial cylinders between which the measured cylinder must lie. The Least-Square (LS) fitting method (Osborne, 1985) is used to calculate the cylindricity.
- *Diameter:* The diameter of LS fitted cylinder is used to represent the hole size.
- *Roundness*: The 12 points in a section are analyzed to calculate the roundness. The roundness vs. depth of circle in the micro-hole is investigated.
- *Straightness:* The measured points 1, 2, 3 and 4, as defined in Figure A.9(a), of the 12 sections are used to calculate the straightness. The LS fitted line of measurement points in 12 sections is used to represent the straightness at points 1, 2, 3 and 4 of the micro-hole.
- *Taper:* Two pairs of lines 1-2 and 3-4 determine two taper values of the micro-hole. Taper is the difference in distances between these two lines at entrance and exit ends of the micro-hole, i.e., difference in size of the hole. Positive taper, as shown in Figure A.2(a), is defined to have the positive value of the taper.

A parameter called tilted angle is used to determine the accuracy of the alignment. Tilt angle is defined as the angle between the axis of the cylinder representing the micro-hole and the vector perpendicular to the plane representing the 12 measurement points in a section.

A.3.4. Gage R&R

For each measurement group, the range R and average $\overline{X}$ of measured dimension characteristics were identified for each of the three micro-holes. Definitions of standard deviation for repeatability, reproducibility, and gage R&R, are based on the Measurement Systems Analysis Reference Manual (1990). The standard deviation for repeatability, $\sigma_{repeatability}$, is:

$$\sigma_{repeatibility} = \frac{\overline{R}}{d_2'} \tag{A.2}$$

where $\overline{R}$ is the average of range R for both measurement groups, and d_2' is a coefficient depending on the number of trials, samples, and measurement groups (Measurement Systems Analysis Reference Manual, 1990). In this study, the number of trials is 4 and the number of samples times the number of measurement group is 6 (=3×2). The value of d_2' is 2.09.

The standard deviation for reproducibility, $\sigma_{reproducibility}$, is:

$$\sigma_{reproducibility} = \sqrt{\left(\frac{R_0}{d_2''}\right)^2 - \frac{\sigma^2_{repeatability}}{nr}} \tag{A.3}$$

where R_0 is the range of the average of $\overline{X}$ for both measurement groups, n is the number of samples, r is the number of trials, and d_2'' is again dependent on the number of measurement setup. In this study, the number of measurement group is 2 and the number of range calculation is 1. The value of d_2'' is 1.41.

The standard deviation for gage R&R, $\sigma_{R\&R}$, is:

$$\sigma_{R\&R} = \sqrt{\sigma^2_{repeatability} + \sigma^2_{reproducibility}} \tag{A.4}$$

The value of $5.15\sigma_{R\&R}$ is commonly used to represent 99% population of measurements for a normal distribution. The ratio $\sigma_{R\&R}/\sigma_{part}$ is used to assess the measurement system capability, where σ_{part} is the standard deviation for part. For a capable measurement system, $\sigma_{R\&R}/\sigma_{part}$ needs to be smaller than 10% (Measurement Systems Analysis Reference Manual, 1990). In practical applications, 30% of $\sigma_{R\&R}/\sigma_{part}$ could be acceptable. The part standard deviation under the 10% and 30% criteria can be calculated from the $\sigma_{R\&R}$.

The value of $5.15\sigma_{part}$ is defined as the capability tolerance of a measurement system. The capability tolerance is used to assess the capability of the multi-sensor CMM for micro-hole measurements. Values for capability tolerance are valuable for product engineers to specify micro-hole tolerances that are measurable and for metrology engineers to quantify the measurement capability and further improve the capability of gages.

A.4. Measurement Results

Table A.2 summarizes the tilted angles and five measured characteristics of three micro-holes.

Table A.2. Measurement results of three micro-holes before and after abrasive flow machining.

		Before AFM			After AFM
Hole number		1	2	3	1
Tilted angle (deg)		0.43	0.45	0.59	0.52
Cylindricity (μm)		16.1	14.7	17.1	29.3
Diameter (μm)		160	157	158	178
Roundness (μm)	Stage 1	2.91	2.42	2.55	1.97
	Stage 2	4.14	4.98	4.50	4.02
	Stage 3	6.69	4.65	6.95	9.01
Straightness (μm)	Point 1	7.29	7.94	10.52	17.13
	Point 2	10.04	9.48	8.40	22.45
	Point 3	12.84	10.53	13.78	20.07
	Point 4	9.19	10.49	9.36	18.22
Taper (μm)	T_{12}	4.86	7.92	6.99	-21.9
	T_{34}	3.24	4.52	3.76	-25.9

The tilted angle is small, ranging from 0.4 to 0.6°. It demonstrates the good alignment of the micro-hole to CMM Z-axis and ensures that the 12 data points in sections perpendicular and parallel to the hole axis can be used to calculate the roundness and straightness of the micro-hole, respectively. The five measured characteristics of three micro-holes are discussed as follows:

- *Cylindricity*: The cylindricity of three micro-holes is 16.1, 14.7, and 17.1 μm, about 10% of the cylinder size.
- *Diameter*: The diameter of three micro-holes is 160, 157, and 158 μm. These holes were drilled using 127 μm diameter tungsten wire electrode. The average gap between the wire and workpiece is about 15 μm. The variation of diameter for the 12

sections of micro-holes is shown in Figure A.10. Without considering the skewness of the hole axis and roundness of the section, Figure A.10 gives a rough representation of the hole shape. The largest diameter of the hole occurs at 0.35 mm depth, near the middle of the micro hole. The smallest diameter of the hole is inside the hole at 0.85 mm depth. This narrow section of the hole is likely contributed by the rounding or sharpening of the electrode tip, as shown in Figure 3(a), near the end of hole drilling. The use of large gap voltage in Stage 3 does enlarge the inside diameter of the hole where the electrode exits the micro hole. The difference between the maximum and minimum diameter of the micro-hole is about 30 μm. At the electrode entry side, the hole diameter is also small, which is likely due to the low gap voltage in electrode dressing in Stage 1. The variation among three holes is not large.

- *Roundness*: The roundness of three holes is shown in Figure A.11. The EDM process parameters in three Stages greatly affect the roundness. The roundness is higher deeper inside the hole. In Stage 1, the roundness is small, about 2.0 to 3.5 μm. In Stage 2, the roundness is consistent at about 4.5 μm. In Stage 3, the variation of roundness becomes very large, ranging from 4.0 to 8.5 μm. Such large variation in roundness measurement can be attributed to three factors: (1) uneven wear of electrode near the end of hole drilling, (2) rough surface due to the large gap voltage in Stage 3, and (3) large measurement uncertainty inside the hole. The measurement uncertainty will be discussed in the next section.
- *Straightness*: The straightness at points 1, 2, 3, and 4 (Figure 9(a)) of three micro-holes are listed in Table A.2. The straightness ranges from 7 to 14 μm. Point 3 has consistently higher straightness than the other three points. During micro-hole EDM,

Point 3 is located at the bottom where the debris accumulated due to gravity. Since de-ionized water was supplied by dribbling and debris cannot be flushed out effectively at Point 3, it is likely to be the cause of poor straightness.

- *Taper*: The taper T_{12} and T_{34}, as listed in Table 2, ranges from 3 to 8 μm. Although Point 3 has high straightness, the taper T_{34} is consistently lower than T_{12}. The taper is also lower than the straightness. All tapers are positive, which is common in micro-holes drilled by EDM.

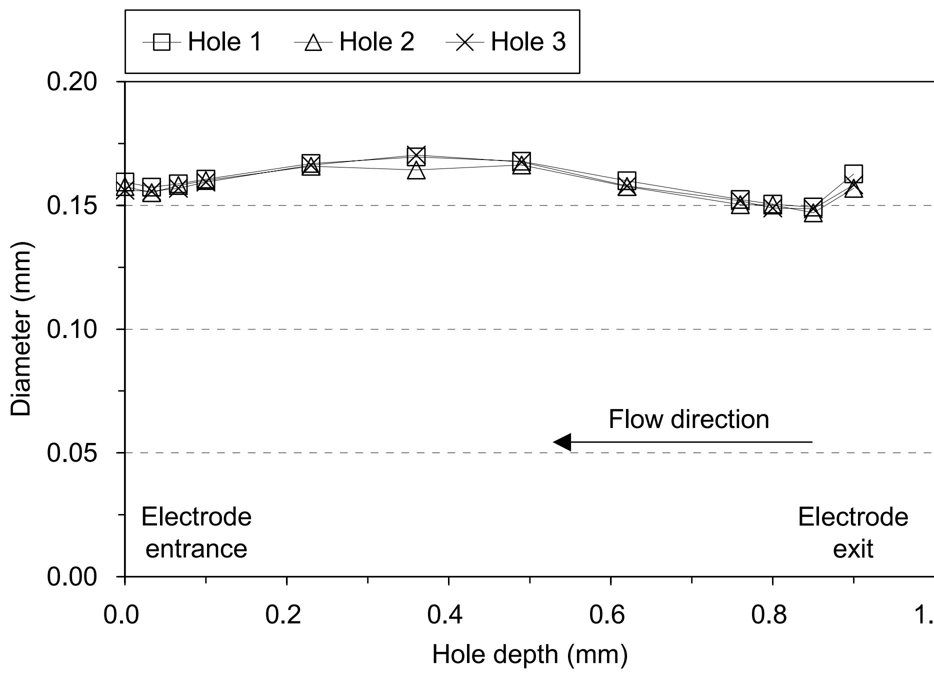

Figure A.10. Diameter of 12 measurement sections in three micro-holes.

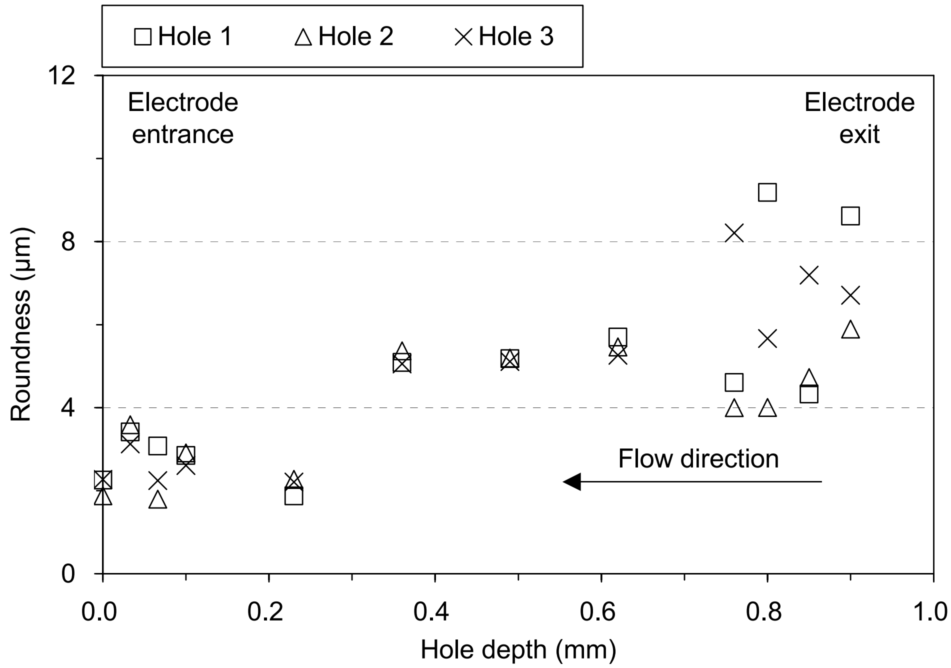

Figure A.11. Roundness of 12 measurement sections in three micro-holes.

A.5. Gage R&R for Micro-Hole Measurements

The $\sigma_{repeatability}$ for roundness of the 12 sections is presented in Figure A.12. The $\sigma_{repeatability}$ gradually deteriorates inside the hole, increasing from 0.5 to 1.7 µm. This is due to the limited accuracy of vision system for measurements of ball positions deep inside the micro-hole. Large $\sigma_{repeatability}$ contributes to the large variation of roundness in Stage 3, as shown in Figure A.11.

The $\sigma_{repeatability}$, $\sigma_{reproducibility}$, and $\sigma_{R\&R}$ of cylindricity, diameter, roundness, straightness, and taper measurements are summarized in Table A.3. The $\sigma_{repeatability}$ represents the repeatability of the CMM for measuring a specific hole characteristic. The zero value for $\sigma_{reproducibility}$ implies that the gage variation is larger than the measurement group variation. The $\sigma_{R\&R}$ is the index of measurement capability of the gage for a specific feature.

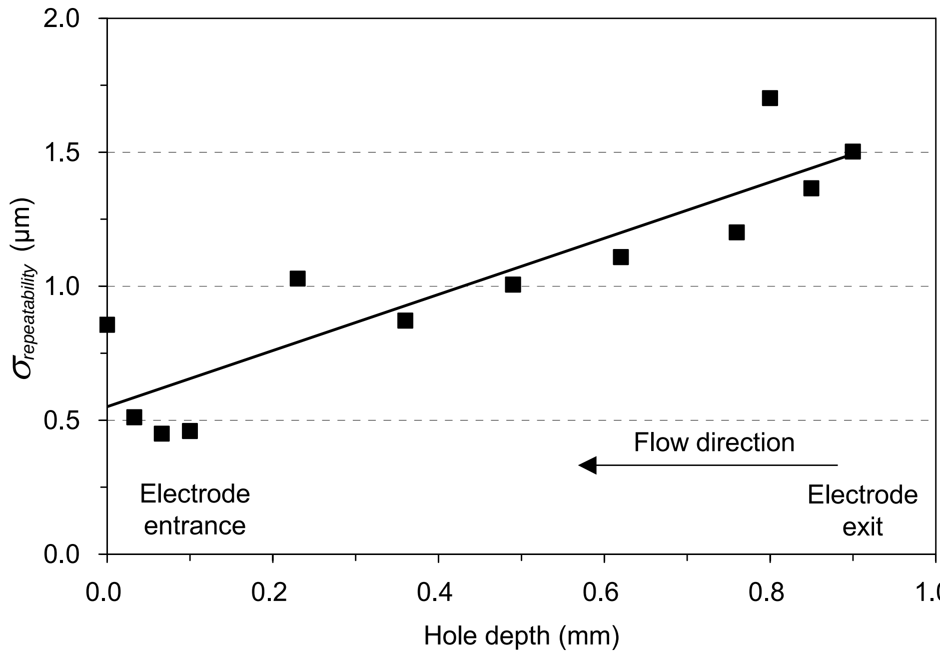

Figure A.12. $\sigma_{repeatability}$ of roundness for 12 measurement sections.

Table A.3. Gage R&R and capability tolerance for CMM micro-hole measurement.

Dimension type		$\sigma_{repeatability}$ (µm)	$\sigma_{reproducibility}$ (µm)	$\sigma_{R\&R}$ (µm)	Capability tolerance (µm)	
					$\sigma_{R\&R}/\sigma_{part}$ <0.3	$\sigma_{R\&R}/\sigma_{part}$ <0.1
Cylindricity		1.36	0	1.36	23.4	70.2
Diameter		0.30	0	0.30	5.15	15.5
Roundness	Stage 1	0.60	0.12	0.63	10.8	32.4
	Stage 2	0.90	0.08	0.91	15.6	46.9
	Stage 3	1.44	0.04	1.45	24.9	74.7
Straightness		0.36	0.14	0.39	6.70	20.1
Taper		1.51	0.54	1.60	27.5	82.5

The capability tolerance (CT) of the CMM for $\sigma_{R\&R}/\sigma_{part}$ < 30% and 10% for each of the hole characteristic are summarized in Table A.3. CT values specify the part tolerance that can be capably measured by the CMM. For cylindricity, the measurement capability is not very good: capable of only 70 μm and marginally capable of 23 μm. For diameter, the measurement is capable of 15 μm and marginally capable of 5 μm. For roundness, the gage is more capable in Stage 1 (outside the hole) than in Stage 3 (inside the hole). This is consistent with the trend of roundness $\sigma_{repeatability}$ in Figure A.12. The gage capability is good for straightness but poor for taper. Results in Table A.3 provide a guideline for designers to specify tolerances for the diesel fuel injector micro-holes and for metrology engineers to further improve the measurement capability.

A.6. Effects of AFM on Micro-Hole Geometry

AFM is a non-traditional machining process applied to improve the surface condition and round the flow entry (electrode exit) of the micro-hole (Stackhouse, 1993). The abrasive media, which is a mixture of abrasive grit and a semi-solid carrier (Loveless et al., 1994), flows through the micro-hole at high pressure to round the inlet or flow entry edge and improve the surface roughness. In this study, SiC abrasive with nominal size of 0.015 mm was used in an ExtrudeHone machine. The flow pressure and process cycle time were set at 27.6 MPa and 25 s, respectively.

The 3D wireframe representations of measured points for Hole 1 before and after AFM process are shown in Figure A.13(a) and (b), respectively. The fuel inlet (electrode exit) edge of the hole has been enlarged and rounded after AFM. The rounding is uneven around the hole circumference of the hole inside edge. More material is removed at Point 3, which is away from the injector tip. The flow pattern of high viscosity media in AFM affects the material removal rate around the circumference of hole edge. Such effect can be quantified using the micro-hole measurement technique developed in this study.

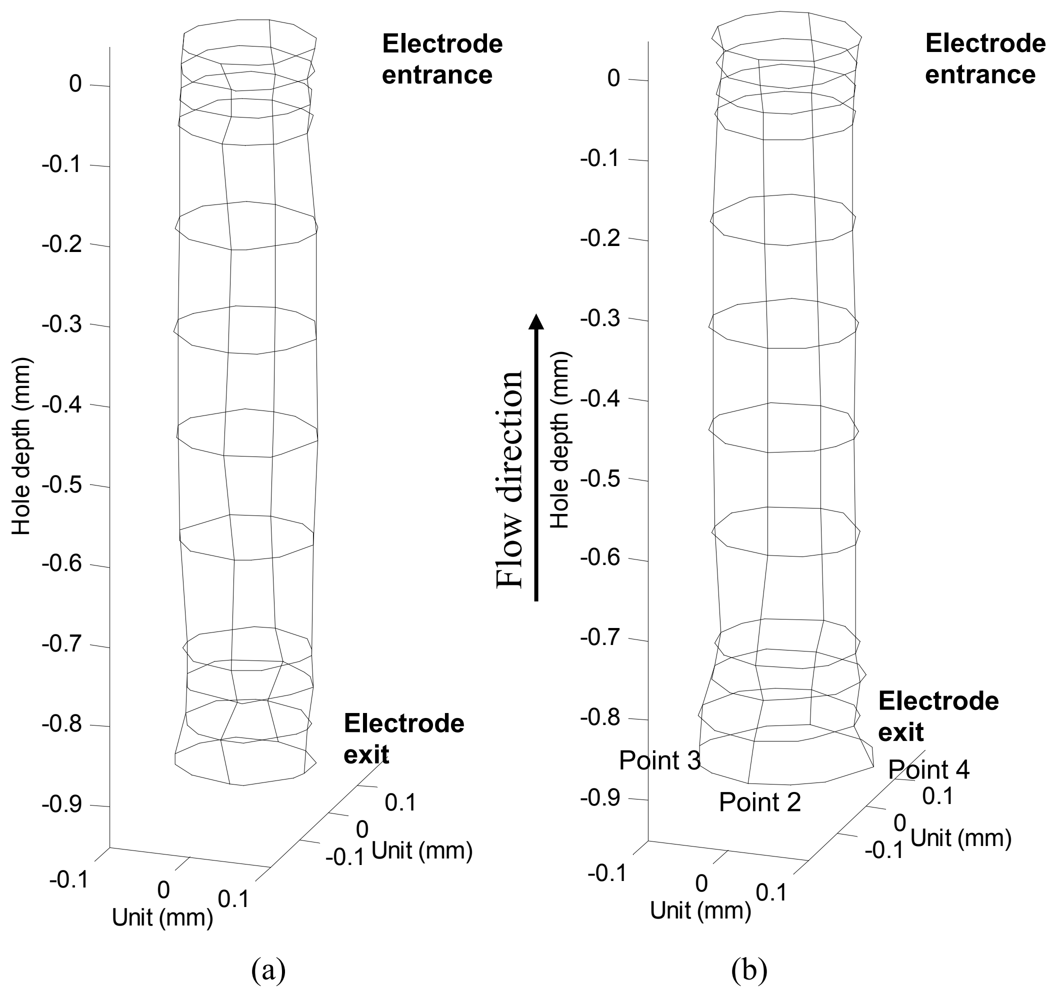

Figure A.13. 3D wireframe representation of Hole 1: (a) before AFM and (b) after AFM.

The cylindricity, diameter, roundness, straightness, and taper of Hole 1 machined after AFM are listed in the last column of Table A.2. Due to the rounding of the hole inside edge, the cylindricity, diameter, and straightness are all increased. The roundness is improved in Stages 1 and 2 regions but worsened in Stage 3 region (near the hole inside edge). The taper becomes negative, which demonstrates the effect of AFM to alter the hole geometry.

The diameter of Hole 1 before and after AFM for 12 sections in the Z-axis is shown in Figure A.14. The diameter after AFM is increased by about 10 to 25 μm in Stages 1 and 2 regions. In the Stage 3 region, the hole diameter is increased by about 35 to 50 μm.

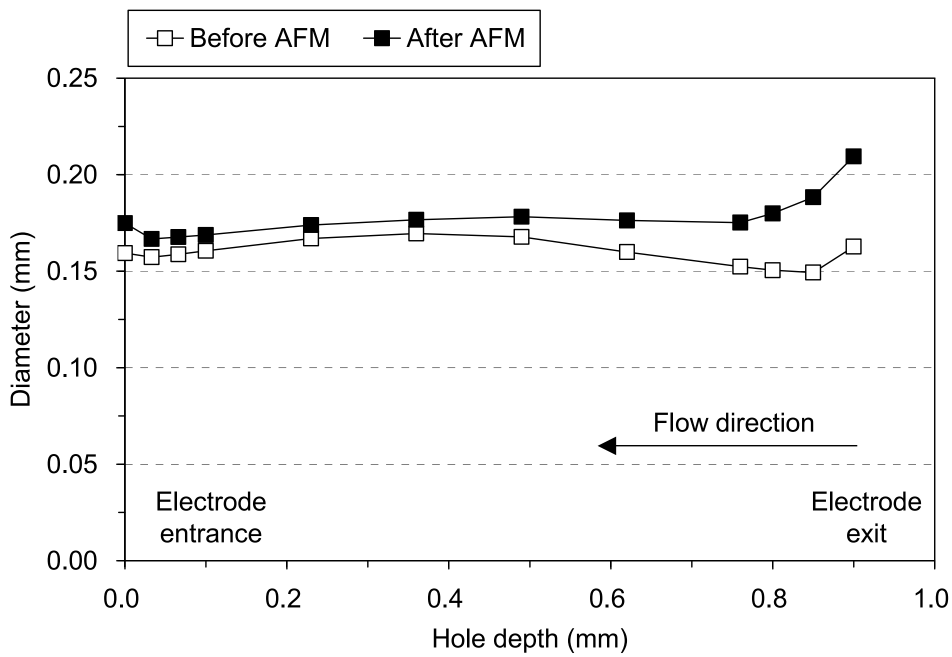

Figure A.14. Effects of AFM on micro-hole diameter.

A.7. Concluding Remarks

In this study, the form measurement and gage R&R of micro-holes was conducted. Geometric (cylindricity, roundness, straightness, and taper) and dimensional (diameter) characteristics of three 160 μm diameter micro-holes were measured. Effects of EDM process parameters on hole geometry were correlated. Capable tolerance specifications for micro-holes were derived from the gage R&R study using the multi-sensor CMM The change of hole geometry, particularly the rounding of hole inside edge on one side and enlarging of the hole size, using the AFM were revealed using the micro-hole measurement technique.

The measurement capability of the CMM for micro-hole measurement is certainly limited, compared to that of large hole measurement. Further improvements of measurement technology, both in imaging and scanning contact probe, will further advance the gage R&R. Using the scanning probe, more points can be acquired for accurate roundness, straightness, taper, cylindricity, and the overall form measurement of micro-holes. The measured data points can be processed to create 3D representation of micro-hole and to further understand and correlate effects of hole machining (laser, EDM, etc.) and post-machining (AFM) processes on the hole geometry, spray pattern, and engine emissions. Such link between manufacturing and product engineering is important for the development of future clean diesel combustion technology.

Appendix B

Negative Tapered Micro-Hole EDM Drilling

The geometry of the Diesel fuel injection spray holes has crucial effects on the spray propagation as well as the air/fuel mixture formation, and thus directly influences exhaust gas emissions. State-of-the-art spray holes usually have positive taper shape, as shown in Figure A.2., due to the limitation of current EDM drilling technology. Positive tapered spray holes would cause the cavitation, a phenomenon which bubbles and cavities generated inside the spray hole at localized pressure changes (Blessing et al., 2003). Negative tapered spray holes can effectively minimize the cavitation and generate better fuel spray pattern for more efficient emissions (Blessing et al., 2003). The requirement of diameter difference between flow inlet and outlet is about 15 to 20 μm for state-of-the-art diesel injector spray holes.

Current EDM drilling techniques for negative tapered spray holes primarily use the mechanical method, using a rotating wire guide which is designed to slant at a small angle to the hole axis to fabricate the negative tapered spray hole (Diver et al., 2004; Cusanelli et al., 2007). A multi-stage EDM drilling is proposed in this research to achieve the goal of negative tapered spray holes by proper process parameter control, which can significantly save the new equipment cost. For the multi-stage EDM drilling, a small pilot hole is first drilled to prevent debris accumulation and provide smooth debris flushing. The pilot hole drilling has been proposed in a sequential, hybrid micro-hole drilling using laser and EDM (Li et al., 2006) and proved beneficial for the maintenance of hole dimension consistency. The debris accumulation around the hole inlet, or the flow exit, would cause the secondary discharge and enlarge the flow exit, as shown in Figure B.1. After the pilot hole is drilled, the deionized water flushing can flow smoothly downward to prevent the debris accumulation and secondary discharges, as shown in Figure B.2. In addition to the pilot hole drilling, a method using coated electrodes to prevent secondary discharges in micro-EDM was developed by Richardson and Gianchandani (2005).

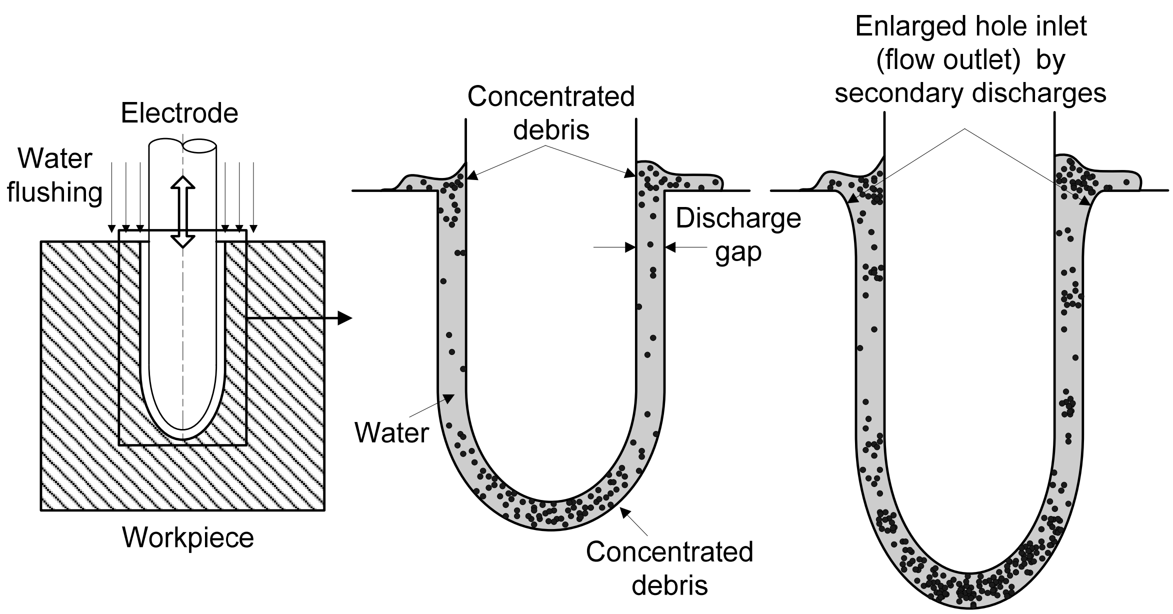

Figure B.1. Debris accumulation and hole exit enlargement due to secondary discharges.

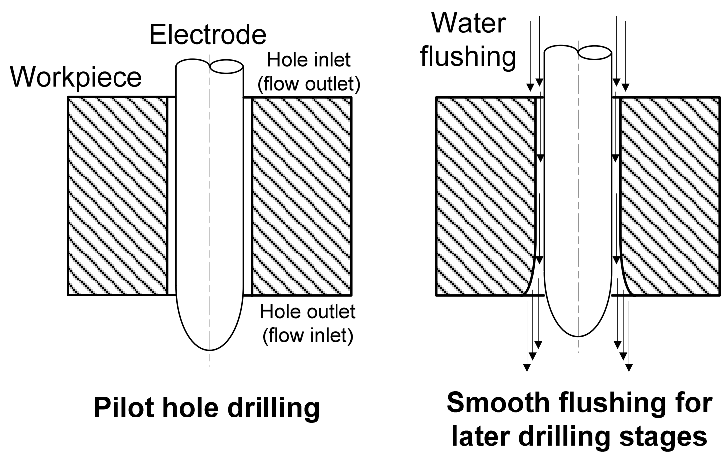

Figure B.2. Effects of the pilot hole in multi-stage EDM drilling.

In addition to the pilot hole drilling, another characteristic of multi-stage EDM drilling is the utilization of electrode dressing to enlarge the hole diameter. As shown in Figure 2.5, the diameter of electrode tip is increased after the electrode dressing. The enlarged electrode tip as well as localized arc and short circuit pulses, generated due to the reverse polarity (Kao and Shih, 2006), are used together to enlarge the hole diameter at specific location near the hole outlet. Experimental results of 150 μm diameter electrode on 1.14 mm thick AISI 52100 hardened steel are shown in Figure B.3.

Pictures embedded in Figure B.3 compare the diameter of the negative tapered micro-hole and Werth CMM probe. The multi-stage EDM micro-hole drilling can effectively fabricate negative tapered micro-holes and an 18 μm difference between flow inlet and outlet is achieved.

Further studies are necessary to enhance the process stability and obtain precise control over the negative taper dimension.

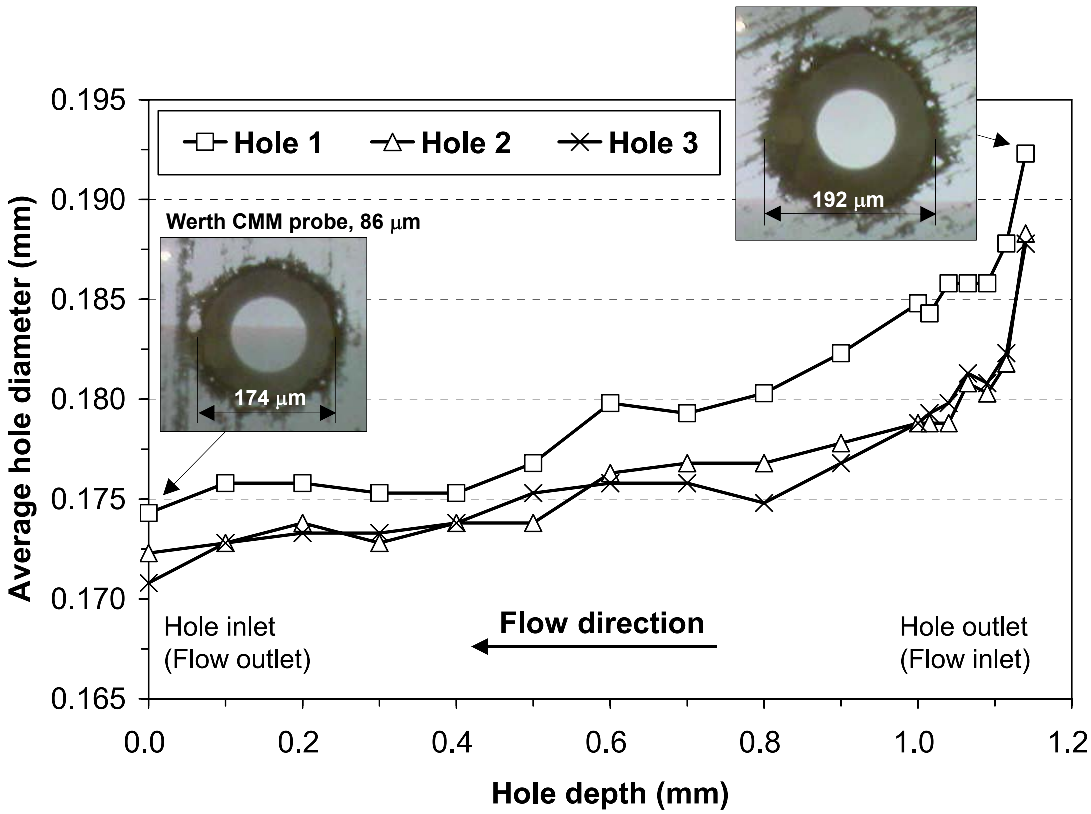

Figure B.3. Negative tapered micro-holes measurement using Werth CMM.

Appendix C

The Ringing Model

Due to the parasitic inductance and capacitance inherent in the electronic circuit under high speed switching in micro-hole EDM, the oscillation (or ringing) of decaying gap voltage at the end of each spark and arc pulse is inevitable (Kuo et al., 2002). For micro-hole EDM, as shown in the sample spark and arc pulses in Figure 2.2, the ringing of gap voltage occupies over 60% of pulse off time. Modeling the oscillation of gap voltage can help give a better understanding of the ringing effect and lead to more efficient EDM circuit design and process parameter selection.

C.1. Modeling of Voltage Oscillation After Discharging

A *RLC* circuit model, as shown in Figure C.1, was developed. Parameters used in this model are: gap voltage V_g, parasitic resistance R_p, parasitic capacitance C_p, parasitic inductance of electrode L_e, parasitic inductance of the jumper cable for the voltage probe L_p, and a DC voltage source representing the open-circuit voltage across discharge gap E_o (Takahata and Gianchandani, 2002). A schematic diagram of each component of the circuit corresponding in the EDM setup and the arrangement of voltage probe and jumper cable are illustrated in Figure C.2.

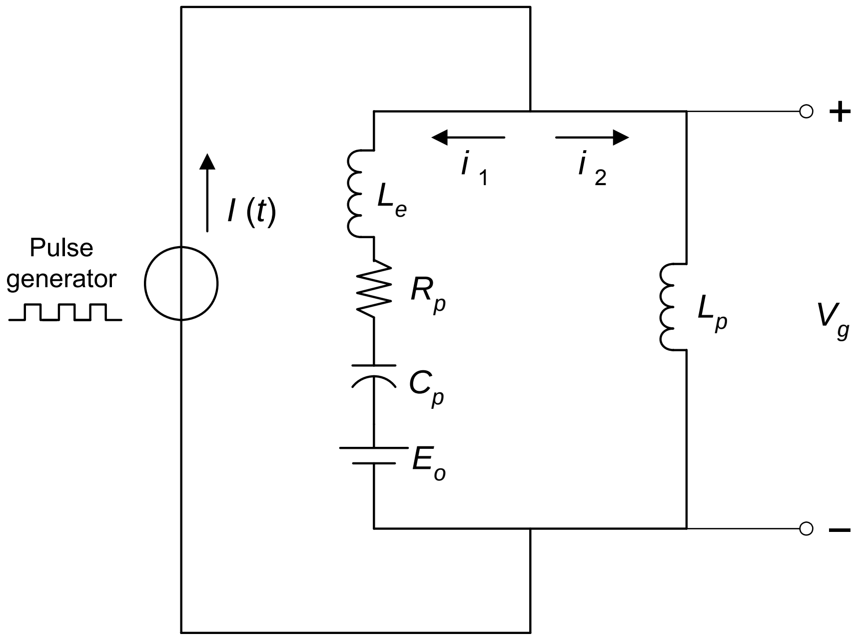

Figure C.1. A *RLC* circuit for the modeling of ringing effect.

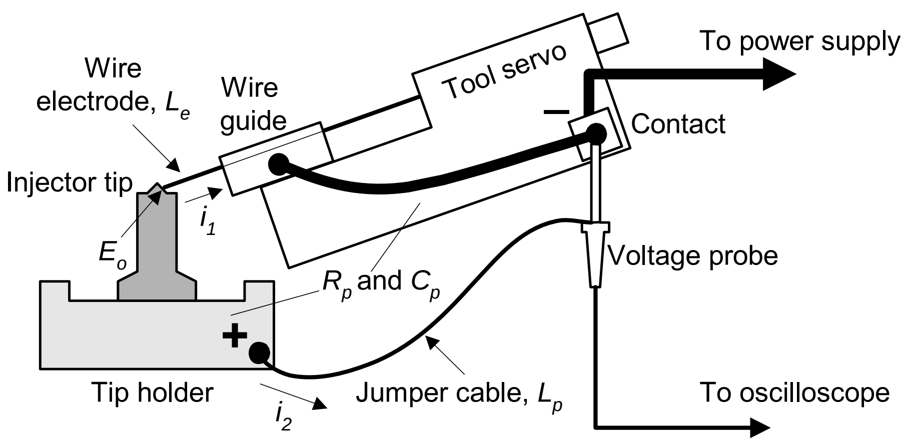

Figure C.2. Schematic diagram of the micro-hole EDM setup.

Values of L_e and L_p can be estimated by the work of Grover (1946):

$$L = 0.002l\left[\ln\frac{2l}{\rho} - \frac{3}{4}\right] \tag{C.1}$$

where ρ is the wire radius in cm, l is the wire length in cm, and the unit of L is μH.

The second-order differential equation of the *RLC* circuit shown in Figure C.1 is:

$$\frac{d^2V_g}{dt^2} + \frac{R_p}{L_e + L_p}\frac{dV_g}{dt} + \frac{1}{(L_e + L_p)C_p}V_g = 0 \tag{C.2}$$

Equation (C.2) can be rewritten as:

$$\frac{d^2V_g}{dt^2} + 2\xi\omega_n\frac{dV_g}{dt} + \omega_n^2 V_g = 0 \tag{C.3}$$

where $\xi = R_p/2\omega_n(L_e+L_p)$ is the damping ratio and $\omega_n=\sqrt{1/(L_e + L_p)C_p}$ is the resonant frequency of the EDM circuit. The homogenous solution of Eq. (C.3) is from Inman (2001):

$$V_g = Ae^{-\xi\omega_n t}\sin(\omega_d t + \phi) \tag{C.4}$$

where A is the amplitude of voltage oscillation, called the ringing amplitude, ω_d

($=\omega_n\sqrt{1-\xi^2}$) is the damped frequency, and ϕ is the phase shift.

In this study, the ringing oscillates from negative voltage to zero. The envelope curve to represent the oscillating decay is given by

$$V_g = -Ae^{-\xi\omega_n t} \tag{C.5}$$

The ξ and ω_n are solved by processing the data of gap voltage V_g vs. time t in the ringing region. The decay rate $\xi\omega_n$ and period of decay oscillation T are identified from the six data points, as marked in Figure C.3, in Period VI. Three examples of the ringing of spark pulses in Stage 2 using 100, 125, and 225 μm diameter wire electrodes are shown in Figure C.3 to demonstrate the data processing procedure. The t = 0 is defined at the end of Period V when the current is zero. The first data point is located at t = 0. The following five peaks in Period VI are identified. The average of three time spans between adjacent peaks 2, 3, 4, and 5 is used to represent the period T. Fitting the six data points using Eq. (C.4), the decay rate $\xi\omega_n$ can be determined. It is important to note that the 0.5 ns high speed data acquisition is crucial to accurately determine T and $\xi\omega_n$. Knowing T ($=2\pi/\omega_d$), $\xi\omega_n$, L_e, and L_p, the values of C_p and R_p are obtained from Eqs. (C.6) and (C.7).

$$C_p = \frac{1}{(L_e + L_p)\omega_n^2} \tag{C.6}$$

$$R_p = 2\xi\omega_n(L_e+L_p) \tag{C.7}$$

These two variables are intrinsic system parameters and should not change under different EDM setups. Two sets of experiments, one varying wire electrode diameter and the other changing open circuit voltage, are conducted to test the variation of C_p and R_p to validate the proposed *RLC* circuit for ringing model.

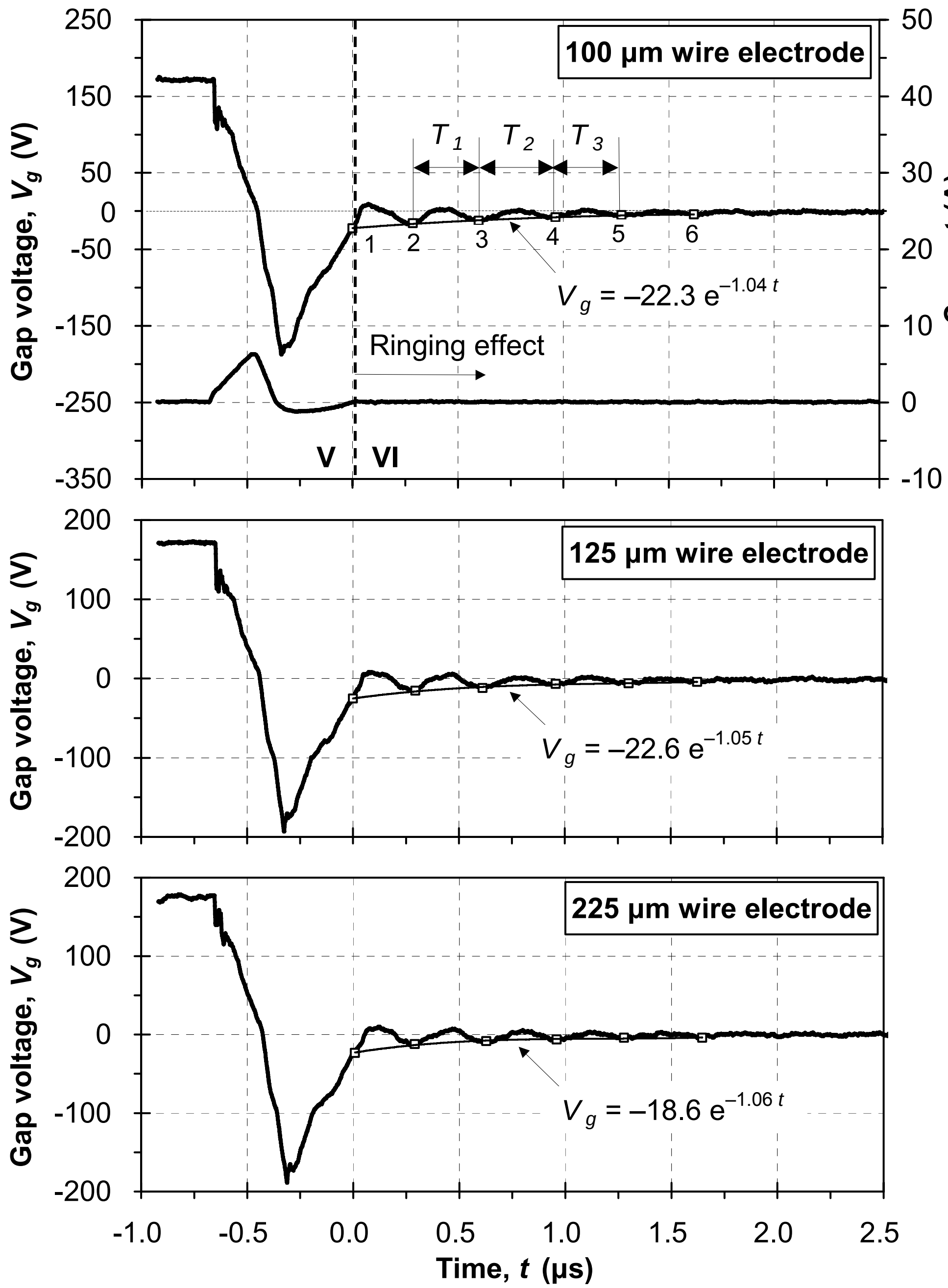

Figure C.3. Envelope curves of the ringing effect for 100, 125, and 225 µm diameter wire electrodes. (V_o = 200 V)

C.2. Influence of the Electrode Size

The spark pulse in Stage 2 of 100, 125, and 225 μm diameter electrodes, as shown in Figure C.3, are used to find the C_p and R_p. Using Eq. (C.1), the parasitic inductance L_p = 0.288 μH (l = 25 cm and ρ = 0.075 cm) and L_e = 0.069, 0.066, and 0.060 μH for l = 5 cm and ρ = 0.005, 0.0063, and 0.011 cm, respectively.

For the 100, 125, and 225 μm diameter wire electrodes, T = 0.33, 0.32, and 0.32 μs and $\xi\omega_n$ = 1.04, 1.05, and 1.06 s^{-1}, respectively. The ringing time T_r is about 2.3 μs for three wire electrodes. Results of the parasitic capacitance C_p and parasitic resistance R_p are listed in Table C.1. Both C_p and R_p are almost the same for all three electrode diameters. This confirms the proposed ringing model.

Table C.1. Parasitic properties C_p and R_p with different electrode size (V_o = 200 V, L_p = 0.288 μH).

Electrode diameter (μm)	100	125	225
L_e (μH)	0.069	0.066	0.060
Parasitic capacitance C_p (nF)	7.61	7.35	7.62
Parasitic resistance R_p (Ω)	0.743	0.743	0.738

C.3. Influence of the Open Circuit Voltage

The open circuit voltage vs. time data in five experiments at 160, 180, 200, 230, and 250 V open circuit voltage is used to find the variation of C_p and R_p. The electrode diameter is 125 μm, the parasitic inductances L_p = 0.288 μH and L_e = 0.066 μH. The ringing time T_r is about 2.3 μs for the five voltage setups. As listed in Table C.2, C_p varies from 7.32 to 7.64 nF and R_p ranges from 0.687 to 0.828 Ω. The variation of C_p is small, while a reasonable variation of R_p, which increases with open circuit voltage, exists. A possible cause for the variation of R_p is the resistance variation across the discharge gap due to different levels of open circuit voltage. The ringing effect occurs at the end of discharging, while the heat-induced explosion destroys the plasma channel and generates a cavity within the dielectric fluid. A higher open circuit voltage corresponds to a higher pulse energy level and generates a stronger explosion, which cleans away the previous plasma channel more completely. This will reduce the concentration of remnant ions and electrons within the discharge gap and result in a higher resistance.

Table C.2. Parasitic properties C_p and R_p with different open circuit voltage V_o (diameter of wire electrode = 125 μm, parasitic inductance L_e= 0.066 μH, and L_p = 0.288 μH).

Open circuit voltage V_o (V)	160	180	200	230	250
Parasitic capacitance C_p (nF)	7.51	7.60	7.36	7.64	7.32
Parasitic resistance R_p (Ω)	0.687	0.729	0.743	0.807	0.828

C.4. Concluding Remarks

A *RLC* circuit was proposed to model the ringing effect generated at the end of discharge. The inductance of the voltage probe jumper cable and the wire electrode was calculated and two parameters, parasitic capacitance C_p and resistance R_p, of the *RLC* circuit were calculated from the measured decaying voltage waveforms. Results showed that the proposed *RLC* circuit could model the ringing phenomenon, the electrode diameter had negligible effect on ringing, and high open voltage increased the parasitic resistance and improved the damping in ringing.

The modeling of ringing phenomenon can help understand the effects of key circuit components and, in the future, help to reduce the ringing time. A reduction of ringing time can increase the pulse frequency as well as the electrode feed rate for more efficient EDM drilling.

BIBLIOGRAPHY

Bibliography

Adler, U., 1994, *Diesel Fuel Injection*, Robert Bosch GmbH, Stuttgart.

Ahmed, M.S. and Duffield, A., 1989, “Deep hole drilling using ECM,” SME Technical Paper Series, MS89-816.

Albus, J.S., 1992, “A theory of intelligent machine systems,” Proceedings of the IEEE/RSJ International Workshop on Intelligent Robots and Systems – IROS '91, Osaka, Japan, pp. 3-9.

Allen, D.M. and Lecheheb, A., 1996, “Micro electro-discharge machining of ink jet nozzles: optimum selection of material and machining parameters,” Journal of Materials Processing Technology, 58(1), pp. 53-66.

Automotive Industry Action Group, 1990, *Measurement Systems Analysis Reference Manual*, 1st edition, AIAG publications, Southfield, MI.

Bhattacharyya, S.K. and El-Menshawy, M.F., 1978, “Monitoring the E.D.M. process by radio signals,” International Journal of Production Research, 16(5), pp. 353-363.

Bhattacharyya, S.K. and El-Menshawy, M.F., 1980, “Monitoring and controlling the E.D.M. process,” Journal of Engineering for Industry, 102(3), pp. 189-194.

Blessing, M., König, G., Krüger, C., Michels, U., Schwarz, V., 2003, “Analysis of flow and cavitation phenomena in diesel injection nozzles and its effects on spray and mixture formation,” SAE Technical Paper series, 2003-01-1358.

Boccadoro, M. and Dauw, D., 1995, “About the application of fuzzy controllers in high-performance die-sinking EDM machines,” Annals of the CIRP, 44(1), pp. 147-150.

Chiu, S. and Togai, M., 1988, “A fuzzy logic programming environment for real-time control,” International Journal of Approximate Reasoning, 2(2), pp. 163-175.

Chiueh, T., 1991, “Optimization of fuzzy logic implementation,” Proceedings of the

Twenty-First International Symposium on Multiple-Valued Logic, Victoria, Canada, pp. 348-355.

Christoph, R., 2004, “Multisensor coordinate metrology: Flexible measurements of form size and location," VDI Berichte, 1860 pp. 157-163.

Cusanelli, G., Minello, M., Torchia, F., Ammann, W., Grize, P.-E., 2007, "Properties of micro-holes for nozzles by micro-EDM," 15th International Symposium on Electromachining, Pittsburgh, PA, pp. 241-245.

Dauw, D.F., Snoeys, R., Dekeyser, W., 1983, "Advanced pulse discriminating system for EDM process analysis and control," Annals of the CIRP, 32(2), pp. 541-549.

Diver, C., Atkinson, J., Helml, H.J., Li, L., 2004, "Micro-EDM drilling of tapered holes for industrial applications," Journal of Materials Processing Technology, 149(1–3), pp. 296-303.

Evans, J.M., Messina, E.R., Albus, J.S., 2002, "Knowledge Engineering for real time intelligent control," Proceedings of the 2002 IEEE International Symposium on Intelligent Control, Vancouver, Canada, pp. 421-427.

Furutani, K., Mohri, N., Higuchi, T., 1997, "Self-running type electrical discharge machine using impact drive mechanism," IEEE/ASME International Conference on Advanced Intelligent Mechatronics, Tokyo, Japan, 1997, p 88.

Gangadhar, A., Shunmugam, M.S., Philip, P.K., 1992, "Pulse train studies in EDM with controlled pulse relaxation," International Journal of Machine Tools and Manufacture, 32(5), pp. 651-657.

Giedl, R., Helml, H.J., Wagner, F.X., Wild, M.J., 2003, "Geometrical aspects of laser-drilled high precision holes for flow control applications," Proceedings of SPIE 5063, Fourth International Symposium on laser Precision Microfabrication, Bellingham, WA, pp. 389-394.

Goldberg, D.E., 1989, *Genetic Algorithm in Search, Optimization, and Machine Learning*, Addison-Wesley, Reading, MA.

Grover, F.W., 1946, *Inductance calculations*, D. Van Nostrand Company, Inc., New York.

Han, F., Wachi, S., Kunieda, M., 2004, "Improvement of machining characteristics of micro-EDM using transistor type isopulse generator and servo feed control," Precision Engineering, 28, pp. 378-385.

Hebbar, R.R., 1992, "Micro-hole drilling by electrical discharge machining," Ph.D. Dissertation, Purdue University.

Her, M.G. and Weng, F.T., 2001, "Micro-hole machining of copper using the electro-discharge machining process with a tungsten carbide electrode compared with a copper electrode," International Journal of Advanced Manufacturing Technology, 17(10), pp. 715-719.

Higuchi, T., Furutani, K., Yamagata, Y., Takeda, K., 1991, "Development of pocket-size electro-discharge machine," Annals of the CIRP, 40(1), pp. 203-206.

Ho, K.H. and Newman, S.T., 2003, "State of the art electrical discharge machining (EDM)," International Journal of Machine Tools and Manufacture, 43(13), pp. 1287-1300.

Holland, J., 1975, *Adaptation in natural and artificial systems*, University of Michigan Press, Ann Arbor.

Holt, D.J., 2004, *The Diesel Engine*, SAE, Warrendale, PA.

Hu, B., Mann, G.K.I., Gosine, R.G., 1999, "New methodology for analytical and optimal design of fuzzy PID controllers," IEEE Transactions on Fuzzy Systems, 7(5), pp. 521-539.

Imai, Y., Nakagawa, T., Miyake, H., Hidai, H., Tokura, H., 2004, "Local actuator module for highly accurate micro-EDM," Journal of Materials Processing Technology, 149(1-3), pp. 328-333.

Inman, D.J., 2001, *Engineering Vibration*, second edition, Prentice Hall, New Jersey.

Isermann, R., 1998, "On fuzzy logic applications for automatic control, supervision, and fault diagnosis," IEEE Transactions on Systems, Man, and Cybernetics – Part A: Systems and Humans, 28(2), pp. 221-235.

Iwata, K. and Moriwaki, T.,1981, "Basic study of high speed micro deep drilling," Annals of the CIRP, 30(1), pp. 27-30.

Johnson, T.V., 2003, "Diesel emission control in review – the last 12 months," SAE technical paper series, 2003-01-0039.

Kaminski, P.C. and Capuano, M.N., 2003, "Micro hole machining by conventional penetration electrical discharge machine," International Journal of Machine Tools and Manufacture, 43(11), pp. 1143-1149.

Kaneko, T. and Onodera, T., 2004, "Improvement in machining performance of die-sinking EDM by using self-adjusting fuzzy control," Journal of Materials Processing Technology, 149, pp. 204-211.

Kao, C.C. and Shih, A.J., 2006, "Sub-nanosecond monitoring of micro-hole electrical discharge machining pulses and modeling of discharge ringing," International Journal of Machine Tools and Manufacture, 46(15), pp. 1996-2008.

Kao, C.C. and Shih, A.J., 2007a, "Form measurements of micro-holes," submitted to Measurement Science and Technology.

Kao, C.C., Tao, J., Shih, A.J., 2007b, "Water mist near dry wire and drilling electrical discharge machining and gap distance modeling," 15th International Symposium on Electromachining, Pittsburgh, PA, pp. 281-286.

Kao, C.C. Miller, S.F., Shih, A.J., 2007c, "Fuzzy logic control system for micro-hole electrical discharge machining," Proceedings of the 2007 International Manufacturing Science and Engineering Conference, Atlanta, GA, accepted.

Kao, C.C. and Shih, A.J., 2007d, "Fuzzy logic control of micro-hole electrical discharge machining," Journal of Manufacturing Science and Engineering, Transactions of the ASME, submitted.

Kao, C.C. and Shih, A.J., 2007e, "Design and tuning of the fuzzy logic controller for micro-hole electrical discharge machining," International Journal of Machine Tools and Manufacture, submitted.

Kao, J.Y. and Tarng, Y.S., 1997, "A neural-network approach for the on-line monitoring of the electrical discharge machining process," Journal of Materials Processing Technology, 69(1–3), pp. 112-119.

Karakuzu, C., 2000, "An experimental comparison of fuzzy, neuro and classical control techniques," Proceedings of 21st IEEE Convention of the Electrical and Electronic Engineers in Israel, Tel-Aviv, Israel, pp. 160-166.

Kernighan, B.W. and Ritchie, D.M., 1988, *The C Programming Language*, second edition, Prentice Hall, New Jersey.

Kim, B.J., Masuzawa, T., Fujita, H., Tominaga, A., 1998, "Dimensional measurement of microholes with silicon-based micro twin probes," Proceedings of the IEEE Micro Electro Mechanical Systems (MEMS), Heidelberg, Germany, pp. 334-339.

Kim, B.J., Masuzawa, T., Bourouina, T., 1999, "The vibroscanning method for the measurement of micro-hole profiles," Measurement Science and Technology, 10(8), pp. 697-705.

Ko, R.C. and Good, M.C., 2005, "Improving contour accuracy of machine tools using an integral-gain scheduler," Proceedings of the Institution of Mechanical Engineers – Part I:

Journal of Systems and Control Engineering, 219(7), pp. 511-518.

Kruth, J.P., Snoeys, R., Van Brussel, H., 1979, “An adaptive control solution to the problem of automation and optimization of EDM,” Transactions of NAMRC 7, Ann Arbor, MI, pp. 307-314.

Kuo, J.L., Chang, Z.S., Lee, J.D., Chio, Y.C., Lee, P.H., 2002, “Ringing effect analysis of the digital current pulse generator for the linear rail gun,” IEEE Industry Applications Society Annual Meeting, 1, pp. 176-181.

Lebrasseur, E., Pourciel, J.B., Bourouina, T., Masuzawa, T., Fujita, H., 2002, “A new characterization tool for vertical profile measurement of high-aspect-ratio microstructures,” Journal of Micromechanics and Microengineering, 12(3), pp. 280-285.

Li, H.X. and Gatland, H.B., 1996, “Conventional fuzzy control and its enhancement,” IEEE Transactions on Systems, Man, and Cybernetics, Part B: Cybernetics, 26(5), pp. 791-797.

Li, L., Diver, C., Atkinson, J., Giedl-Wagner, R., Helml, H.J., 2006, “Sequential laser and EDM micro-drilling for next generation fuel injection nozzle manufacture,” Annals of the CIRP, 55(1), pp. 179-182.

Li, Y., Guo, M., Zhou, Z., Hu, M., 2002, “Micro electro discharge machine with an inchworm type of micro feed mechanism,” Precision Engineering, 26(1) pp. 7-14.

Lim, H.S., Wong, Y.S., Rahman, M., Edwin Lee, M.K., 2003, “A study on the machining of high-aspect ratio micro-structures using micro-EDM,” Journal of Materials Processing Technology, 140(1-3), pp. 318-325.

Liu, H.S. and Tarng, Y.S., 1997, “Monitoring of the electrical discharge machining process by abductive networks,” International Journal of Advanced Manufacturing Technology, 13(4), pp. 264-270.

Loveless, T.R., Williams, R.E., Rajurkar, K.P., 1994, “Study of the effects of abrasive-flow finishing on various machined surfaces,” Journal of Materials Processing Technology, 47(1-2), pp. 133-51.

Lu, X. and Leng, Y., 2005, “Electrochemical micromachining of titanium surfaces for biomedical applications,” Journal of Materials Processing Technology, 169(2), pp. 173-178.

Masuzawa, T., Tsukamoto, J., Fujino, M., 1989, “Drilling of deep microholes by EDM,” Annals of the CIRP, 38(1), pp. 195-198.

Masuzawa, T., Kuo, C.L., Fujino, M., 1990, "Drilling of deep microholes by EDM using additional capacity," Bulletin of the Japan Society of Precision Engineering, 24(4), pp. 275-276.

Masuzawa, T., Hamasaki, Y., Fujino, M., 1993, "Vibroscanning method for nondestructive measurement of small holes," Annals of the CIRP, 42(1), pp. 589-592.

Masuzawa, T., Kim, B.J., Bergaud, C. Fujino, M., 1997, "Twin-probe vibroscanning method for dimensional measurement of microholes," Annals of the CIRP, 46(1), pp. 437-440.

Masuzawa, T., 2000, "State of the art of micromachining," Annals of the CIRP, 49(2), pp. 473-488.

Mediliyegedara, T.K.K.R., Wijayakulasooriya, J.V., Alahakoon, S., Pathirana, S.D., 2004, "An artificial neural network approach for the process control of electro discharge machining (EDM)," Proceedings of the 36th ISCIE International Symposium on Stochastic Systems Theory and its Applications, Saitama, Japan, pp. 303-308.

MINITAB Inc, 2003, *MINITAB User Manual Release 14 for Windows*, MINITAB Inc..

Mohan, B., Rajadurai, A., Satyanarayana, K.G., 2004, "Electric discharge machining of Al-SiC metal matrix composites using rotary tube electrode," Journal of Materials Processing Technology, 153-154(1-3), pp. 978-985.

Morita, H., Ohyama, S., Mohri, N., 2000, "Electrical discharge device with direct drive method for thin wire electrode," SAE Technical Paper series, 2000-01-1085.

Nagasaka, K., Takagi, T., Koyanagi, K., Yamauchi, T., 2000, "Development of fine atomization injector," JSAE Review, 21, pp. 319-313.

Nordgren, H., Hultqvist, A., Johansson, B., 2004, "Start of injection strategies for HCCI-combustion," SAE technical paper series, 2004-01-2990.

Nunes, U., Araujo, R., Marques, L., 2000, "Towards intelligent machines: theories, technologies, and experiments," Systems Analysis Modelling Simulation, 38, pp. 157-173.

Ogata, K., 2004, *Modern control engineering*, fourth edition, Pearson Education Ltd., Singapore.

Osborne, M.R., 1985, *Finite Algorithms in Optimization and Data Analysis*, John Wiley & Sons Ltd, Chichester, UK.

Pandit, S.M. and Mueller, T.M., 1987, "Verification of on-line computer control of EDM by data dependent systems," Journal of Engineering for Industry, 109(2), pp. 117-121.

Perry, W.B., 1986, "Abrasive flow machining principles and practices," Nontraditional Machining Conference Proceedings, Cincinnati, OH, pp. 121-127.

Postrioti, L. and Ubertini, S., 2006, "An integrated experimental-numerical study of HSDI diesel injection system and spray dynamics," SAE technical paper series, 2006-01-1389.

Pourciel, J.B., Lebrasseur, E., Bourouina, T., Masuzawa, T., Fujita, H., 2001, "Microsystem tool for Microsystems characterization profile measurement of high aspect-ratio microstructures," Proceedings of SPIE 4592, Device and Process Technologies for MEMS and Microelectronics II, Adelaide, Australia, pp. 244-251.

Pourciel, J.B., Jalabert, L., Masuzawa, T., 2003, "Profile and surface measurement tool for high aspect-ratio microstructures," JSME International Journal Series C, 46(3), pp. 916-922.

Rajurkar, K.P. and Pandit, S.M., 1985, "Adaptive control of EDM – technology and research," Transactions of NAMRC 13, Berkeley, CA, pp. 8-14.

Rajurkar, K.P. and Wang, W.M., 1997, "Improvement of EDM performance with advanced monitoring and control systems," ASME Journal of Manufacturing Science and Engineering, 119, pp. 770-775.

Reznik, L., 1997, *Fuzzy Controllers*, Newnes, Oxford.

Richardson, M.T. and Gianchandani, Y.B., 2005, "A passivated electrode batch μEDM technology for bulk metal transducers and packages," Proceedings of the Fourth IEEE Conference on Sensors, Irvine, CA, pp. 219-222.

Sasaki, J., Youoku, S., Tamamushi, K., Ito, A., 2005, "Development of microchannel device for automated microinjection," Proceedings of SPIE - Progress in Biomedical Optics and Imaging, San Jose, CA, pp. 186-193.

Shamma, J.S. and Athans, M., 1992, "Gain scheduling: potential hazards and possible remedies," IEEE Control Systems Magazine, 12(3), pp. 101-107.

Snoeys, R., Dauw, D., Kruth, J.P., 1980, "Improved adaptive control system for EDM processes," Annals of the CIRP, 29, pp. 97-101.

Soni, J.S. and Chakraverti, G., 1994, "Machining characteristics of titanium with rotary electro-discharge machining," Wear, 171(1-2), pp. 51-58.

Stackhouse, J. 1993, "Abrasive flow machining," SME Technical Paper series, MR93-148.

Takahata, K., Shibaike, N., Guckel, H., 2000, "High-aspect-ratio WC-Co microstructure produced by the combination of LIGA and micro-EDM," Microsystem Technologies, 6(5), pp. 175-178.

Takahata, K. and Gianchandani, Y.B., 2002, "Batch mode micro-electro-discharge machining," Journal of Microelectromechanical Systems, 11(2), pp. 102-110.

Tarng, Y.S., Tseng, C.M., Chung, L.K., 1997, "A fuzzy pulse discriminating system for electrical discharge machining," International Journal of Machine Tools and Manufacture, 37(4), pp. 511-522.

Van Ossenbruggen, C., 1969, "Micro-spark erosion," Philips Technisch Tijdschrif, 20, pp. 200-213.

Wang, W.M. and Rajurkar, K.P., 1990, "Monitoring, modeling and control of EDM," ASME Production Engineering Division (Publication) PED, Winter Annual Meeting of the ASME, Dallas, TX, pp. 393-406.

Wang, W.M. and Rajurkar, K.P., 1992, "Modeling and adaptive control of EDM systems," Journal of Manufacturing Systems, 11, pp. 334-345.

Weck, M. and Dehmer, J.M., 1992, "Analysis and adaptive control of EDM sinking process using the ignition delay time and fall time as parameter," Annals of the CIRP, 41(1), pp. 243-246.

Wong, Y.S., Rahman, M., Lim, H.S., Han, H., Ravi, N., 2003, "Investigation of micro-EDM material removal characteristics using single RC-pulse discharges," Journal of Materials Processing Technology, 140(1-3), pp. 303-307.

Yamamoto, M., Kanno, I., Aoki, S., 2000, "Profile measurement of high aspect ratio micro structures using tungsten carbide micro cantilever coated with PZT thin films," Proceedings of the IEEE Micro Electro Mechanical Systems (MEMS), Miyazaki, Japan, pp. 217-222.

Yan, B.H., Huang, F.Y., Chow, H.M., Tsai, J.Y., 1999, "Micro-hole machining of carbide by electric discharge machining," Journal of Materials Processing Technology, 87(1-3), pp. 139-145.

Yan, M.T. and Liao, Y.S., 1998, "Adaptive control of the WEDM process using the fuzzy control strategy," Journal of Manufacturing Systems, 17, pp. 263-274.

Yu, S.F., Lee, B.Y., Lin, W.S., 2001, "Waveform monitoring of electric discharge machining by wavelet transform," International Journal of Advanced Manufacturing Technology, 17(5), pp. 339-343.

Yu, Z.Y., Rajurkar, K.P., Shen, H., 2002, "High aspect ratio and complex shaped blind micro holes by micro EDM," Annals of the CIRP, 51(1), pp. 359-362.

Zhang, J.H., Zhang, H., Su, D.S., Qin, Y., Huo, M.Y., Zhang, Q.H., Wang, L., 2002, "Adaptive fuzzy control system of a servomechanism for electro-discharge machining combined with ultrasonic vibration," Journal of Materials Processing Technology, 129, pp. 45-49.

Zhang, Y., Ying, J., Chen, Z., Chen, W., 1997, "The research on the self adaptive fuzzy control system for electric discharge machining," Proceedings of the IEEE International Conference on Intelligent Processing Systems, Beijing, China, pp. 364-367.

Zhang, Y., 2005, "The study in a new-type self-adaptive fuzzy logic control system in EDM process," Proceedings of the Fourth International Conference on Machine Learning and Cybernetics, Guangzhou, China, pp. 18-21.

Zhao, W.S., Zhang, Y., Wang, Z.L. Jia, B.X. Hu, F.Q. Li, Z.Y., 2004, "Research on a micro EDM equipment and its application," Key Engineering Materials, 259-260, pp. 567-571.